Satellite Remote Sensing of Air Quality
in the Oil Sands Region

Heba S. Marey and Zaher Hashisho

University of Alberta

Long Fu

Alberta Environment and Sustainable Resource Development

June 2014

OSRIN

Oil Sands Research and Information Network

Oil Sands Research and Information Network

The Oil Sands Research and Information Network (OSRIN) is a university-based, independent organization that compiles, interprets and analyses available knowledge about managing the environmental impacts to landscapes and water impacted by oil sands mining and gets that knowledge into the hands of those who can use it to drive breakthrough improvements in regulations and practices. OSRIN is a project of the University of Alberta's School of Energy and the Environment (SEE). OSRIN was launched with a start-up grant of $4.5 million from Alberta Environment and a $250,000 grant from the Canada School of Energy and Environment Ltd.

OSRIN provides:

- **Governments** with the independent, objective, and credible information and analysis required to put appropriate regulatory and policy frameworks in place

- **Media, opinion leaders and the general public** with the facts about oil sands development, its environmental and social impacts, and landscape/water reclamation activities – so that public dialogue and policy is informed by solid evidence

- **Industry** with ready access to an integrated view of research that will help them make and execute environmental management plans – a view that crosses disciplines and organizational boundaries

OSRIN recognizes that much research has been done in these areas by a variety of players over 40 years of oil sands development. OSRIN synthesizes this collective knowledge and presents it in a form that allows others to use it to solve pressing problems.

Citation

This report may be cited as:

Marey, H.S., Z. Hashisho and L. Fu, 2014. Satellite Remote Sensing of Air Quality in the Oil Sands Region. Oil Sands Research and Information Network, University of Alberta, School of Energy and the Environment, Edmonton, Alberta. OSRIN Report No. TR-49. 104 pp.

Copies of this report may be obtained from OSRIN at osrin@ualberta.ca or through the OSRIN website at http://www.osrin.ualberta.ca/en/OSRINPublications.aspx or directly from the University of Alberta's Education & Research Archive at http://hdl.handle.net/10402/era.17507.

Table of Contents

LIST OF TABLES

LIST OF FIGURES

REPORT SUMMARY

The rapid expansion of oil sands activities and massive energy requirements to extract and upgrade the bitumen have led to a need for more comprehensive understanding of their potential environmental impacts, particularly on air quality. There are many oil sands developments and natural sources (point, area and mobile) that generate significant emissions, including nitrogen (NO_2) and sulphur oxides (SO_2), carbon monoxide (CO), and particulate matter. These chemicals are known to affect human health and climate. Thus an environmental monitoring program that measures the ambient air quality is needed to understand air pollutant emissions, their chemical transformation in the atmosphere, long-range transport and subsequent deposition to the local and regional environment.

Several studies have been conducted to understand the impact of the oil sands projects on the air quality over Alberta using ground-based measurements. However, data from these measurements are limited in spatial coverage as they reflect local air quality and cannot provide information about the overall regional air quality. A complementary approach to ground-based measurements is satellite-based monitoring which can provide large spatial and vertical coverage and allow monitoring of local and regional air quality. The objective of this report is to review available remote sensing technologies for monitoring and understanding the tropospheric constituents in the atmosphere, and potential use for monitoring the air quality over the oil sands region. The report includes a summary of the basic principles of remote sensing using satellites for tropospheric composition measurements; a detailed description of the instruments and techniques used for atmospheric remote sensing from space; demonstration of the key findings and results of using satellite data for air quality application; a brief summary of future missions; and, a case study to demonstrate the use of satellite data to study the impact of oil sands and other sources on carbon monoxide levels over Alberta.

The science of atmospheric remote sensing has dramatically evolved over the past two decades and proved to be capable of observing a wide range of chemical species (e.g., aerosols, tropospheric O_3, tropospheric NO_2, CO, HCHO, and SO_2) at increasingly higher spatial and temporal resolution. The integrated use of ground-based and satellite data for air quality applications has proven to be of enormous benefit to our understanding of the global distribution, sources, and trends of air pollutants. Despite the significance of using satellites in characterizations of air quality, there is limited research on using satellite-based remote sensing technology over Alberta. As satellite-based techniques now provide an essential component of observational strategies on regional and global scales, it is recommended to integrate data from satellite, and ground-based measurements as well as chemical transport models for air quality monitoring.

This report provides an in depth review of the developments in the atmospheric remote sensing area that may support air quality management, policy, and decision makers at the national, and regional level to take actions to control the exposure to air pollution.

ACKNOWLEDGEMENTS

1   INTRODUCTION

The industrial revolution and rapid population growth led to an improved standard of living, resulting in increased air pollution on local, regional and global scales. Air pollution negatively impacts human health, causing respiratory disease and chronic illness (McCubbin and Delucchi 1999, Turner et al. 2011), soil (Zhao et al. 2009), and forests (Matyssek et al. 2012). Anthropogenic activity is also changing the normal composition of the atmosphere, causing climate change and global warming. Thus, atmospheric monitoring of these changes, on all scales, is necessary.

Air quality is traditionally measured from ground monitoring stations and through *in situ* monitoring campaigns. Modeling may also be employed for emissions assessment and forecasting, relying heavily on emissions inventories and meteorological models. However, for these traditional methods, the area of land that can be monitored is restricted to discrete points on the Earth's surface. Ground instruments monitor individual pollutants (e.g., carbon dioxide) at specific locations, preventing an accurate description of total air pollution throughout a region and vertical level. Air quality measurements from space, however, may allow for monitoring at regional and national scales, potentially even providing air quality data across the globe. The science of atmospheric remote sensing developed dramatically over the past decade and is now capable of quantifying a wide range of chemical species (e.g., aerosols, tropospheric O_3, tropospheric NO_2, CO, HCHO, and SO_2) at increasingly high spatial and temporal resolutions. Correspondingly, these advanced technologies should be exploited to provide continuous air quality data at the tropospheric level to improve human health and the environment (Borrell et al. 2001, Martin 2008).

Remote sensing in this report refers to the use of electromagnetic radiation to acquire information without physical contact with the object being assessed, which, in this case, is the atmosphere. It relies on interactions between electromagnetic radiation and trace atmospheric constituents that cause changes in the spectral or temporal characteristics of the radiation. These signal changes are translated to quantitative estimates of atmospheric composition (Martin 2008).

The increasing availability of earth observing satellite systems provides a new approach to monitor air quality and assess our scientific understanding of pollution transport, air quality and global climate change. Satellite observations assist in identifying major sources of pollution and the associated pollution distribution patterns so the effectiveness of regulations is ensured (Hutchison 2003). Moreover, the relationship between local features and air pollution distribution can be identified (Wald and Baleynaud 1999). In addition, the presence of satellite products in a user-friendly, archived format allows the information to be conveniently used for a wide range of applications[1].

---

[1] See for example Rochdi, N., J. Zhang, K. Staenz, X. Yang, D. Rolfson, J. Banting, C. King and R. Doherty, 2014. Monitoring Procedures for Wellsite, In-Situ Oil Sands and Coal Mine Reclamation in Alberta. OSRIN Report No. TR-47. 156 pp. http://hdl.handle.net/10402/era.38742

We are currently capable of looking down from space to generate a three-dimensional view of the atmospheric interactions that impact air quality. The integrated use of satellites, ground data, and models will improve our understanding of urban air quality better than using any of the individual techniques. The purpose of this report is to describe the capability of satellite observations for measuring tropospheric composition, including a summary of key findings and results.

2   GEOPHYSICAL AND REMOTE SENSING CONSIDERATIONS

2.1   Orbits

The observation capabilities of satellites are largely based on orbit characteristics and the viewing and scanning properties of the instrument. For instance, the inclination angle (the angle between the equatorial plane and the orbital plane) determines the ground track (the point on the earth directly beneath the satellite) and maximum latitude (north and south). Each orbit covers a path on the earth's surface with width (swath width) dependent on the viewing properties of the instrument – typically ranging from <100 km to nearly 3,000 km. Most satellites are placed on polar orbits (inclination angle close to 90°), which provides for near global coverage because the earth rotates beneath the satellite as it moves between polar regions (Burrows et al. 2011). Most polar orbiting satellites are sun-synchronous, meaning they cross the equator at a fixed local time each day.

The orbiting altitude determines how much of the earth's surface can be observed from a satellite. As satellite altitude increases, observable surface area increases. For high-resolution earth observation, satellite orbits should be on low Earth orbits (LEO; around 800 km) (Wright et al. 2005); these platforms circle the earth every 100 minutes. Accordingly, the choice of a particular orbit for a satellite depends mainly on its intended application. Each satellite orbit cross the equator twice, once in the southward (descending) direction, and once in the northward (ascending) direction (Martin 2008) yielding complete earth coverage every day for wide swaths (> 2,000 km) (Figure 1), or within a few days for narrow swaths.

In contrast, satellites on geo-stationary orbits (GEO) are positioned above the equator at a high altitude with the same rotational period as the earth. Accordingly, they continuously monitor the same part of the earth, providing data related to diurnal variations, which is not possible for polar satellites (Burrows et al. 2011).

<div align="center">a   b</div>
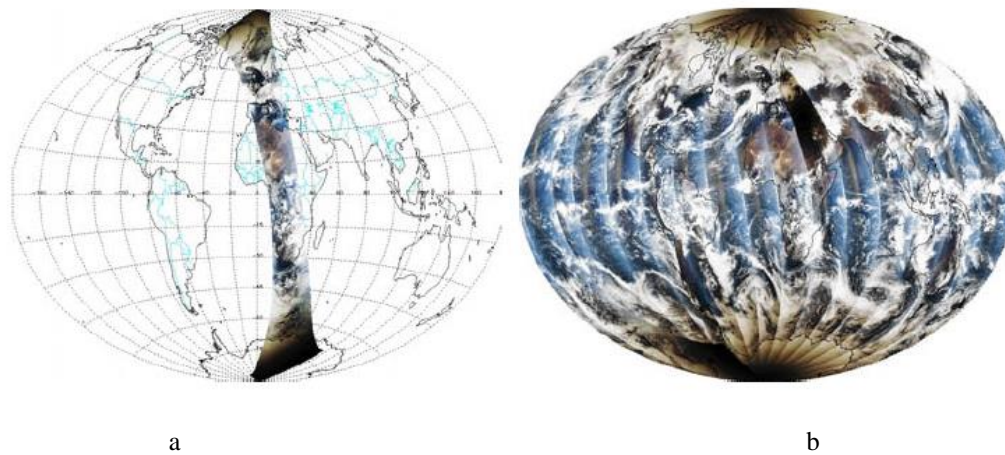
Figure 1.   Example of the measurements from a Sun-synchronous orbit.
             a) single orbit of OMI data plotted on 29 March 2006.
             b) how all the orbits for 29 March 2006 cover the whole globe.
             (Burrows et al. 2011).

2.2   Passive and Active Remote Sensing

Passive remote sensing measures the electromagnetic radiation coming from the sun and the
earth, after it has passed through the atmosphere (Figure 2). Active remote sensing generates
radiation from the satellite and detects back-scattered radiation and temporal changes in intensity
(Figure 2). An example of active remote sensing that has been used on satellites is light
detection and ranging (LiDAR), where short laser pulses are emitted into the atmosphere and
back-scattered energy is measured by a detector (Rothe et al. 1974).

<div align="center">3</div>
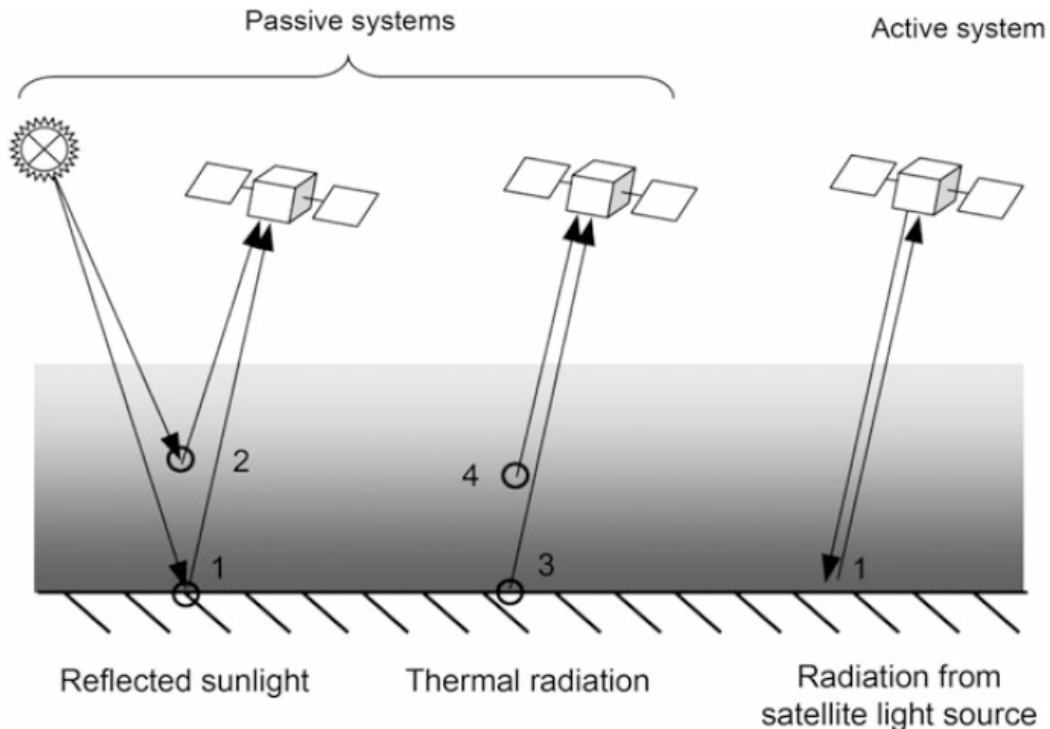
Figure 2. Schematics of active and passive remote sensing systems showing possible radiation
pathways from source to object and sensor.
Direct solar radiance can be reflected from the Earth's surface (1), or scattered in the
atmosphere (2). Long-wave radiation is emitted from the Earth's surface (3) or from
atmospheric gases (4) (Burrows et al. 2011).

2.3   Viewing Geometry

For passive remote sensing, the viewing geometry allows specific parts of atmospheric
composition to be probed. The satellite viewing geometry can be either nadir or limb. Nadir
geometry refers to all downward looking observations directly beneath the satellite. This
geometry allows for observations of the entire atmospheric column, including the boundary layer
(Figure 3) (Martin 2008). Satellites with limb geometry detect scattered light laterally and can
be used to derive information about the stratosphere and vertical trace gas concentration profiles
by varying the tangent altitudes (Figure 3). Spatial coverage with limb measurements is limited
since it is dependent on the position of the light source. SCanning Imaging Absorption
SpectroMeter for Atmospheric CHartographY (SCIAMACHY) is an example of an onboard
satellite instrument that uses limb geometry as well as nadir view (Figure 3) (Clerbaux et al.
2011).
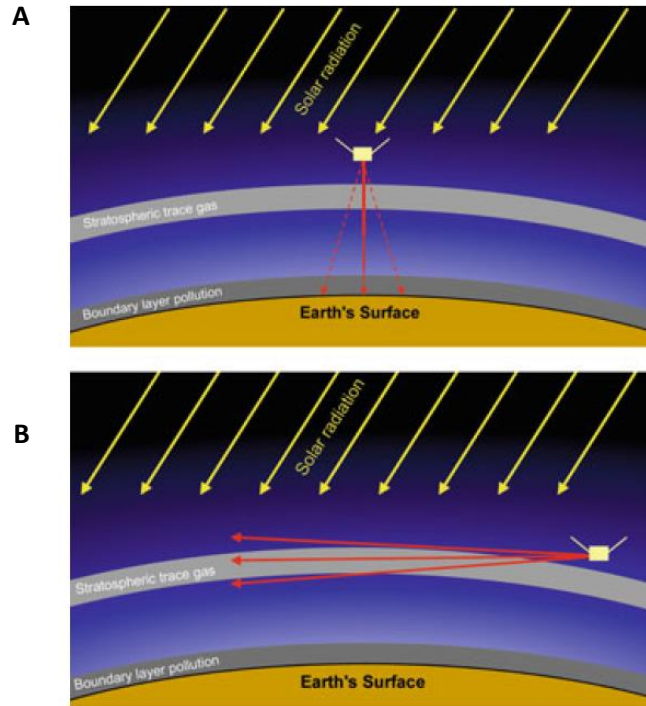
Figure 3.   Schematic representation of nadir (a) and limb (b) viewing geometries used by SCIAMACHY (Clerbaux et al. 2011).

2.4   Retrievals

The inferred concentration of chemical species, known as retrieval, is determined by a complex set of spectral fitting and radiative transfer calculations, well described by Martin (2008). Satellite retrievals of the lower atmosphere depend on spectral coverage and resolution. Satellite instruments detect spectral regions in the ultraviolet (UV), visible (Vis), infrared (IR), and microwave regions (i.e., 250 nm to 10 cm wavelengths). To measure a certain atmospheric constituent, the instrument should measure the spectral range in which that constituent absorbs, emits, or scatters radiation. The extent of radiation interactions, together with the resolution and signal-to-noise ratio of the instrument, governs the accuracy of the measurement.

Instruments fall broadly into two categories, observing either solar backscatter in the UV-Vis region or thermal IR emissions. The combination of equation solutions that best reproduces observed radiation is used for calculating retrieval. This approach is a forward, radiative transfer model that predicts atmospheric compositions. Often, external information about geophysical fields, atmospheric properties, and viewing conditions are required. An inversion method is applied to the developed forward model to derive the unknown parameter (e.g., ozone profile or column) from the measured reflectance. Parameters are adjusted until the squared-sum difference between modeled and measured reflectance is minimized. If the forward model is linear, the minimum is easily found by inverting the forward model's matrix. Unfortunately, most forward models are non-linear (Martin 2008).

Differential Optical Absorption Spectroscopy (DOAS) is a type of retrieval that is used to differentiate between absorption properties of multiple species in a single system, allowing for simultaneous quantification of multiple pollutants in a given atmospheric column. The retrieved quantity is the slant column density, which is defined as the column density along the average solar light path through the atmosphere. The slant column density and the air mass factor (AMF) are used to calculate the vertical column density. For many tropospheric trace gas retrievals, the largest uncertainty results from the AMF calculation (Boersma et al. 2004).

The aim of tropospheric monitoring is to produce column densities and/or concentration profiles of gases and aerosols. The retrieval process is often underdetermined, where there are too many unknown parameters (e.g., concentrations at various altitudes or pressures) than information in the measurement to solve the set of equations determined for the given system. In the case of profile retrieval, the unknown parameters are a set of concentrations at various altitudes or pressures. Many contaminants have trace concentrations in the troposphere, but notably larger stratospheric concentrations, making altitude discrimination essential. Since the measurements provide limited information on vertical concentration profiles, *a priori* information is required to stabilize the retrieval and solve the system of equations. The optimal estimation method (Rodgers 2000) is the most common for such profile retrievals. Contaminants including O_3, NO_2, CO, HCHO, SO_2, and CO_2, have been detected and vertically differentiated using these satellite techniques.

2.4.1 *Solar Back Scattered Radiation for Atmospheric Remote Sensing*

Atmospheric sensing with solar back scatter uses visible, near-infrared, and UV electromagnetic radiation. The intensity of reflected solar radiation from targets on the ground is attenuated as it traverses the atmospheric layers (Martin 2008). Land surface reflectivity at ultraviolet and short visible wavelengths is typically <5% (Herman and Celarier 1997, Koelemeijer et al. 2003), hence, observed backscattered radiation is directly related to the absorption spectra of atmospheric constituents. Another advantage of using satellite observations in the UV-Vis spectral region is that information is available for all atmospheric heights (including the near surface layers), making UV-Vis satellite observations a powerful tool for monitoring ground-level emission sources. Little or no information on the vertical distribution of trace gases is observed, however, which contrasts with observations for the microwave and/or thermal IR regions. Atmospheric gases show absorption features in the UV-Vis spectral range and thus their concentration can in principle be inferred. Aerosols can also be measured by quantifying their contribution to solar radiation scattering (Figure 4), allowing for observing the pattern of atmospheric aerosols, such as, dust storms, forest fires and other aerosol events. For select aerosols (e.g., dust and soot), solar radiation absorption can be measured to determine concentrations (Burrows et al. 2011).
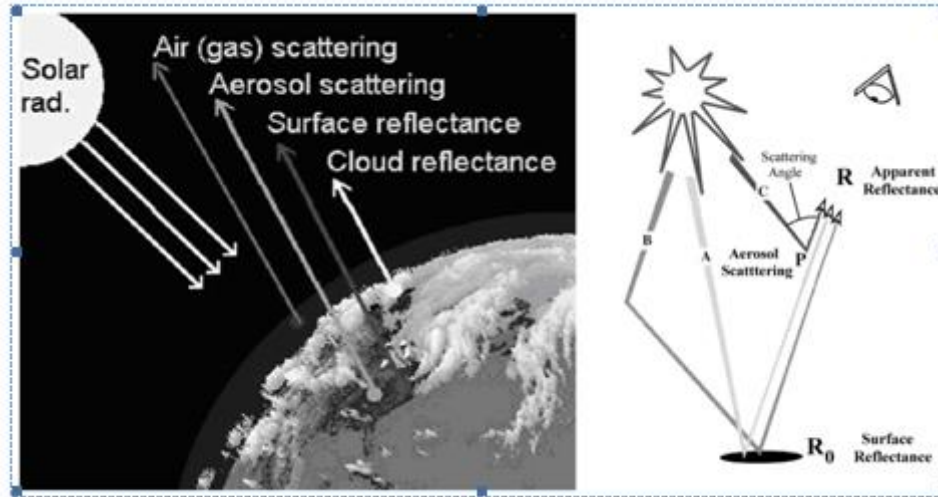
Figure 4.   Schematic representation of solar backscatter reflected from surface, cloud, and atmosphere (Husar 2011).

2.4.2   *Thermal Infrared Absorption and Emission for Atmospheric Remote Sensing*

Thermal infrared radiation (or radiative heat) is associated with thermal or heat radiation from the atmosphere and the earth's surface (McCartney 1983). Thus, retrievals in this region to infer trace gas concentrations require a comparison of absorbed and emitted radiation. Thermal emissions can be characterized at any time (day and night) because they do not require solar radiation.

Many atmospheric gases exist in specific rotational and vibrational quantum states, causing them to absorb and re-emit infrared photons as they move from one vibrational-rotational mode to another. All transitions that change the dipole moment of the molecule correspond to infrared spectral features that are characteristic of the given gas. Hetero-nuclear, diatomic molecules (e.g., CO, NO, HF, HCl) and most polyatomic molecules (e.g., H_2O, N_2O, CH_4, NO_2, HNO_3, OCS, SO_2) show strong absorption in and emission of thermal infrared energy. The main atmospheric constituents (N_2 and O_2) are symmetric, so their transitions do not result in a dipole moment change. Therefore, they do not have significant spectral features in the thermal infrared region (Clerbaux et al. 2011).

Atmospheric gases (e.g., CO and O_3) can be identified and quantified by the positions (wavenumbers) and areas of their absorption lines, respectively. Absorption and emission of infrared photons are sensitive to temperature, so the shape of the line provides information about the altitude distribution of the absorbing gas due to vertical variability in atmospheric temperature. Absorption line-widths can provide further information on vertical profiles because they depend on pressure, which also varies vertically. These pressure effects, however, require high spectral resolution to be detected. While infrared instruments rely on thermal contrast, surface sensitivity is enhanced when the difference between skin (temperature of the surface layer of the Earth) and air temperatures is highest (Bowman et al. 2006, Deeter et al. 2003).

Thus, the remote sensing capability of nadir-viewing satellite instruments for trace gases and aerosols is based on surface reflectivity or emissivity, cloud coverage, viewing geometry, and retrieval wavelength (Martin 2008).

2.5   Vertical Sensitivity

Instrument sensitivity in the middle and upper troposphere is typically high; however, near the ground, sensitivity depends on aerosol solar back scattering and surface conditions. The detection of trace gases and UV-absorbing aerosols is constrained by atmospheric scattering, which prevents part of the actual intensity from passing through the boundary layer. Strong scattering at UV wavelengths affects sensitivity when measuring absorbing aerosols (Klenk et al. 1982). On other hand, sensitivity when measuring trace gases with thermal infrared energy is reduced as the thermal contrast between the atmosphere and surface decreases (Pan et al. 1995, 1998).

A useful parameter that describes the vertical resolution of retrieved profiles is the averaging kernel (A). For example, if the retrieved profiles cover 10 pressure levels, A is a matrix that describes the sensitivity ratio of the retrieved values to the actual values at different altitudes. The averaging kernel is a function of the sensitivities of the top of atmosphere spectral radiances to species concentrations at different altitudes, signal-to-noise of the measurements, and *a priori* constraints used in the retrievals (Rodgers 2000). The trace of A is defined as Degrees Of Freedom for Signal (DOFS), which is an index that describes the number of independent elements of information in the retrieved vertical profile (Deeter et al. 2004, Rodgers 2000). DOFS depends on instrument characteristics and atmospheric physics. For example, DOFS for CO and O_3 profiles is 1 to 2 in the tropics and < 1 at the poles (Buchwitz et al. 2007, Deeter et al. 2004, Liu et al. 2005, Worden et al. 2004, 2013).

3   SATELLITE OVERVIEW

Satellite remote sensing for air quality applications began in 1978 with the launch of the Total Ozone Mapping Spectrometer[2] (TOMS) instrument onboard the Nimbus 7 satellite, which provided information about stratospheric ozone depletion (Molina and Rowland 1974). Ozone in a column of air is expressed in Dobson units (DU), where 1 DU has a value of 2.69×10^{16} molecules of ozone per square centimetre. Total O_3 column retrieval is based on backscattered ultraviolet (BUV) detection. This technique was developed (Hudson et al. 1995, Hudson and Thompson 1998, Kim et al. 1996) to give a tropical tropospheric O_3 product (Fishman 1991, Fishman et al. 1990). Additionally, information about volcanic SO_2 (Krueger 1983) and ultraviolet absorbing aerosols (Herman and Celarier 1997) was provided by the TOMS instrument.

---

[2] See http://disc.sci.gsfc.nasa.gov/acdisc/TOMS

The last TOMS instrument was deactivated in 2007, but the Ozone Monitoring Instrument[3] (OMI) on the Earth Observing System[4] (EOS) Aura satellite inherited the TOMS series and is discussed below.

Aerosol and tropospheric CO retrievals from space started nearly three decades ago. Aerosol retrieval was initially accomplished only over water, and only in the last decade have above-land measurements become available (Lee et al. 2009). Observations from the Multi Spectral Scanner[5] (MSS) on board the Earth Resources Technology Satellite[6] (ERTS-1) were first used to determine aerosol optical depth in 1972 (Griggs 1975, Mekler et al. 1977). The first generation of operational aerosol products were performed using data from the Advanced Very High Resolution Radiometer[7] (AVHRR) onboard TIROS-N in 1978 (Stowe et al. 2002). TOMS provided the longest measurement of global aerosols, although it was not designed for aerosol monitoring (Torres et al. 2002).

Space measurements of tropospheric CO started when the Measurements of Atmospheric Pollution from Satellites (MAPS) instrument was deployed four times between 1981 and 1994 (Reichle et al. 1986, 1990, 1999). The instrument measured CO in nadir view using a fixed-cell correlation radiometer operating in the 4.7 µm region, providing the first measurements of CO distributions in the middle and upper troposphere (Connors et al. 1999, Newell et al. 1999). Subsequently, the Interferometric Monitor of Greenhouse Gases (IMG), a part of the Japanese Advanced Earth Observing System[8] (ADEOS) satellite, provided CO data from August 1996 until June 1997, when the instrument's solar array failed (Kobayashi et al. 1999). This was the first high-resolution nadir infrared tropospheric sounder of several trace gases (H_2O, CO_2, N_2O, CH_4, O_3, CO, CFCs, and HNO_3), using a Fourier transform spectrometer (Barret et al. 2005, Clerbaux et al. 2003, Turquety et al. 2004).

Table 1 summarizes the capabilities of major satellite instruments designed for remote sensing of aerosols or trace gases in the lower troposphere. All of these instruments are in sun-synchronous, polar orbits and are discussed in more detail below.

---

[3] See http://en.wikipedia.org/wiki/Ozone_Monitoring_Instrument

[4] See http://eospso.gsfc.nasa.gov/

[5] See https://www.fas.org/irp/imint/docs/rst/Intro/Part2_16.html

[6] See http://en.wikipedia.org/wiki/Landsat_1

[7] See http://en.wikipedia.org/wiki/Advanced_Very_High_Resolution_Radiometer

[8] See http://kuroshio.eorc.jaxa.jp/ADEOS/

Table 1.   Major satellite instruments designed for remote sensing of aerosols and trace gases in the lower troposphere.

Instrument	Platform	Measurement Period	Nadir Resolution EW x NS (km)	Global Coverage (days)	Main Products
GOME	ERS-2	1995 to 2003	320×40	3	NO_2, HCHO, SO_2, O_3
MOPITT	Terra	2000 –	22×22	3.5	CO
MISR	Terra	2000 –	18×18	7	Aerosol optical depth (AOD)
MODIS	Terra	2000 –	10×10	2	AOD
	Aqua	2002 –			
AIRS	Aqua	2002 –	14×14	1	CO, SO_2
SCIAMACHY	ENVISAT	2002 –	60×30	6	NO_2, HCHO, SO_2, O_3, CO
OMI	Aura	2004 –	24×13	1	NO_2, HCHO, SO_2, O_3, AOD
TES	Aura	2004 –	8×5	16	O_3, CO
PARASOL	PARASOL	2004 –	7×6	2	AOD
CALIOP	CALIPSO	2006 –	0.335	16	AOD
GOME-2	MetOp	2006 –	80×40	1.5	NO_2, HCHO, SO_2, O_3
IASI	MetOp	2006 –	12×12	0.5	O_3, CO

3.1   ERS-2 (GOME-1)

New and improved tropospheric trace gas measurements began in 1995 with the launch of the Global Ozone Monitoring Experiment[9] (GOME) instrument aboard the second European Research Satellite (ERS-2) (Burrows et al. 1999). GOME-1 measures solar backscatter radiance in the 240 to 790 nm region with a spectral resolution between 0.2 and 0.4 nm. It is a nadir viewing instrument that flies on a polar sun-synchronous orbit, approximately 800 km above the earth and crossing the equator at 10:30 AM local time. It has a spatial resolution of 320×40 km,

---

[9] See http://gome.aeronomie.be/

achieving global coverage in three days. Data output from GOME is accumulated at the German Processing and Archiving Facility, providing information on tropospheric O_3, NO_2, H_2O, BrO, SO_2, and HCHO, in addition to clouds and aerosol properties (Borrell et al. 2001). GOME-1 global measurements stopped in June 2003 and the operational follow-on (GOME-2) was launched aboard MetOp in 2006.

The large spatial footprint of GOME makes data validation with *in situ* measurements challenging. Aircraft measurements over the Mediterranean Sea, the southeast United States, and central Europe were employed to validate HCHO retrievals and tropospheric NO_2 columns, and the results showed consistency within uncertainty limits (Heland et al. 2002, Ladstatter-Weißenmayer et al. 2003, Martin et al. 2004). O_3 columns retrieved with GOME were within 5 Dobson Units of *in situ* profiles from ozonesondes (Hoogen et al. 1999, Liu et al. 2005) and the MOZAIC aircraft program (Liu et al. 2006).

3.2   Terra (**MOPITT, MODIS, MISR**)

The U.S. National Aeronautics and Space Administration (NASA) launched a Terra satellite carrying five instruments to study the Earth's atmosphere, surface, and oceans on December 18, 1999 and began collecting data on February 24, 2000 as part of the EOS program (Kaufman et al. 1998). Terra operates in a polar sun-synchronous orbit at 705 km above the earth's surface, crossing the equator at 10:30 AM local time in 16-day cycles. Three of the on-board instruments, Measurements of Pollution in the Troposphere[10] (MOPITT), Moderate Resolution Imaging Spectroradiometer[11] (MODIS), and Multi-Angle Imaging SpectroRadiometer[12] (MISR), measure atmospheric constituents.

MOPITT is a Canadian contribution to the Terra mission for measuring CO (Drummond and Mand 1996). It is a nadir correlation radiometer with a spatial resolution of 22×22 km and a scanning swath of about 650 km (29 pixels), covering the globe in about 4 days (Deeter et al. 2003). MOPITT is unique because it measures CO simultaneously in both the thermal infrared (TIR) band (4.7 µm) and the near-infrared (NIR) band (2.3 µm). NIR observations provide information about the total CO column, while TIR observations provide CO measurements in the middle and upper-troposphere. The multispectral instruments, therefore, demonstrates higher sensitivity to CO in the lower troposphere (Deeter et al. 2011, 2013, Worden et al. 2010). MOPITT validation indicates that measurements are within the target accuracy and precision over much of the globe (Deeter et al. 2013, Emmons et al. 2004, 2007). Data from MOPITT are presented as the total CO column and vertical profiles of CO mixing ratios. The data are available online at https://eosweb.larc.nasa.gov/project/mopitt/mopitt_table.

MODIS (Barnes et al. 1998) and MISR (Diner et al. 1998) instruments provide improved aerosol retrievals (Diner et al. 1998, Remer et al. 2005) with high spatial resolution. MODIS measures

---

[10] See http://en.wikipedia.org/wiki/MOPITT

[11] See http://modis.gsfc.nasa.gov/

[12] See http://www-misr.jpl.nasa.gov/

upwelling thermal radiation and solar reflectance in 36 wavelengths between 0.4 and 14.5 µm. Twenty-six bands are used to derive atmospheric properties such as cloud mask, aerosol properties, and cloud properties with 10×10 km spatial resolution. Two MODIS algorithms are used to retrieve aerosol properties over land (Kaufman et al. 1997) and water (Tanré et al. 1997), and they are described in detail elsewhere (Remer et al. 2005). Retrieving aerosol properties over a bright surface is challenging because of high reflectance in the red to NIR spectral region. Hsu et al. (2004) proposed a new approach, called "Deep Blue", to retrieve aerosol properties over bright land surfaces such as arid, semiarid, and urban areas where reflectivity is decreased in the blue-band region (i.e., wavelength 500 nm). Thus, the surface reflected contribution can be isolated from the satellite-receiving radiance.

The main aerosol parameter retrieved by MODIS is aerosol optical depth (AOD, a measure of the integrated aerosol load through the atmosphere) at various wavelengths and fine mode fraction (FMF, the ratio of small mode AOD (sub-micron) to the total AOD). The wavelength dependence is expressed by the Angstrom coefficient parameter. Validation studies using data from the ground-based Aerosol Robotic Network[13] (AERONET) (Levy et al. 2007, Mi et al. 2007) and from a hand-held sun-photometer (Li et al. 2007) indicate that the MODIS AOD determinations are within uncertainty limits. Daily MODIS atmospheric products are produced at a spatial resolution of 10 x 10 km and are available online from NASA's Atmosphere Archive and Distribution System at http://ladsweb.nascom.nasa.gov/data/search.html.

The MISR instrument has a unique combination of multiple viewing angles and wavelengths. It uses nine push-broom cameras to view the Earth: one at nadir and eight symmetrical views at 26.1, 45.6, 60.0, and 70.5 degrees forward and aft of nadir. MISR obtains images at four spectral bands (443, 558, 672, and 866 nm) with a horizontal resolution of 1.1 km in non-red bands and 275 m in the red band (Diner et al. 1998). The multi-view feature enables MISR to provide detailed aerosol properties including size, sphericity (Chen et al. 2008, Kalashnikova and Kahn 2006), and elevation of aerosol plumes (Diner et al. 1998, Kahn et al. 2007). Instruments with several viewing directions provide the ability to assess multiple paths through the atmospheric boundary layer, which is especially useful for aerosol retrieval.

MISR's retrieval algorithm differs over water, dense dark vegetation (DDV), and heterogeneous land (Martonchik et al. 1998, 2002), and it can retrieve aerosol information over bright surfaces (Martonchik et al. 2004). Validation of MISR AODs using AERONET data has been conducted multiple times (e.g., Abdou et al. 2005, Kahn et al. 2005). Cheng et al. (2012) completed a ten-year comparison study (2001 to 2011) and showed that 66.8% of MISR retrieved AODs fall within the error value. MISR data are available online at https://eosweb.larc.nasa.gov/PRODOCS/misr/level3/download_data.html

---

[13] See http://aeronet.gsfc.nasa.gov/

3.3   Aqua (MODIS, AIRS)

Aqua is NASA's second largest EOS satellite mission, after Terra, and was launched in May 2002 in a sun-synchronous orbit at an altitude of 705 km crossing the equator at 1:30 PM local time. It was the first of a group of NASA satellites termed the Afternoon Constellation, or the A-Train (Figure 5). The A-Train strives to combine information from several sources to deliver a more integrated view than would be possible from any single satellite (Parkinson 2003).
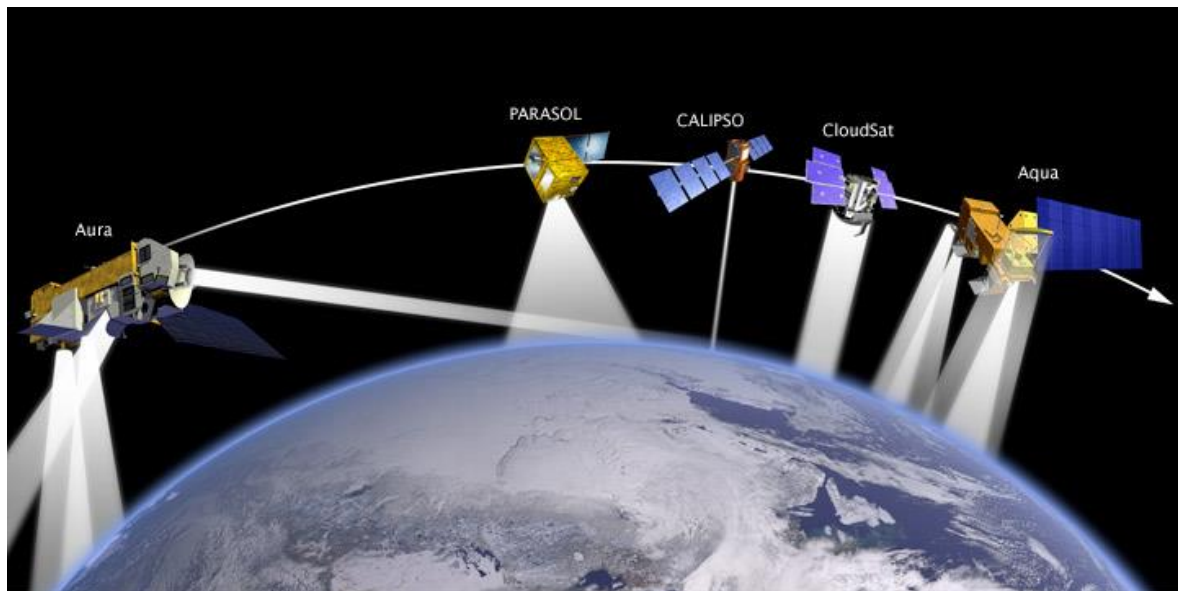
Figure 5.   The NASA international Afternoon Constellation, called A-train, includes Aqua, CALIPSO, CloudSat, PARASOL, and Aura.

Aqua carries six instruments for studying land, oceans, biosphere, and cryosphere. The satellite's two atmospheric sensors are Atmospheric Infrared Sounder[14] (AIRS) and MODIS. Aqua's MODIS instrument is the same as the Terra instrument discussed above. AIRS is a high-spectral-resolution instrument that has 2,378 spectral channels from 3.74 to 15.4 μm. Spatial resolutions are 13.5×2.3 km for infrared measurements and near-infrared measurements, respectively, in the nadir field of view. It provides atmospheric temperature and humidity profiles from the surface to an altitude of 40 km, while also measuring trace greenhouse gases (e.g., CO, O_3, and CH_4) and, to a lesser extent, CO_2 (Crevoisier et al. 2004, Parkinson 2003). CO measurements are conducted at 4.7 mm with a spatial resolution of 45 km at nadir (McMillan et al. 2005). Measurements from AIRS have also retrieved volcanic SO_2. Comparisons between CO measurements from AIRS and MOPITT showed a positive bias (15 to

---

[14] See http://airs.jpl.nasa.gov/

20 ppb$_v$) for AIRS relative to MOPITT over the ocean and consistency between AIRS and MOPITT (within 10 to 15 ppb$_v$) over land (Warner et al. 2007).

3.4   ENVISAT (SCIAMACHY)

The European earth observation environmental satellite[15] (ENVISAT) launched in February 2002 is in a polar, sun-synchronous orbit crossing the equator at 10:00 AM local time and carrying the SCIAMACHY instrument[16]. In contrast to NASA instruments, which analyze specified wavelengths, SCIAMACHY performs continuous measurements of transmitted, reflected, and scattered sunlight for the entire solar spectrum – from UV to short wave IR (240 to 2,380 nm) – at moderate resolution (0.2 to 1.5 nm). Additionally, SCIAMACHY functions in three observation geometries: nadir, limb, and occultation measurement modes (Bovensmann et al. 1999). These wide spectral radiance measurements assist in providing information about several atmospheric constituents, including NO_2 (Martin et al. 2006), O_3 (Ebojie et al. 2013, Tan et al. 2013), SO_2 (Fioletov et al. 2013, Lee et al. 2008), BrO, OClO, CO (Gloudemans et al. 2006), CO_2, CH_4, H_2O, and HCHO (Dufour et al. 2009, Wittrock et al. 2006) with a spatial resolution of 30×60 km and global coverage of 6 days. Trace gas concentrations are determined by subtracting limb measurements from the total columns determined with nadir measurements (Sierk et al. 2006).

Validations of SCIAMACHY CO, CH_4, CO_2 and N_2O columns were conducted using Fourier transform infrared spectroscopy (FTIR) (Dils et al. 2006), aircraft remote sensing measurements (Heue et al. 2005) and aircraft *in situ* measurements (Martin et al. 2006). Although SCIAMACHY was designed for the retrieval of trace gas concentrations, its data have also been used for retrieving aerosol properties (Penning de Vries et al. 2009, Sanghavi et al. 2012). All data are available online at http://www.iup.uni-bremen.de/sciamachy/dataproducts/index.html.

3.5   Aura (OMI, TES)

Aura is a NASA EOS satellite launched in July 2004 into a sun-synchronous, near polar orbit at 705 km above the Earth, crossing the equator at approximately 1:45 PM local time. Aura is part of the A-Train satellite constellation, flying behind the Aqua platform. It studies stratospheric and tropospheric composition with its four instruments: Microwave Limb Sounder[17] (MLS), Tropospheric Emission Spectrometer[18] (TES), OMI and the High Resolution Dynamics Limb Sounder[19] (HIRDLS) (Schoeberl et al. 2006).

OMI is the successor to TOMS, continuing to record total ozone and other parameters related to ozone chemistry and climate. OMI observes solar backscatter radiation in the visible and UV

---

[15] See http://en.wikipedia.org/wiki/Envisat

[16] See http://www.sciamachy.org/

[17] See http://mls.jpl.nasa.gov/

[18] See http://www.nasa.gov/centers/jpl/missions/tes.html

[19] See http://aura.gsfc.nasa.gov/scinst/hirdls.html

regions with ground resolution of 13×24 km, in nadir view. OMI uses a wide swath (2,600 km), enabling it to achieve global coverage in one day. It measures $O_{3 \text{ and }} NO_2$ (Bucsela et al. 2006), SO_2 and BrO (Koo et al. 2012, Suleiman et al. 2013), and aerosols (Levelt et al. 2006). Retrieved aerosol properties include AOD and absorbing aerosol optical depth (AAOD), single-scattering albedo, layer height, and aerosol index (Veihelmann et al. 2007). Absorbing aerosols located over bright surfaces and cloudy areas can be detected using the absorbing aerosol index (AAI). Moreover, measurements in the UV region provide complementary information on aerosol type, which instruments such as MODIS and MISR that do not include UV analyses cannot provide. Therefore, different aerosol types can be identified, including smoke, dust, and sulfates, using OMI UV measurements (Torres et al. 2007). Validation studies were conducted using ground-based remote sensing, aircraft, and ground-based *in situ* measurements (Boxe et al. 2010, Fu et al. 2013, Lamsal et al. 2010, Wong et al. 2013). OMI data are available online at http://mirador.gsfc.nasa.gov/cgi-bin/mirador/collectionlist.pl?keyword=omno2.

TES is a Fourier transform spectrometer (FTS) that provides observations in both limb and nadir viewing modes. It is capable of measuring vertical profiles of ozone, CO, and H_2O with ground resolution of 5×8 km, in nadir view, obtaining global coverage every 16 days. Ozone retrievals are sensitive to both the lower and upper troposphere, with vertical resolution of about 6 km when clouds are absent (Bowman et al. 2006). Validations of ozone retrievals were performed using ozonesonde measurements (Boxe et al. 2010, Worden et al. 2007) and data provided by different satellites (e.g., Osterman et al. 2008). These studies show that TES tropospheric O_3 measurements have a positive bias of 3 to 10 ppb_v.

TES measures CO at 4.7 μm, similar to MOPITT and AIRS, however, it uses *a priori* profiles that vary by region and season (Rinsland et al. 2006). Validation of TES CO measurements using aircraft data shows a slightly negative (<10%) bias in mid-latitudes and a slightly positive bias (<10%) in the tropics (Lopez et al. 2008, Luo et al. 2007). Tropospheric methanol observations from TES are evaluated using a combination of aircraft observations and chemical transport model over North America. Retrievals agreed well with aircraft observations when DOFS is >0.5 (Wells et al. 2012). TES data are available online at https://eosweb.larc.nasa.gov/project/tes/tes_table.

3.6   PARASOL (POLDER)

The PARASOL satellite[20] launched in December 2004 carrying the POLDER instrument[21] as part of the A-train constellation on a sun-synchronous orbit crossing the equator at 1:30 PM local time at an altitude of 705 km. POLDER measures spectral, directional, and polarized light reflected by the earth-atmosphere system at 0.490 μm, 0.670 μm, and 0.865 μm. Measuring polarized light in different directions allows for improved characterization of aerosols and clouds compared to traditional methods that depend on spectral signature only (Tanré et al. 2011). The

---

[20] See http://smsc.cnes.fr/PARASOL/GP_satellite.htm

[21] See http://smsc.cnes.fr/POLDER/GP_instrument.htm

ground resolution is 5.3×6.2 km at nadir, with global coverage achieved within two days. It can discriminate large spherical marine aerosols from non-spherical desert aerosols (Herman et al. 2005, 2011). The POLDER algorithm over land only retrieves the optical depth of fine particles ($d_p < 2.5$ μm) (Maignan et al. 2009). An evaluation of POLDER aerosol measurements against sun-photometer measurements was performed by Bréon et al. (2011). They showed that POLDER and MODIS retrievals are of similar quality over the oceans, while over land POLDER provided a better fine mode estimate than MODIS.

3.7 CALIPSO (CALIOP)

The CALIOP LiDAR[22], also part of the A-Train, launched in April 2006 onboard the Cloud Aerosol LiDAR and Infrared Pathfinder Satellite Observations[23] (CALIPSO) satellite with equator-crossing times of about 1:30 PM and 1:30 AM, and a 16-day cycle. CALIOP is an active instrument, setting it apart from the previously discussed instruments. Processing LiDAR data makes it possible to retrieve vertical distributions of aerosols and clouds, which is not possible for passive sensors. However, measurements are limited to the satellite sub-track – CALIOP does not have cross-track imaging capabilities (the swath width is very narrow). Thus, validation is challenging because it is difficult to find active measurements sites that coincide with validation sites (Winker et al. 2009, 2010). The sampling resolution of CALIOP is 30 m vertical and 335 m horizontal, producing simultaneous backscatter intensities at 1,064 and 532 nm during the day and night. CALIOP algorithms were developed to classify aerosol layers and evaluate AODs as low as 0.01 (Liu et al. 2011, Omar et al. 2009).

3.8 MetOP (GOME-2, IASI)

The MetOp mission was initiated by ESA and the European Organization for the Exploitation of Meteorological Satellites (EUMETSAT). MetOp-A was launched on October 19, 2006 as the first of three successive MetOp satellites. For air quality measurements, MetOp-A carried GOME-2 (Callies et al. 2000), an update to the original ERS-2 instrument, and the Infrared Atmospheric Sounding Interferometer[24] (IASI) (Clerbaux et al. 2009). GOME-2 is a nadir-scanning, double spectrometer that covers wavelengths from 240 to 790 nm. It observes the same species as GOME-1 at a typical resolution of 40×80 km with global coverage in 1.5 days (Nowlan et al. 2011).

IASI measures key species relevant to climate forcing and atmospheric chemistry, including CO (Turquety et al. 2004), O_3 (Boynard et al. 2009), CH_4 (Razavi et al. 2009), HNO_3 (Wespes et al. 2012), NH_3 (Clarisse et al. 2009, 2010), and CH_3OH (Razavi et al. 2011). In addition, IASI has excellent horizontal coverage that results from its wide swath (2,200 km), allowing for global coverage every 12 h with a 12 km footprint diameter.

---

[22] See http://www.ti.com/solution/satellite_payload_lidar

[23] See http://www-calipso.larc.nasa.gov/

[24] See http://www.eumetsat.int/website/home/Satellites/CurrentSatellites/Metop/MetopDesign/IASI/index.html

CO measurements are most sensitive in the middle troposphere, where limited vertical profile information is available. George et al. (2009) compared total CO column distributions from IASI to columns measured with other space-based remote sensors. The authors showed 10% to 17% discrepancies between IASI and three sounders in the Northern Hemisphere and the equatorial region. Comparisons of tropospheric O_3 measurements from ground-based FTIR, the MOZART-4 model, and IASI were performed at Eureka (Canada) and Thule (Greenland). These comparisons showed that IASI measurements capture temporal variations and spatial structure of tropospheric O_3 in the Northern Hemisphere, although the satellite observations showed lower sensitivity in the lower troposphere (Wespes et al. 2012).

Although there is strong absorption by water vapor in the same spectral region, weakly absorbing molecules, such as SO_2 released during volcanic eruptions were analyzed using the IASI instrument. However, detection of SO_2 is most sensitive at high altitudes and for strong sources (high concentrations) (Clarisse et al. 2008). Recent studies report the possibility of also detecting CH_3OH, $HCOOH$, PAN, C_2H_4, C_3H_6, and C_4H_4O with IASI if their concentrations are above ambient levels (Clarisse et al. 2011, Clerbaux et al. 2009, Razavi et al. 2011, Stavrakou et al. 2011).

4   APPLICATIONS

Tropospheric air pollution can be measured at progressively higher spatial and temporal resolutions using the new generation of satellite measurements. Numerous applications for satellite data have emerged, and most primary air pollutants can now be detected by one or more instruments and the corresponding data are openly accessible. In this section, applications that take advantage of the readily available air quality data are described. Some applications use satellite data as stand-alone products, while others combine satellite and surface measurements with air quality models. Four main applications of tropospheric satellite data will be discussed in this section; analyses of events that affect air quality, modeling evaluation, hemispheric transport of air pollution and emission estimates.

4.1   Analyses of Events That Affect Air Quality

Satellite data complement ground-based measurements by adding synoptic and geospatial context. Such context is applied for qualitative and quantitative analyses of events that affect air quality.

Gautam et al. (2013) employed satellite data from MODIS and CALIOP to better understand regional aerosol characteristics during Indochina's pre-monsoon season, quantifying aerosol optical properties and vertical distribution. Specifically, the researchers showed a strong correlation between AOD and biomass burning from 2001 to 2010. Multi-year (2007 to 2011) analysis of aerosol extinction profiles from CALIOP show high aerosol loading that starts in the lower troposphere and extends to higher altitudes (4 km) (Figure 6b). Analysis of the CALIOP-derived depolarization ratio product and ground-based sun-photometer AERONET data indicates that smoke pollution is dominated by fine particulate matter (Figure 6c) (Gautam et al. 2013).
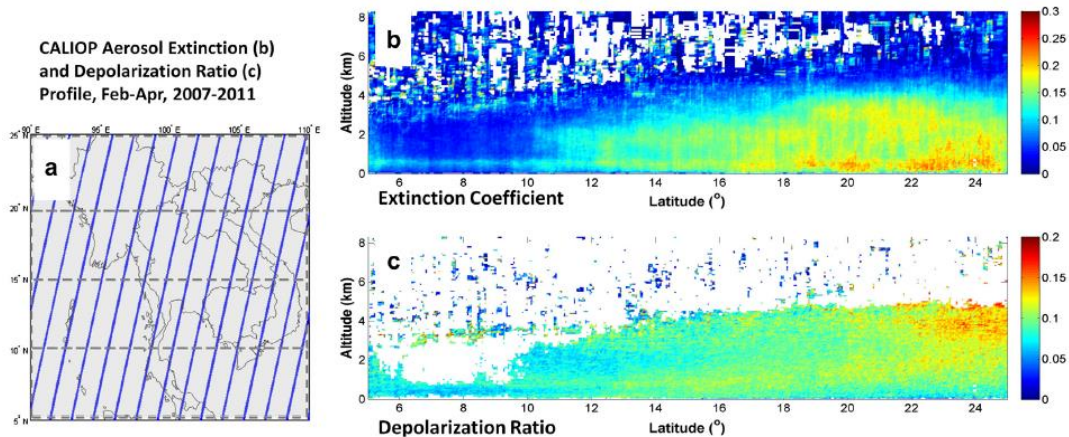
Figure 6.   CALIOP aerosol extinction and depolarization ratio profile measurements averaged
              over the Indochina peninsula domain.
              (a) each blue line represents about 40 overlapping CALIOP tracks (with 608 total
              tracks available) for the February to April, 2007 period, (b) latitudinal mean aerosol
              extinction profile (km), and (c) depolarization ratio, from 5° N to 25° N (Gautam et
              al. 2013).

Spatio-temporal variability of a dust episode over Northern China was analyzed using AOD
retrieved from MODIS, OMI, MISR, and CALIPSO. Although there are differences in
characterizations among instruments, all techniques identified the same locations of aerosol
layers in the region of interest (Figure 7). CALIOP LiDAR results showed that dust layers are
located near the surface, threatening human health (Figure 8). Passive sensors (e.g., MODIS)
provide AOD columns, while active sensors (e.g., CALIOP LiDAR) capture the vertical location
of aerosol layers and identify aerosol types. Combining active and passive sensors, therefore,
adds valuable information to air quality assessments and models (Schrader et al. 2013).

Additionally, Zhao et al. (2013) combined MODIS AOD and daily air pollution index (API) data
to assess air quality variability in East China (Shanghai) during the past decade. This study
concluded that environmental initiatives for reducing air pollution are effective, improving air
quality over Shanghai in the range of 1.9% to 22%.
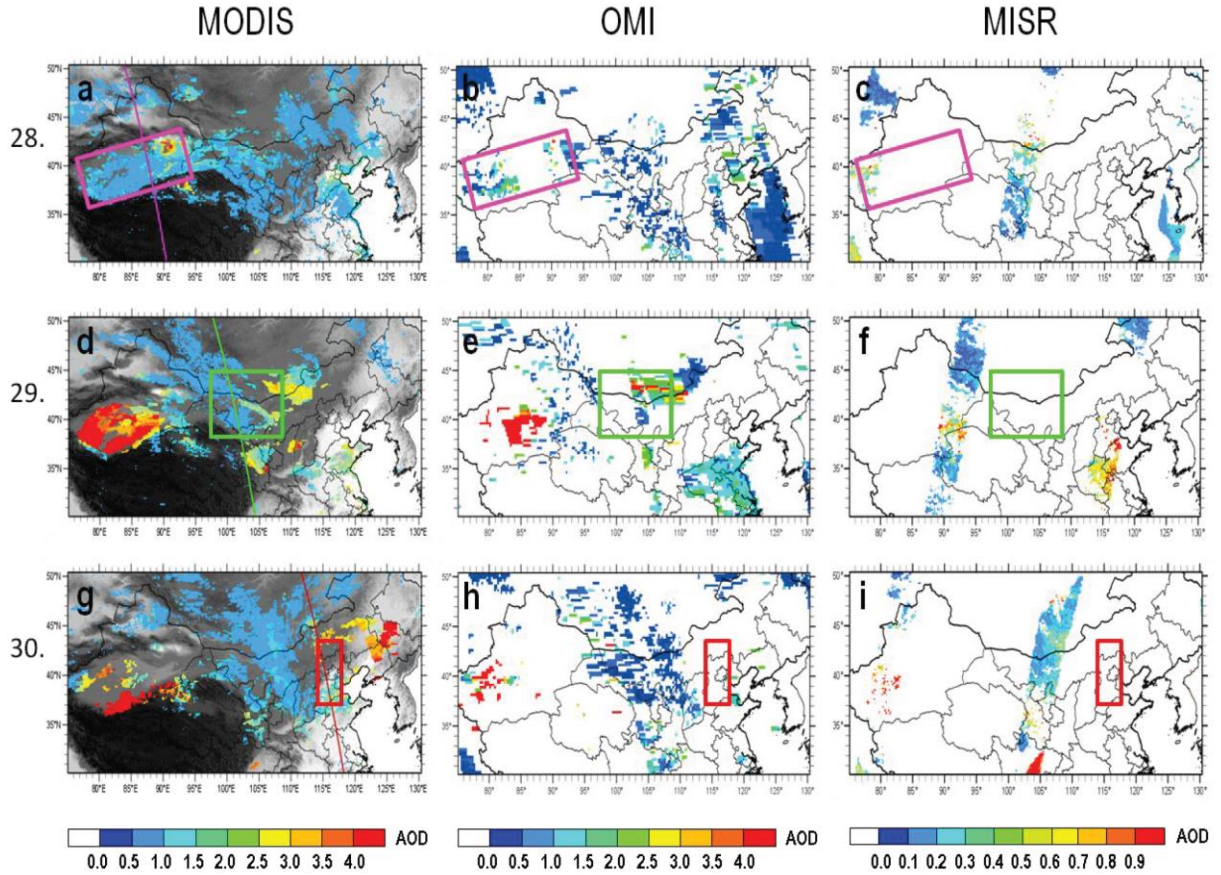
Figure 7.   Multi-satellite AOD data for April 28, 29 and 30, 2011.
The first column shows MODIS Deep Blue AOD for April 28 (a), April 29 (d), and April 30 (g) and topography (in grey colour).
The second column shows OMI AOD for 500 nm for April 28 (b), April 29 (e), and April 30(h).
The third column shows MISR AOD for 555 nm for April 28 (c), April 29 (f), and April 30 (i).
The coloured lines in images (a), (d) and (g) represent the corresponding CALIPSO path for each day.
The coloured boxes show the specific areas of interest for each day: the pink colour box in the Taklamakan Desert on April 28, the green colour box in the Central Chinese desert areas on April 29, and the red colour box in the Beijing area on April 30 (Schrader et al. 2013).
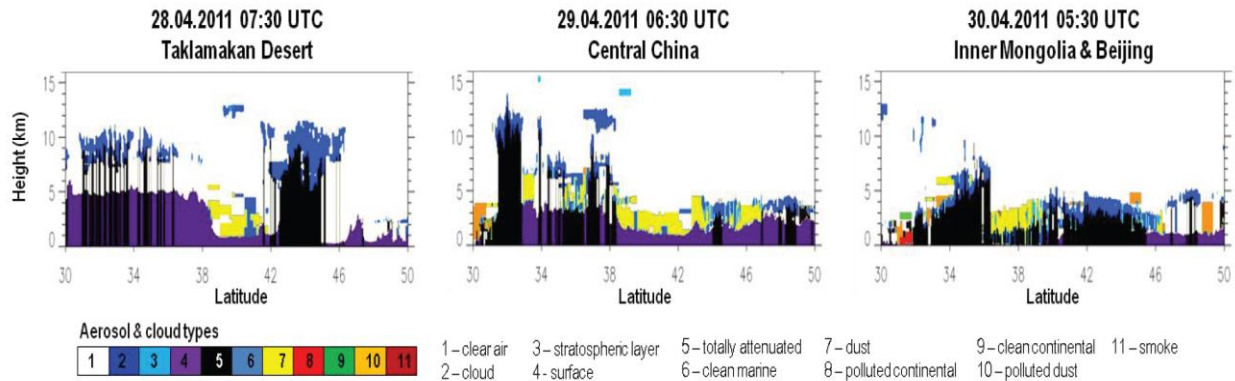
Figure 8.   The CALIPSO feature mask for the three paths over the Taklamakan Desert on April 28, Central China on April 29, and Beijing on April 30 (Schrader et al. 2013).

Nitrogen oxides (NO_x) are precursors to tropospheric ozone and aerosols, cause acidification, and negatively impact human health. NOx emission factors vary according to fuel type and combustion conditions, so emissions can be difficult to predict. Accordingly, satellite measurements are employed to aid in estimating NO_x emissions given the relationship between NO_x emissions and NO_2. The correlation between regional NO_x pollution and Indian thermal power plants was investigated using NO_2 column data derived from four satellites (GOME-1, SCIAMACHY, GOME-2, and OMI) from 1996 to 2010. The results showed that emissions from coal fired power plants should be more stringently regulated because their NOx emissions are about 96% of total power sector NOx emissions (Lu and Streets 2012).

Dupont et al. (2012) used TES and the Real-time Air Quality Modeling System[25] (RAQM) to investigate attribution and dynamic evolution of ozone and CO in Asian wildfire plumes during spring 2008. In addition to photochemical production due to ozone precursors, they found that O_3 concentrations in biomass burning plumes are significantly influenced by exchange between the stratosphere and the troposphere after the smoke plumes is lofted to high altitudes (Figure 9).

Tropospheric BrO vertical columns derived from two satellite measurements (OMI and GOME-2) were combined with surface, aircraft, and ozonesonde measurements to investigate Arctic ozone depletion (Koo et al. 2012). A negative correlation between tropospheric BrO and the O_3 column was attributed to convective transport of free-tropospheric BrO through the unstable boundary layer (Koo et al. 2012).

---

[25] See http://raqms-ops.ssec.wisc.edu/
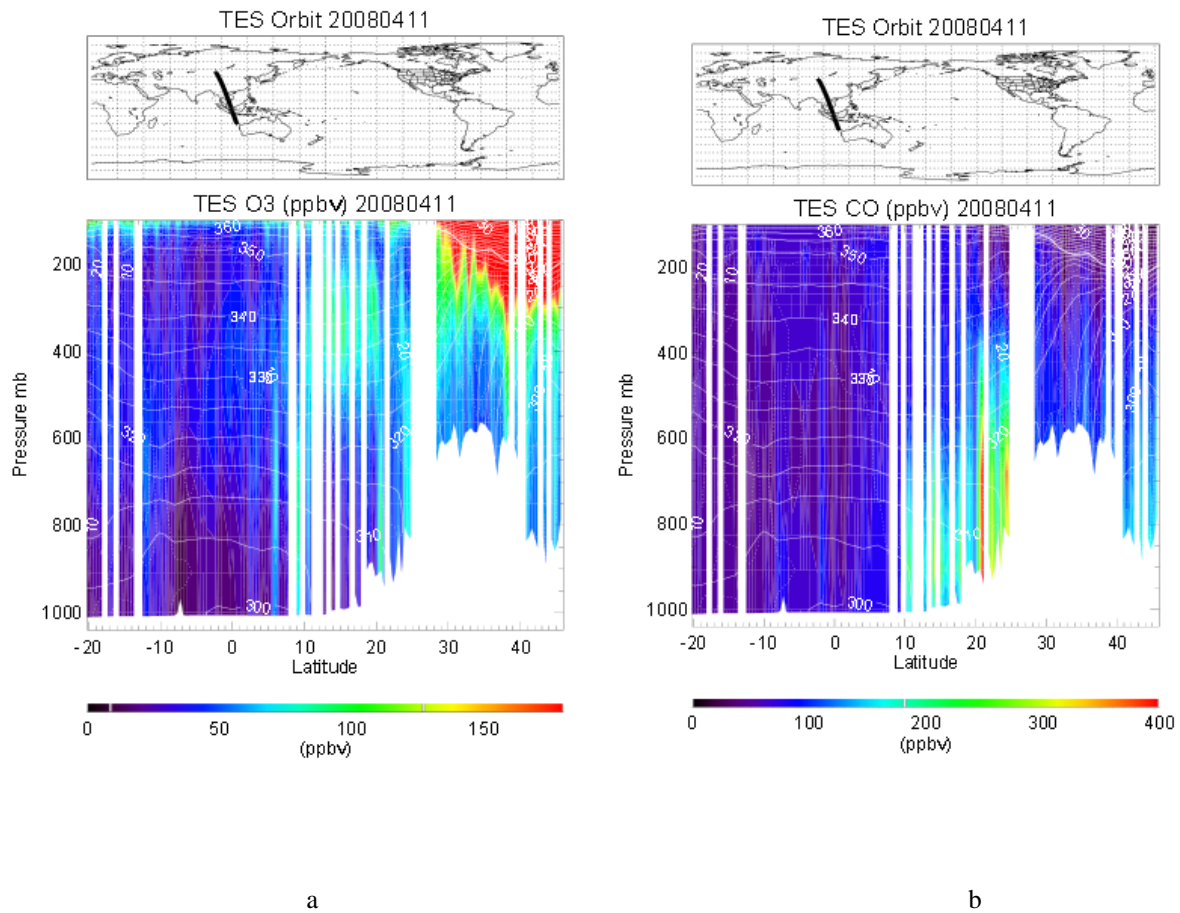
Figure 9. TES ozone and CO profiles.
(a) Observed TES ozone over Thailand and south of the Himalayas, and (b) observed TES CO (Dupont et al. 2012).

Wespes et al. (2012) identified O_3 plumes transported to the Arctic from fires or anthropogenic emissions using the IASI satellite (Figure 10). Combining global models with remote sensing instruments improved detection and allowed for quantification of long-range pollution transport.
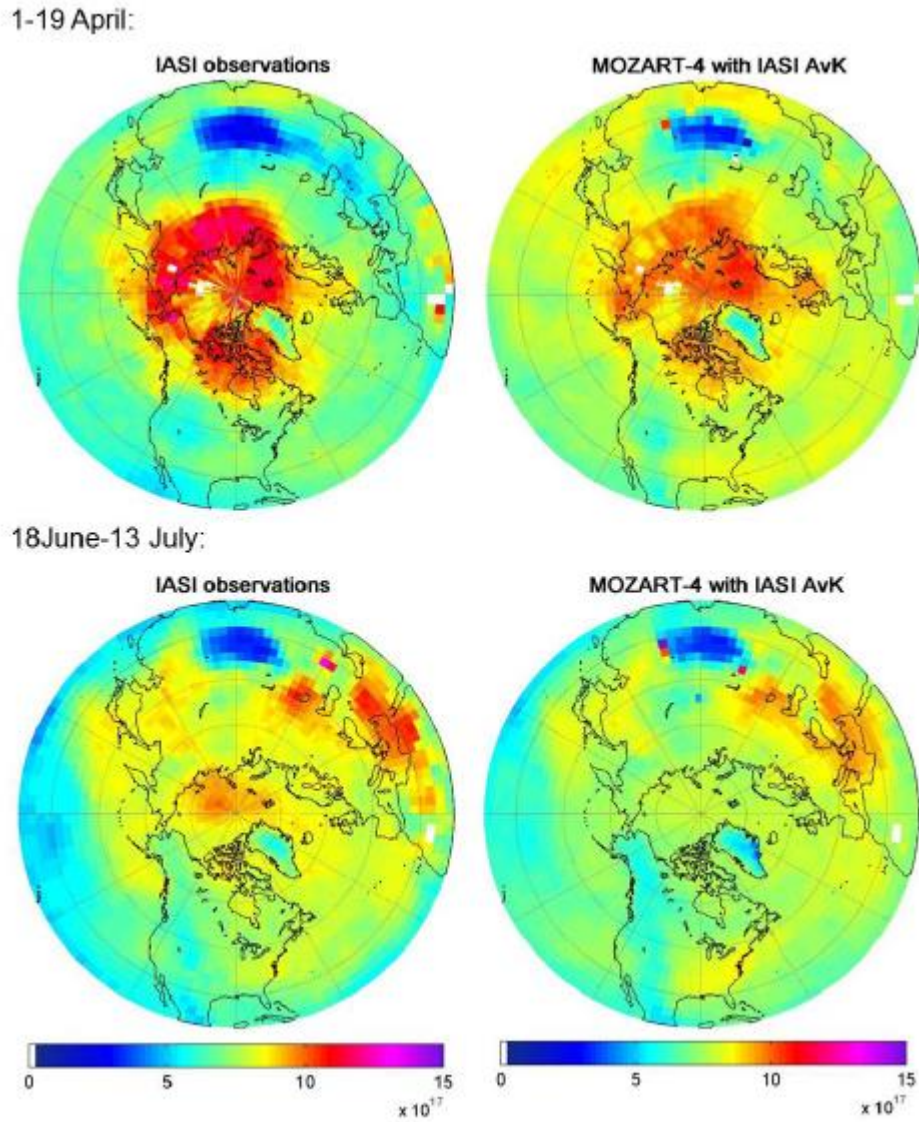
Figure 10. Mean O_3 columns ($\times 10^{17}$ molecules cm^{-2}) from ground to 300 hPa during spring (from April 1 to 19, 2008) and summer (from June 18 to July 13, 2008) campaigns. Observed by the IASI satellite and simulated by MOZART-4, smoothed according to the averaging kernels of the IASI observations (Wespes et al. 2012).

4.2   Model Evaluations

Satellite observations are used to evaluate model simulations, which in many cases are the best way to bound model estimates. Voulgarakis et al. (2011) extracted tropospheric O_3 and CO concentrations from TES data to evaluate chemistry-climate models (G-PUCCINI and UKCA) and explore photochemical characteristics and seasonal variability (Figure 11). Results revealed that correlation between O_3 and CO varies by area and season. For example, there is a positive

correlation in the tropical biomass burning regions for both seasons and a negative correlation in the Sahara Desert and Middle East.
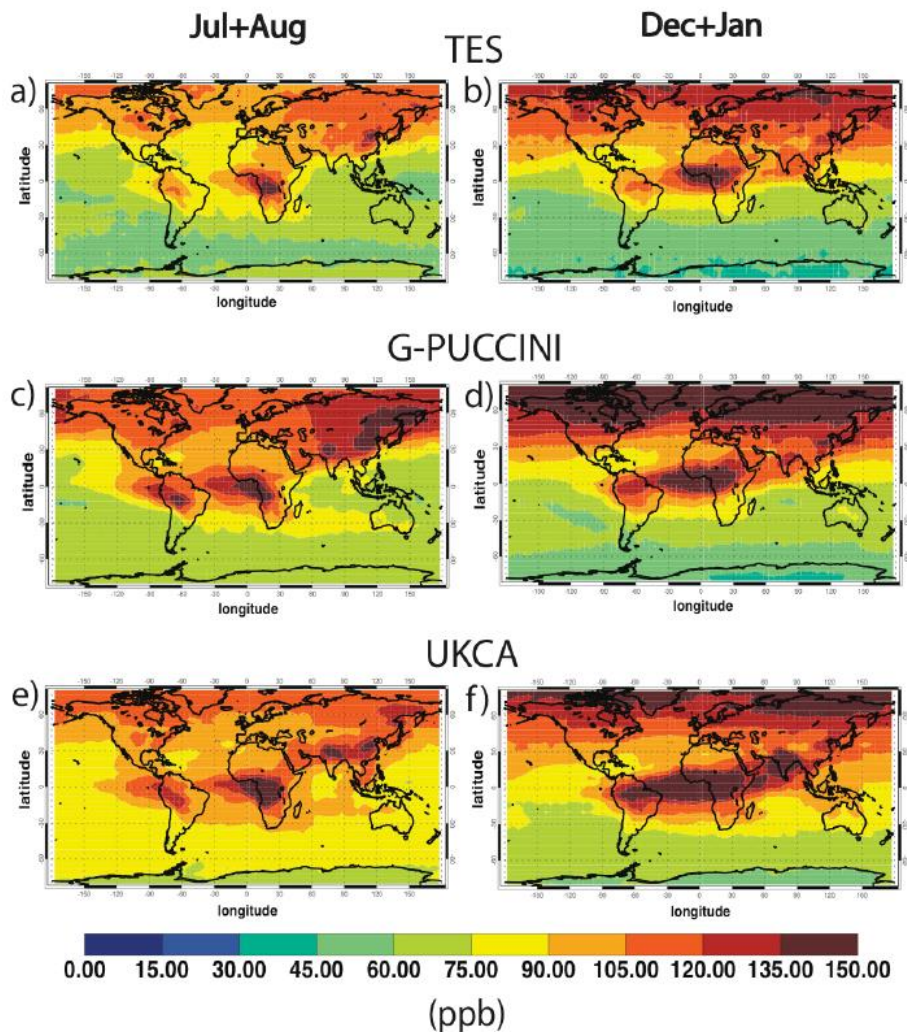
Figure 11. Mean 2005 to 2008 middle/lower free tropospheric CO concentrations.
TES (a, b), G-PUCCINI (c, d), and UKCA (e, f) in July and August (left panels) and December and January (right panels).
Data from 7 TES pressure levels between 800 and 400 hPa were used (Voulgarakis et al. 2011).

Miyazaki et al. (2012) used observations from multiple satellites to develop advanced chemical data assimilation. OMI, TES, MOPITT, and MLS were used simultaneously to simulate NO_2, O_3, CO, and HNO_3 data for a global chemical transport model, CHASER. The study indicated that satellite data can provide a powerful global constraint for understanding modeled tropospheric chemical processes.

4.3   Hemispheric Transport of Air Pollution

Growth in satellite observations over the past decades has advanced understanding of the magnitude and impact of hemispheric transport of air pollution. The broad spatial and temporal coverage of satellite observations allows for tracking the evolution of an aerosol episode, including dust storms, wildfire smoke, and volcanic eruption plumes (Ansmann et al. 2009, Ben-Ami et al. 2010). Providing satellite images of major aerosol events assists in the characterization of transport plumes. For example, Asian outflow and trans-Pacific transport of CO and O_3 have been tracked using satellites, aircraft, and models (Heald et al. 2003). A high CO episode was detected over China with MOPITT and shown to arise from long range transport of the pollutant generated from biomass and/or biofuel burning located in the border areas of Pakistan and India (Zhao et al. 2007). AIRS CO data have also been used to observe long-range transport of the pollutant (Stohl et al. 2007, Zhang et al. 2008).

Hsu et al. (2006) used TOMS AAI to track Asian dust plume transport across the Pacific Ocean by merging images from successive days (Figure 12). Hsu et al. (2012) also investigated trans-Pacific transport in autumn with A-train satellites. SO_2 plumes over East Asia were first detected with OMI and tracked to North America in 5 to 6 days. The AIRS instrument showed similar patterns for CO, suggesting that these plumes were most likely derived from anthropogenic sources. This study highlighted the importance of trans-Pacific transport in autumn where the long-range transport of Asian sulfur species happens frequently and could exert strong impacts on large downstream areas.
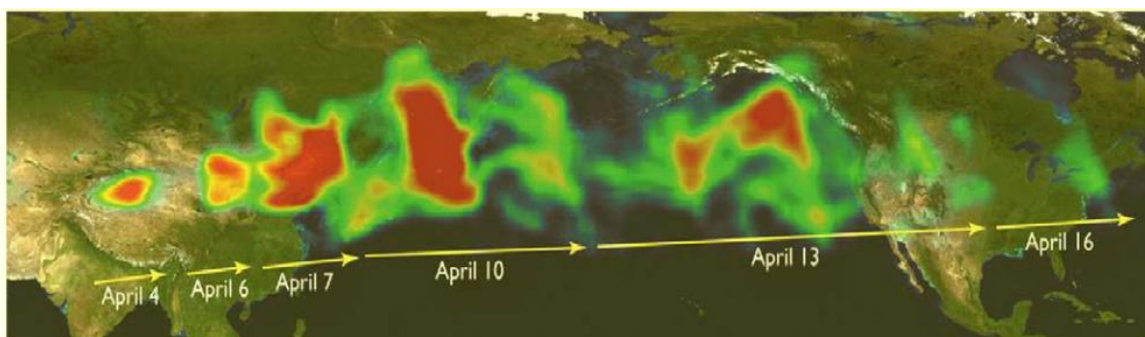
Figure 12.   Time series of TOMS AAI composite in April 2001.
            The track shows long-range transport of Asian dust across the Pacific Ocean,
            reaching as far as the east coast of the US (Hsu et al. 2006).

Quantifying aerosol transport, as well as particle properties, can be accomplished by measuring AOD from numerous satellite sensors. Combining successive CALIOP curtains simultaneously with other satellite sensors or models has been used to analyze dust transport across the Pacific Ocean (Uno et al. 2011, Yu et al. 2008). Yu et al. (2012) studied the long range transcontinental transport of aerosols using MODIS and CALIOP measurements. They found that the mass of

aerosols arriving at North American shores from overseas is comparable to the total mass of particulates emitted domestically.

Kalashnikova and Kahn (2008) analyzed MISR and MODIS aerosol products to identify AOD, particle size, and particle shape during trans-Atlantic dust transport. They reported various size and shape characteristics as the plumes traveled from the coast of North Africa to the Caribbean Sea. Transport height was provided by vertical profiles determined with CALIPSO (LiDAR), and particle shapes were identified using depolarization ratios. The LiDAR depolarization method (Winker and Osborn 1992) assumes that irregularly shaped particles (e.g., dust particles) induce a depolarization signal while spherical particles (e.g., smoke, sea salt) do not (Tesche et al. 2009).

Liu et al. (2008) analyzed transport of dust from the Sahara desert that originated on August 17, 2006 for a period of 10 days. They utilized CALIPSO colour and depolarization ratio products and found that dust plumes mixed with other aerosols (e.g., smoke) over the Gulf of Mexico after they were transported to the Caribbean region. Moreover, CALIOP measurements of LiDAR backscatter, colour, and depolarization ratios have isolated the influence of clouds on trans-Atlantic dust properties. Results revealed the complexity of dust mixing with other water-soluble aerosols (Yang et al. 2012).

Uno et al. (2009) made use of successive CALIPSO LiDAR profiles and aircraft data to track trans-Pacific dust transport of aerosol to the Arctic during the spring 2008. The CALIOP April 2008 global distribution of the aerosol backscatter revealed two regions with large backscatter below 2 km: the Northern Atlantic between Greenland and Norway, and Northern Siberia. The aerosol colour ratio indicated a growth of the aerosol size once transported to the Arctic. The distribution of the aerosol optical properties in the mid troposphere agreed with the known main transport pathways between mid-latitudes and the Arctic (Figure 13) (Ancellet et al. 2014).

Combining model and satellite data is useful for characterizing transport events. CALIOP, OMI, and MODIS measurements together with the chemical transport model and Lagrangian back-trajectories were used to monitor transport of East Asian aerosols to the Arctic (Di Pierro et al. 2011) and Patagonian dust to Antarctica (Li et al. 2010). Detection in Polar Regions is challenging because aerosol concentrations are low compared to the LiDAR's detection limit.
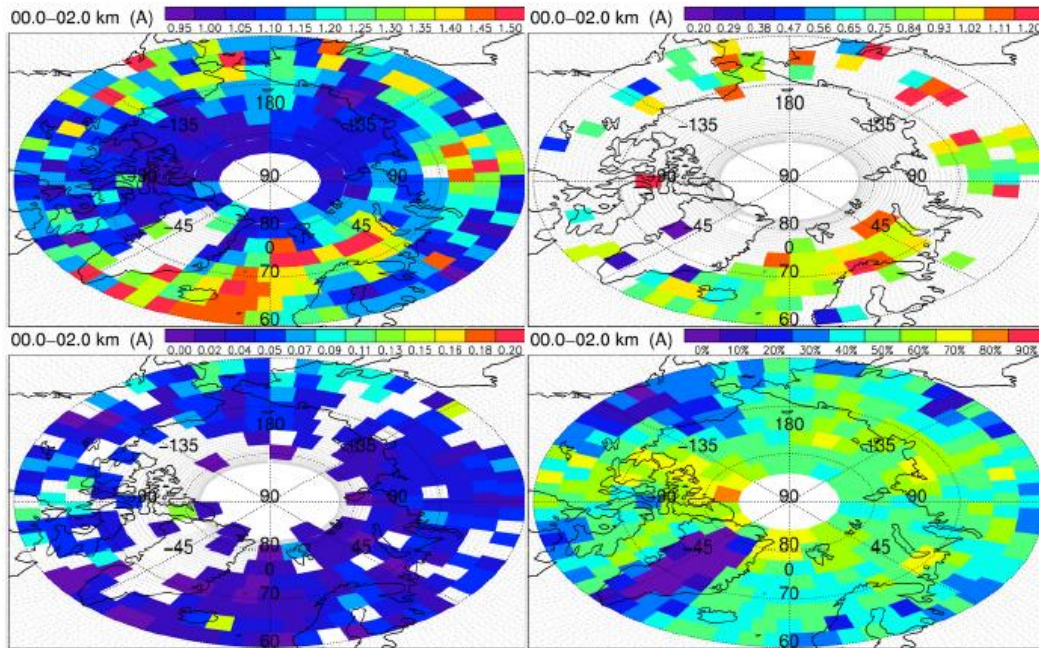
Figure 13. Map of the 532 nm backscatter ratio, aerosol colour ratio, pseudo depolarization ratio and fraction of cloudless observations using the April 2008 filtered level 1 CALIOP data in the 0 to 2 km altitude range (Ancellet et al. 2014).

Hemispheric transport of smoke plumes from volcanic eruptions and forest fires have been characterized by numerous satellite measurements. Satellites including MODIS, TOMS, and GOME were employed to investigate hemispheric transport of air pollutants associated with forest fires in southeast Russia in May 2003. Results illustrate that the fires produced NO_2, CO, and other combustion products that can be transported in two directions: Smoke travelling northwestwards towards Scandinavia was lifted over the Urals and arrived over the Norwegian Sea. Smoke travelling eastwards to the Okhotsk Sea was also lifted, then crossed the Bering Sea to Alaska from where it proceeded to Canada and was later even observed over Scandinavia and Eastern Europe on its way back to Russia. Additionally, transport routes simulated by a Lagrangian particle dispersion model were validated using the satellite images (Damoah et al. 2004).

Similarly, Dirksen et al. (2009) used OMI and CALIOP measurements to track a smoke plume released during intense forest fires in Australia. The study showed the front of the plume traversing the globe in 12 days.

Winker et al. (2012) used CALIOP data to characterize the plumes of volcanic eruption transported from the Icelandic volcano Eyjafjallajökull in April 2010 during both day and night. Their results suggest that layers reporting strong LiDAR depolarization are dominated by ash compared to sulfate, so polarized LiDAR backscatter signals can be used to discriminate between

volcanic ash and the sulfate aerosol resulting from volcanic SO_2 emissions. Walker et al. (2012) developed a scheme to exploit IASI retrievals to track SO_2 in the presence of clouds and volcanic ash. Additionally, GOME-2 has successfully measured BrO columns and SO_2 plume heights associated with volcanic eruptions (Rix et al. 2012). CO emissions from a volcano have similarly been observed using MOPITT data (Martínez-Alonso et al. 2012).

Loyola et al. (2008) used GOME, SCIAMACHY, and GOME-2 instruments along with a trajectory model to identify plume heights from volcanic eruptions in Central and South America. As a result, they suggested developing a near-real-time SO_2 data delivery service to warn of aviation hazards arising from volcanic ash clouds.

4.4   Estimates of Surface Emissions

4.4.1   *Inverse Modeling Techniques*

Surface emissions can be assessed following a bottom-up or top-down approach. The bottom-up method uses detailed emissions inventories (EI) at a model resolution. EIs are developed based on several factors, including fuel consumption from all sectors and corresponding measurements of emission rates for different species (Streets et al. 2003), economic growth, land-use, and fire-burned areas (van der Werf et al. 2006). The top-down method estimates surface emissions by inverse modeling of atmospheric observations, as reviewed by Rodgers (2000) and Jacob (2006). Top-down information is being used to evaluate and improve bottom-up EIs because they often have large uncertainties (Streets et al. 2003) and a number of limitations. First, EIs are often not up-to-date, because it is difficult (and expensive) to characterize all types of sources. Second, the temporal resolution of EIs is typically on monthly or annual scales, which is not adequate for assessing daily or diurnal emission variability. Third, there is a lack of spatial coverage for estimating emissions due to limited data availability as EIs for several important sources (e.g., wildfires, volcanic eruptions, and agricultural activities) are not available. All of these reasons make regional modeling with a uniformly fine resolution challenging (Wang et al. 2006, Xu et al. 2013).

Inverse modeling develops emissions constraints by combining observations of atmospheric composition with knowledge of atmospheric processes (e.g., transport, chemistry). Satellites identify sources and then estimate emissions using inverse modeling techniques, making them a major source of observations (Sandu and Chai 2011, Streets et al. 2013). A chemical transport model (CTM), known as the forward model (for the inversion y = F(x), x is a set of emissions to be estimated and y is a set observed atmospheric concentrations (e.g., satellite data)), solves the continuity equation to predict concentrations as a function of emissions. An inverse model then optimizes emission estimates by fitting the CTM to observed concentrations, subject to error weighting and *a priori* information (i.e., initial and/or background concentrations) on emissions. There is an optimal concentration value that minimizes an error-weighted least squares (χ^2) scalar cost function, derived from Bayes' theorem with the assumption of Gaussian errors (Rodgers 2000). Different top-down techniques have been developed to estimate emissions from satellite observations (e.g., Heald et al. 2004, Lamsal et al. 2011, Lee et al. 2011a, Wang et al. 2012).

Several studies have analyzed trace gas sources using top-down methods, including:

- using MOPITT to identify CO sources over Asia (Heald et al. 2004, Kopacz et al. 2009) and across the globe (Kopacz et al. 2010, Stavrakou and Müller 2006)

- using TES to identify CO_2 surface flux (Nassar et al. 2011)

- using multiple satellites to identify NO_x emissions (Lamsal et al. 2011, Lin et al. 2010, Martin et al. 2003), and

- using SCIAMACHY and OMI to identify SO_2 sources (Lee et al. 2011a).

NH_3 can be quantified using remote-sensing to overcome a lack of surface measurements. TES is capable of resolving spatial and temporal gradients in surface NH_3 concentrations (Pinder et al. 2011). Heald et al. (2012) used IASI measurements to investigate NH_3 concentrations over the U.S., finding underestimation of emissions in California and the Midwest. Zhu et al. (2013) showed that TES observations of NH_3 can be used to constrain monthly average emissions. Overall, remote-sensing constraints indicate that NH_3 emissions are underestimated in many parts of the U.S., especially in the West.

Satellite observations also provide a unique resource for constraining CH_4 emissions through inverse modeling using satellite measurements of solar backscatter and TIR instruments (Frankenberg et al. 2005, Xiong et al. 2009, 2010). Additionally, IASI estimates of global methanol emissions were used to represent global methanol emission sources (Stavrakou et al. 2011).

Near-real time data from satellites can be used to update bottom-up emission trends. Lamsal et al. (2011) showed that satellite observations of NO_2 provide current information about changes in anthropogenic NO_x emissions. Using this approach, they highlighted NOx reductions over the U.S., Japan, and parts of Europe, and increases over Eastern China (Figure 14).

The growth in NO_x emissions from Indian power plants was investigated by Lu and Streets (2012) by combining results from four satellites: GOME, SCIAMACHY, OMI, and GOME-2. Shipping emissions of NO_2 were analyzed using SCIAMACHY and GOME-2, providing monthly estimates (Franke et al. 2009).
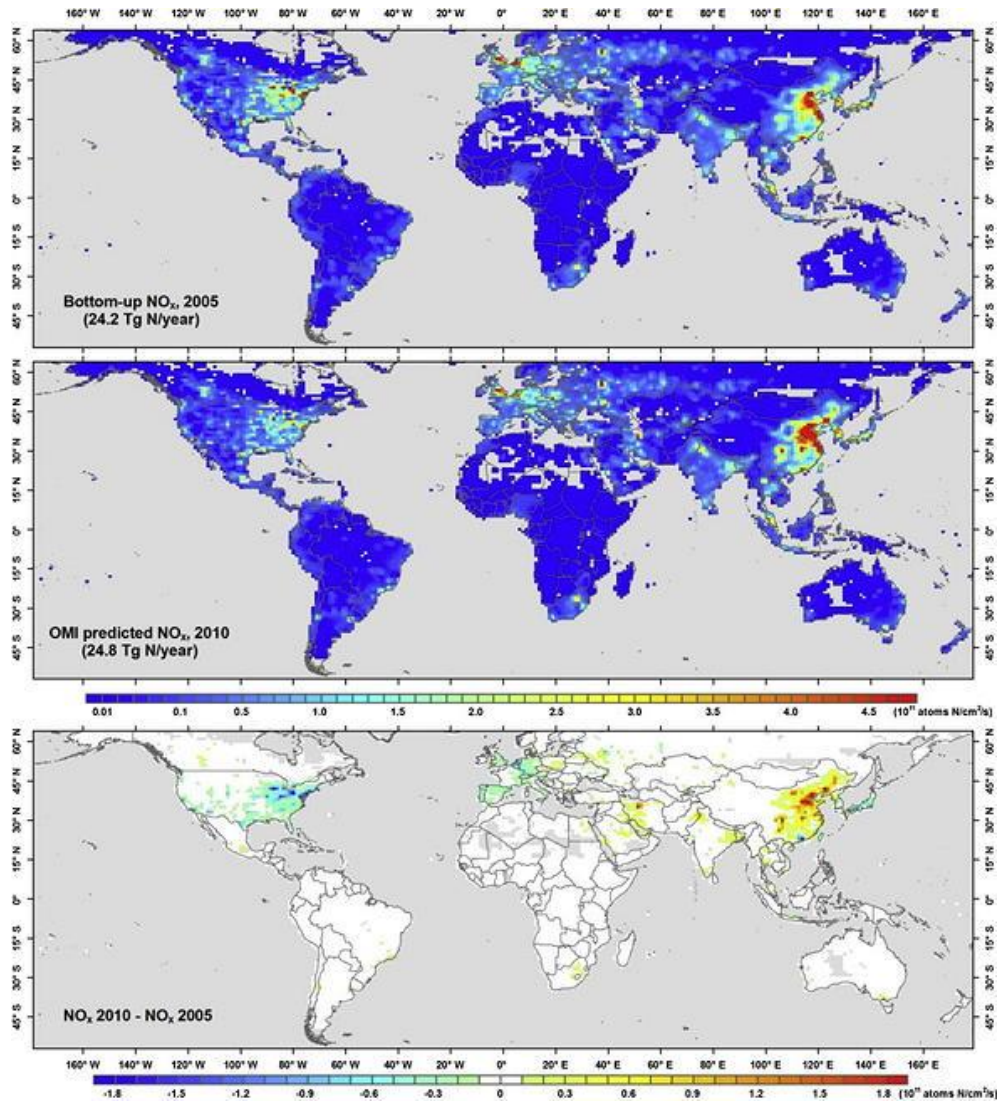
Figure 14.   Spatial distributions of anthropogenic NOx emissions.
Bottom-up inventory for 2005 (top); inventory predicted from OMI NO_2 observations for 2010 (middle). The difference between the OMI-derived emissions for 2010 and the bottom-up emissions for 2005 is shown at the bottom (Lamsal et al. 2011).

Figure 15 compares methane concentrations over North America, as observed by SCIAMACHY (column mixing ratios), a NASA aircraft campaign (INTEX-A, mixing ratios below 700 hPa), and the corresponding GEOS-Chem model values. SCIAMACHY observations are correlated with INTEX-A vertical profile data (96%). Comparison to the GEOS-Chem model shows CH_4 underestimation in the Central U.S. and overestimation along the east coast (Streets et al. 2013).
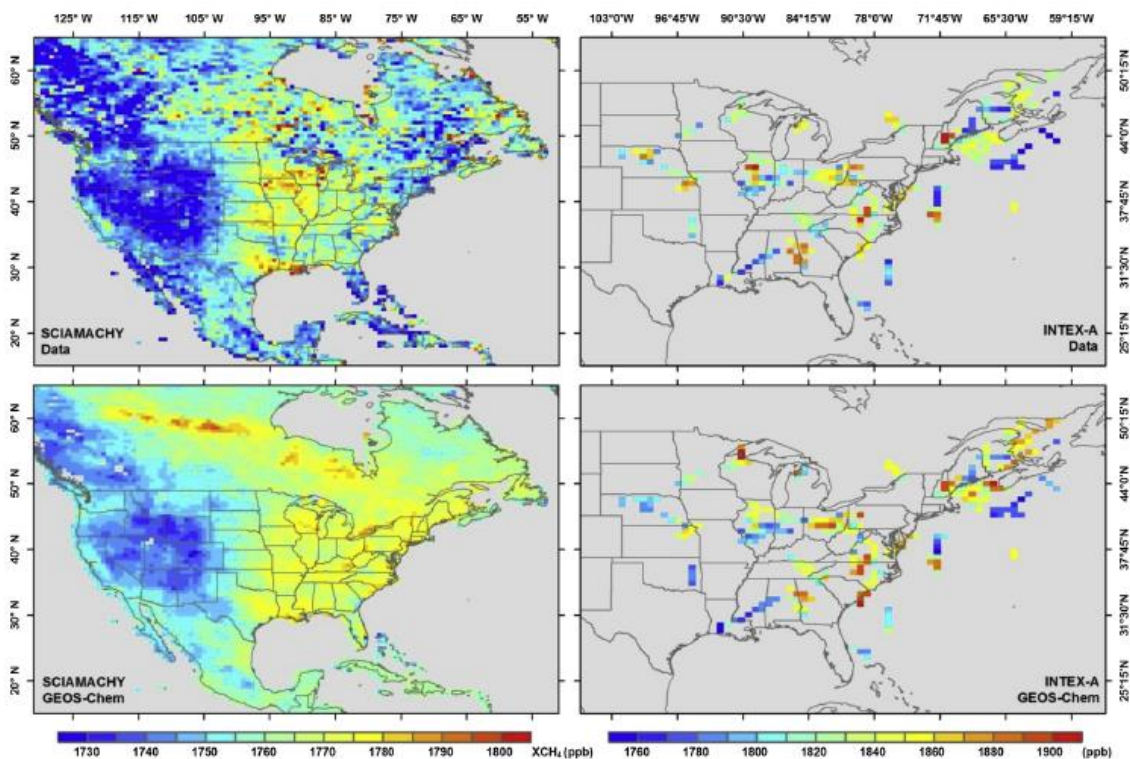
Figure 15. Methane concentrations over North America in June to August 2004, as observed by SCIAMACHY (column mixing ratios) and a NASA aircraft campaign (INTEX-A, mixing ratios below 700 hPa).

The bottom panels show the corresponding GEOS-Chem model values (Streets et al. 2013).

Formaldehyde (HCHO) is a high-yield product of isoprene oxidation, so satellite observations of HCHO can provide useful constraints on isoprene emissions (Palmer et al. 2003). HCHO columns have been detected in urban areas, under very polluted conditions using satellite observations which were used to infer isoprene emissions in different parts of the world, using HCHO-isoprene relationships derived from a CTM (Marais et al. 2012, Millet et al. 2008, Shim et al. 2005).

A challenge related to using remote sensing for developing top-down emissions constraints is determining uncertainties in the resulting inventories. Additionally, emissions of trace gases cannot be fully constrained with satellite-based counterpart products because some gases react. For example, SO_2 can react with other gases such as NH_3 to form $(NH_4)_2SO_4$ aerosols. As a result, satellite measurements are necessarily partial constraints on the emission of the corresponding trace gases. It is beneficial, therefore, to combine measurements of multiple species, including both gases and aerosols, to provide a more complete representation of total pollution (Streets et al. 2013). Recently, Huneeus et al. (2012) simultaneously estimated global emissions of aerosols (e.g., dust, sea salt, black carbon, and organic carbon) by assimilating

MODIS total and fine-mode AOD. Miyazaki et al. (2012) integrated observations of four interrelated species NO_2, O_3, CO, and HNO_3 from four satellites OMI, TES, MOPITT, and MLS with additional aircraft and ozonesonde data. More work, however, is needed before top down-estimates can be used for quantifying multiple species (such as NO_2 and VOC or NO_2 and O_3). Comparisons against independent satellite, aircraft, and ozonesonde data show that the data assimilation results are improved for various chemical compounds. These improvements include a reduced negative tropospheric NO column bias (by 40% to 85%), a reduced negative CO bias in the Northern Hemisphere (by 40% to 90%), and a reduced positive O_3 bias in the middle and upper troposphere (from 30% to 40% to within 10%).

4.4.2 *Oversampling/Spatial Averaging*

Oversampling, or spatial averaging, generates higher resolution data from coarse observations, creating better defined plumes with stronger signals and reduced noise. This technique has been widely used for NO_2 measurements (e.g., Beirle et al. 2004, Lamsal et al. 2008, Martin et al. 2003) and was recently applied to SO_2 measurements from the OMI sensor, improving resolution to 3×3 km for retrievals above Mexico City (de Foy et al. 2009). By averaging OMI NO_2 columns to a grid resolution of 0.025×0.025 deg., Russell et al. (2011) identified spatial patterns in weekday-weekend concentrations in the Los Angeles basin. Beirle et al. (2013) used this technique to identify the volcanic emission rate and lifetime of SO_2 from GOME-2 satellite measurements.

A promising application for space-based spectrometers is SO_2 measurements, although interference with O_3 is problematic (Fioletov et al. 2011). Fioletov et al. (2011) used spatial averaging techniques to successfully quantify the relationship between OMI SO_2 observations and SO_2 emissions from coal-fired power plants in the Eastern US, on a 2 x 2 km grid (Figure 16). They showed that an individual source (or multiple sources within 50 km) produces a statistically significant signal in 3-year averaged OMI pixels within a 12 km radius of the source. Additionally, for sources greater than 70 kT y^{-1}, average OMI SO_2 concentrations around the source were correlated (93%) with annual SO_2 emissions. Fioletov et al. (2011) also observed reductions in the SO_2 column with decreases in emissions from 2005 to 2007 and 2008 to 2010.
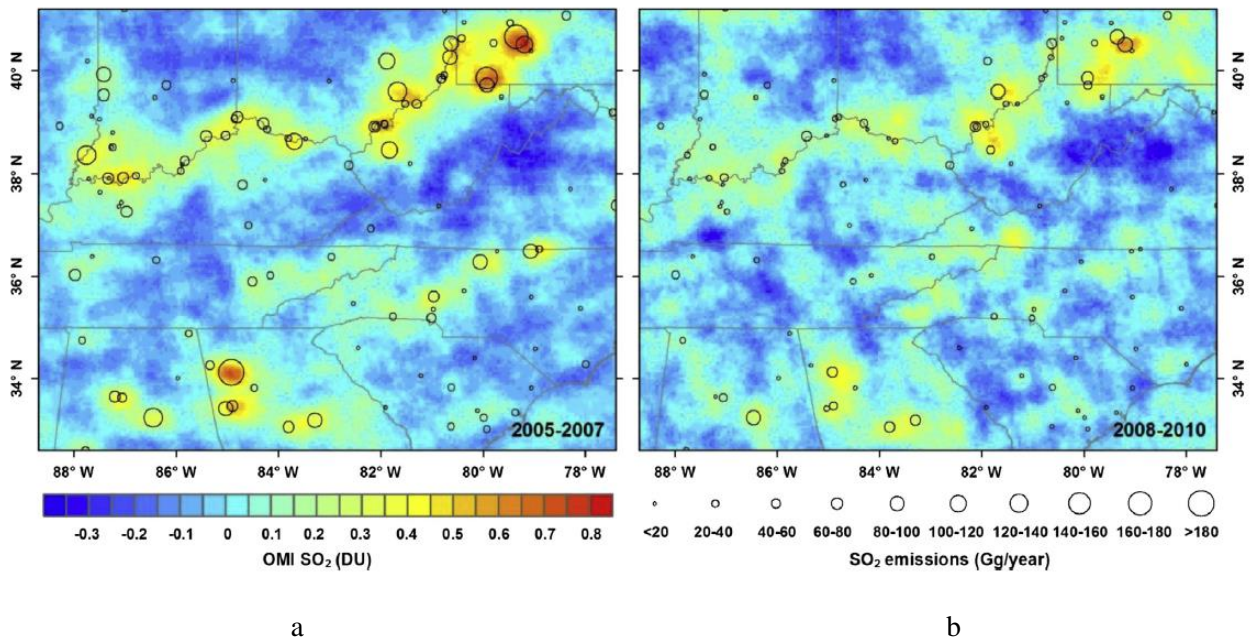
Figure 16.   Mean SO_2 concentrations over the Ohio River Basin measured by OMI.
(a) 2005 to 2007 and (b) 2008 to 2010 (Fioletov et al. 2011).

4.4.3   *Emissions from Oil Fields and Oil Sands*

Fioletov et al. (2013) developed a technique to identify locations with elevated SO_2 emissions using SCIAMACHY, GOME-2, and OMI data, allowing for SO_2 detection at oil fields in the Gulf of Mexico (Figure 17). All three instruments generally agree on the SO_2 sources (e.g., volcanoes, anthropogenic sources). OMI, however, detected smaller sources better than the other two instruments due to its improved resolution. As such, OMI can detect SO_2 when emissions are as low as 70 kT yr^{-1}, compared to 300 kT yr^{-1} for SCIAMACHY and GOME-2.

McLinden et al. (2012) applied the spatial averaging technique described by Fioletov et al. (2011) to produce high resolution emission distribution maps of NO_2 for Alberta. Spatial averaging significantly improved detection and quantification of oil sand NO_2 emissions, showing distinct increases in NO_2 concentrations resulting from surface mining and processing by averaging OMI NO_2 columns between 2005 and 2010 over an area of 30×50 km (Figure 18). Time series analyses illustrate an increasing rate of NO_2 columns by $10.4 \pm 3.5\%$ that is consistent with increases in annual bitumen production (McLinden et al. 2012). Further work is needed to characterize aerosol emissions and complement previous studies in the oil sands region (Howell et al. 2014).
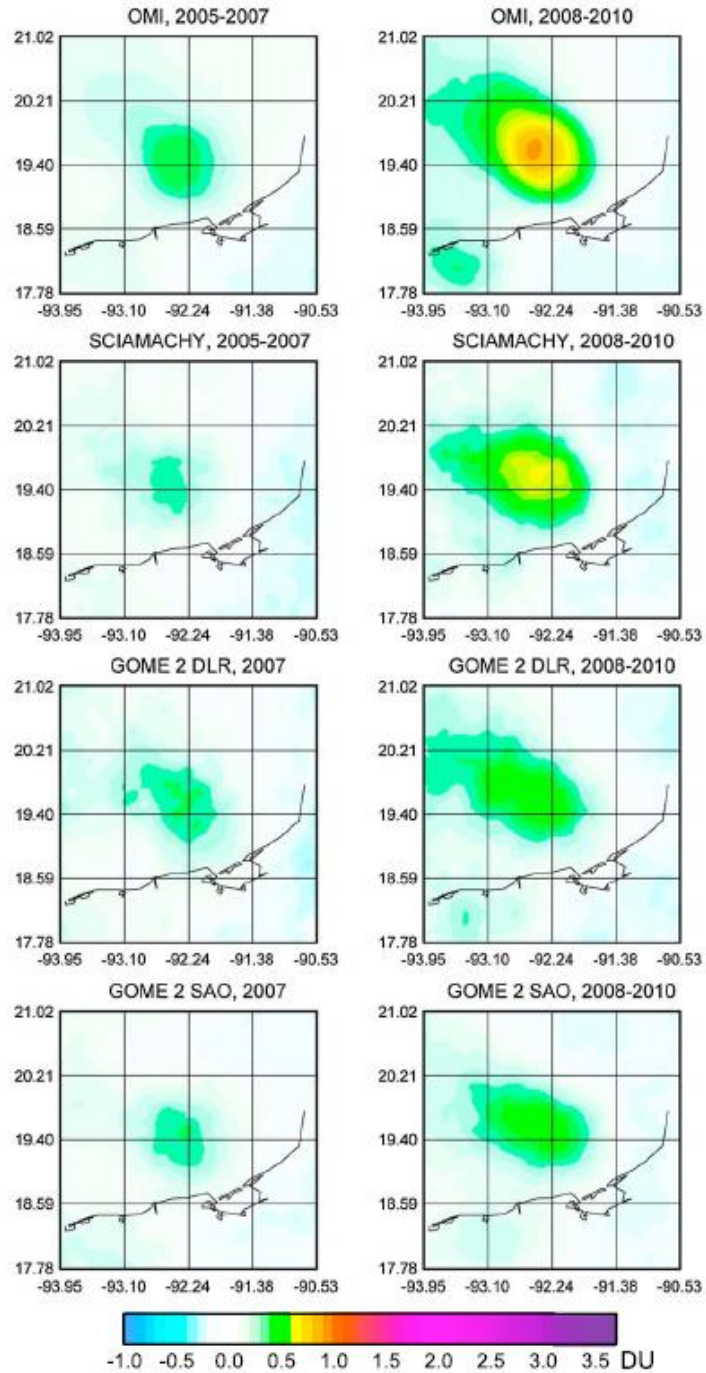
Figure 17. Mean SO₂ distribution over Cantarell and Ku-Maloob-Zaap Oil Fields, Gulf of Mexico, for 2005 to 2007 and 2008 to 2010.
Data are smoothed using the averaging radius of 60 km (Fioletov et al. 2013).

33
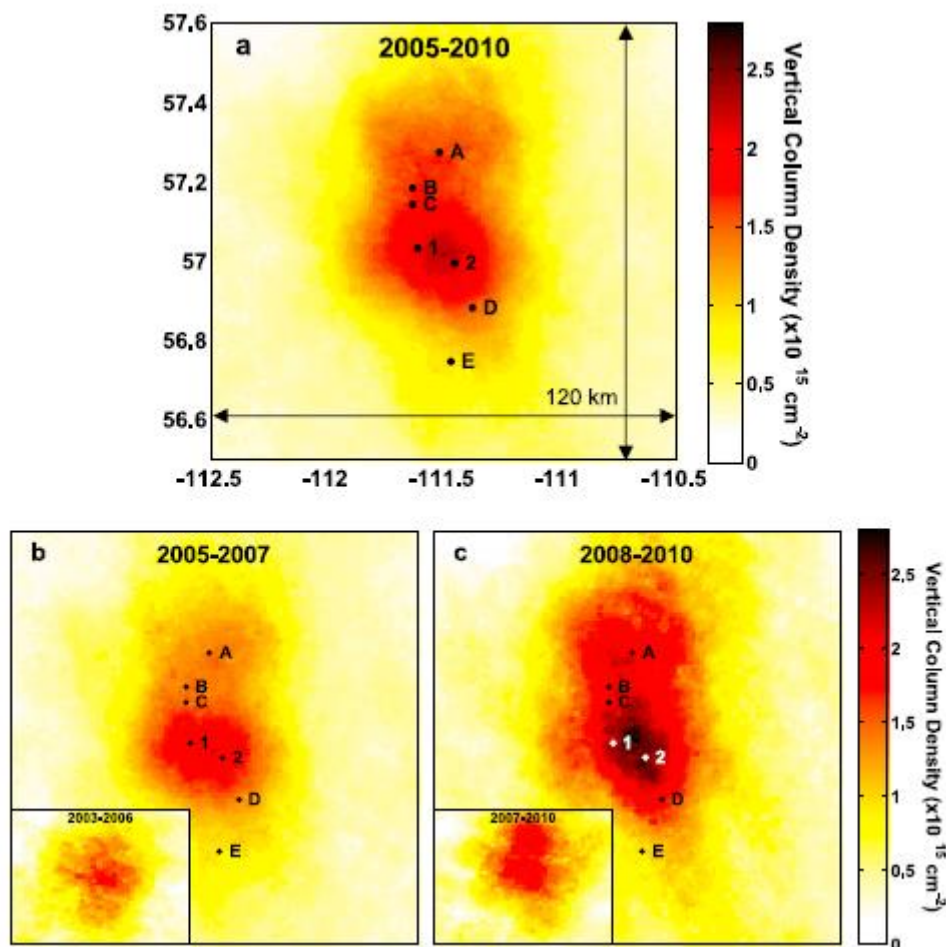
Figure 18. OMI annual mean tropospheric NO$_2$ vertical column in the oil sands region.
(a) averaged over 2005 to 2010, shown on a 1×1 km grid and calculated using an averaging radius of 8 km.
(b) and (c) as in (a) but separated into 2005 to 2007 and 2008 to 2010 averaging periods, respectively.
Monitoring stations equipped with in-situ NO instruments are located at locations A to D for comparison.
Large NO$_2$ emission sources are denoted with '1' and '2' (McLinden et al. 2012).

4.5   Inference of Particulate Matter

The inference of ground-level particulate matter (PM) concentrations from retrieved AOD is a principal application for satellite observations. Since fine particulate matter (dp < 2.5 µm, PM$_{2.5}$) exposure is associated with negative human health impacts, most studies have emphasized the relationship between AOD and surface PM$_{2.5}$ concentrations. Satellite-derived estimates of PM$_{2.5}$ are broadly involved in health impact assessments (Lim et al. 2012) and epidemiological studies (e.g., Anderson et al. 2012, Crouse et al. 2012, Villeneuve et al. 2011). Analytical

34

methods have progressed from semi-quantitative descriptions of air pollution patterns, using correlations and simple linear regressions, to more sophisticated, multivariate spatial and temporal models (Kloog et al. 2011, Lee et al. 2011b, Liu et al. 2012, van Donkelaar et al. 2010). Additional work, however, is still required to improve the accuracy and precision of satellite-derived $PM_{2.5}$ estimates.

Given that passive nadir satellite observations provide little information about vertical profiles, satellite-derived estimates of $PM_{2.5}$ need a conversion factor to relate retrieved AOD to $PM_{2.5}$. This factor should include information about local aerosol optical properties and the aerosol vertical profile, both of which are temporally and spatially variable. The conversion factor can be calculated through various empirical techniques (e.g., Kloog et al. 2011, Zhang et al. 2009) or by using a CTM (e.g., Liu et al. 2004, van Donkelaar et al. 2011). The CTM estimate is based on meteorological data sets, emissions inventories, and equations that represent the physical and chemical behavior of atmospheric constituents, as they are the inputs of the model.

van Donkelaar et al. (2010) used AOD from the Terra satellite-based MODIS and MISR instruments with CTM-simulated AOD-$PM_{2.5}$ to derive global 0.1×0.1 deg. satellite-based $PM_{2.5}$ estimates (Figure 19). Their $PM_{2.5}$ estimates showed promising agreement with *in situ* monitors over North America (r = 0.77) and globally (r = 0.83). The same group recently developed an estimation tool for determining global $PM_{2.5}$ concentrations using MODIS (van Donkelaar et al. 2013). In some regions, correlation improved compared to previous estimation methods (e.g., North America, r = 0.82). In other regions (e.g., San Joaquin Valley, California), however, correlations decreased compared to previous methods.
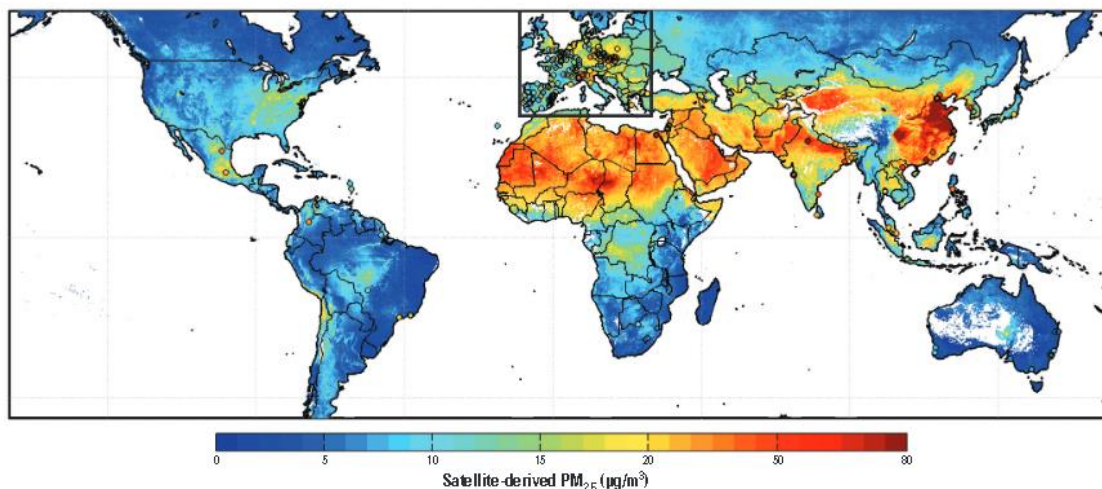

Figure 19. Global satellite-derived $PM_{2.5}$ averaged over 2001to 2006.
White space indicates water or locations containing <50 measurements.
Circles correspond to values and locations of comparison sites outside Canada and the United States; the black box outlines European sites (Van Donkelaar et al. 2010).

35

4.6 Case Study

Spatial and Temporal Variation of CO over Alberta Using Measurements from Satellite, Aircrafts, and Ground Stations – The full case study is presented in Appendix1.

The process of bitumen extraction and upgrading releases trace gases and aerosols to the atmosphere. In this study we present satellite-based analysis to explore, for the first time, various contributing factors that affect tropospheric CO levels over Alberta. The multispectral product that uses both NIR and the TIR radiances for CO retrieval from MOPITT are examined for the 13 year period from 2000 to 2012. The MODIS thermal anomaly product from 2001 to 2012 is employed to investigate the seasonal and temporal variations of forest fires. Additionally, in-situ CO measurements at industrial and urban sites are compared to satellite data. Furthermore, the available MOZAIC/IAGOS aircraft CO profiles (April 2009 to December 2011) are used to validate MOPITT CO data.

The climatological time curtain plot and spatial maps for CO over northern Alberta indicate the signatures of transported CO for two distinct biomass burning seasons, summer and spring. Distinct seasonal patterns of CO at the urban sites (Edmonton and Calgary) point to the strong influence of traffic. Meteorological parameters play an important role in the CO spatial distribution at various pressure levels. Northern Alberta shows stronger upward lifting motion which leads to pronounced CO total column values while the poor dispersion in central and south Alberta exacerbate the surface CO pollution. Inter-annual variations of satellite data depict a slightly decreasing trend for both regions while the decline trend is more evident from ground observations, especially at the urban sites.

MOPITT CO vertical averages and MOZAIC/IAGOS aircraft profiles were in good agreement within the standard deviations at all pressure levels. There is consistency between the time evolutions of high CO episodes monitored by satellite and ground measurements and the fire frequency peak time which implies that biomass burning has affected tropospheric CO distribution in northern Alberta. These findings have further demonstrated the potential use of the MOPITT V5 multispectral (NIR+TIR) product for assessing a complicated surface process.

5 CONCLUSIONS

Monitoring of atmospheric key parameters with instruments mounted on satellites orbiting the Earth has remarkably progressed in the last two decades. The prominent pollutants that can be observed using satellite based instrumentation are: O_3, NO_2, CO, and, SO_2. It is now also possible to observe some selected VOCs. Additionally some of the products from photo-oxidation (such as CH_3OH, and HCHO), intensive agriculture (such as NH_3), as well cloud and aerosol optical parameters can be detected. The accumulation of advanced satellite observations has resulted in a new understanding of our atmospheric environment, the impact of natural processes, and anthropogenic activities on air quality and trans-boundary pollution. The findings have important implications for air pollution control and climate mitigation. Combining information from different sensors and ground-based measurements as well as chemical transport models provides valuable information to air quality assessments. Additionally, satellite

measurements have provided several significant inputs for constraining chemical transport models, and valuable datasets for evaluating and improving model simulations of air quality

Despite the emerging importance of using satellite in air quality applications, there are no studies using them over Alberta until 2012, when McLinden et. al. (2012) employed the Ozone Monitoring Instrument (OMI) instrument for NO_2 and SO_2 assessment over the oil sand region. They presented high-resolution maps that revealed distinct increases over background levels for both species in the area of intensive surface mining. In this work, a study to explore various contributing factors that affect tropospheric CO levels over the oil sand region and some cities using satellite remote sensing observations has been accomplished. It demonstrates the potential use of MOPITT CO multi spectral product measurements to better understand and quantify the CO sources over Alberta. Further work is needed to analyze SO_2, NO_2, and aerosol features over oil sand region especially during the episodic events.

Major progress has been achieved in both passive and active remote sensing from space, providing better boundary layer sensitivity, improved AOD accuracy and aerosol type (size, and shape) characterization. The evolution of active remote instruments (e.g., CALIPSO) offers the advantage of getting vertical distribution of aerosol measurements. Despite the significant progress in atmospheric remote sensing, substantial effort is needed in the future to develop new and enhanced satellite missions. Improvements of the spatial and temporal resolution are required to observe the detailed changes in concentrations of long and short lived active gases.

Current satellites for tropospheric measurements use low Earth orbits, so the maximum temporal resolution is once per day. When considering cloud coverage and noise, only weekly or monthly resolution is practical. Some current instruments have exceeded their designed lifetime and few new satellites have been commissioned. Thus, the National Research Council (NRC) (2007) recently made recommendations about future missions for satellites using remote sensing to determine air quality, including the development of missions with geo-stationary orbits (GEO). Observation from GEO would be of substantial value for air quality investigations, providing continuous mapping on a continental scale to improve air quality forecasts, monitor pollutant emissions, and understand pollutant transport. The NASA Geostationary Coastal and Air Pollution Events[26] (GEO-CAPE) mission was recommended for detecting tropospheric constituents from GEO. This mission, expected to occur by 2020, would measure trace gases and aerosols hourly over North America with a ground resolution of 4×4 km (Fishman et al. 2012, Streets et al. 2013).

In November 2012, a new mission called TEMPO (Tropospheric Emissions: Monitoring of Pollution[27]) was selected under NASA's Earth Venture Instrument program. The mission uses GEO and ultraviolet/visible spectroscopy to monitor North America. It will take measurements from Mexico City to the Canadian oil sands, and from the Atlantic to the Pacific Oceans at hourly timescales and with spatial resolution of 2.0×4.5 km. TEMPO is scheduled to launch no

---

[26] See http://eospso.gsfc.nasa.gov/missions/geostationary-coastal-and-air-pollution-events

[27] See http://eospso.gsfc.nasa.gov/missions/tropospheric-emissions-monitoring-pollution

later than 2020 and will provide measurements of O_3, NO_2, SO_2, H_2CO, $C_2H_2O_2$, H_2O, aerosols, cloud parameters, and radiation (Chance et al. 2013). TEMPO could be a precursor to or component of the larger GEO-CAPE suite of instruments. In addition, the Korea Aerospace Research Institute (KARI) is planning to launch an atmospheric chemistry satellite with a geo-stationary orbit over East Asia around 2018 (Streets et al. 2013).

In Europe, ESA is planning the Sentinel 4 and Sentinel 5 missions, continuing the legacy of EUMETSAT meteorological satellites, to measure atmospheric composition. The ESA Sentinel-5 Precursor (S-5P) polar-orbiting satellite is scheduled to launch in 2015 with a TROPOspheric Monitoring Instrument[28] (TROPOMI) instrument with a 7 year lifetime aimed at global observations of atmospheric composition for air quality and climate. TROPOMI is a nadir viewing spectrometer with bands in the ultraviolet, visible, near infrared, and shortwave infrared regions. It will make daily global observations, with resolution of 7×7 km, of key atmospheric constituents, including O_3, NO_2, SO_2, CO, CH_4, CH_2O, and aerosols. It expands upon the current data records from OMI on NASA EOS Aura and SCIAMACHY on ESA Envisat, with improved spatial resolution and signal-to-noise ratio (Veefkind et al. 2012). Diurnal variations over Europe will be observed by the geo-stationary Sentinel 4 mission after 2018 (Streets et al. 2013). Multiple satellites in a variety of orbits are needed to infer diurnal variation information at high spatial resolution on a global scale.

6   REFERENCES

Abdou, W.A., D.J. Diner, J.V. Martonchik, C.J. Bruegge, R.A. Kahn, B.J. Gaitley, K.A. Crean, L.A. Remer and B. Holben, 2005. Comparison of coincident multiangle imaging spectroradiometer and moderate resolution imaging spectroradiometer aerosol optical depths over land and ocean scenes containing aerosol robotic network sites. Journal of Geophysical Research 110, D10S07. doi:10.1029/ 2004JD004693.

Anderson, H.R., B.K. Butland, A. van Donkelaar, M. Brauer, D.P. Strachan, T. Clayton, R. van Dingenen, M. Amann, B. Brunekreef, A. Cohen, F. Dentener, C. Lai, L.N. Lamsal, R.V. Martin and I.P. One, 2012. Satellite-based estimates of ambient air pollution and global variations in childhood asthma prevalence. Environmental Health Perspectives 120(9): 1333-1339.

Ancellet, G., J. Pelon, Y. Blanchard, B. Quennehen, A. Bazureau, K.S. Law and A. Schwarzenboeck, 2014. Transport of aerosol to the Arctic: Analysis of CALIOP and French aircraft data during the spring 2008 POLARCAT campaign. Atmospheric Chemistry and Physics Discussion 14: 5721-5769. doi:10.5194/acpd-14-5721-2014.

Ansmann, A., H. Baars, M. Tesche, D. Müller, D. Althausen, R. Engelmann, T. Pauliquevis and P. Artaxo, 2009. Dust and smoke transport from Africa to South America: LiDAR profiling over Cape Verde and the Amazon rainforest. Geophysical Research Letters 36: L11802. http://dx.doi.org/10.1029/2009GL037923.

---

[28] See http://www.tropomi.eu/TROPOMI/Home.html

Barnes, W.L., T.S. Pagano, V.V. Salomonson, E.S. Directorate, N. Center and M.D. Greenbelt, 1998. Prelaunch characteristics of the moderate resolution imaging Spectroradiometer (MODIS) on EOS-AM1. IEEE Transactions on Geoscience and Remote Sensing 36: 1088-1100.

Barret, B., S. Turquety, D. Hurtmans, C. Clerbaux, J. Hadji-Lazaro, I. Bey, M. Auvray and P-F. Coheur, 2005. Global carbon monoxide vertical distributions from space borne high-resolution FTIR nadir measurements. Atmospheric Chemistry and Physics 5: 2901-2914.

Beirle, S., C. Hörmann, M. Penning de Vries, S. Dörner, C. Kern and T. Wagner, 2013. Estimating the volcanic emission rate and atmospheric lifetime of SO_2 from space: A case study for Kīlauea volcano, Hawai'i. Atmospheric Chemistry and Physics Discussion 13: 28695-28727. doi:10.5194/acpd-13-28695-2013.

Beirle, S., U. Platt, M.Wenig and T. Wagner, 2004. Highly resolved global distribution of tropospheric NO_2 using GOME narrow swath mode data. Atmospheric Chemistry and Physics 4, 1913-1924.

Ben-Ami, Y., I. Koren, Y. Rudich, P. Artaxo, S.T. Martin and M.O. Andreae, 2010. Transport of North African dust from the Bodele depression to the Amazon Basin: A case study. Atmospheric Chemistry and Physics 10: 7533-7544. http://dx.doi.org/10.5194/acp-10-7533-2010.

Boersma, K.F., H.J. Eskes and E.J. Brinksma, 2004. Error analysis for tropospheric NO_2 retrieval from space. Journal of Geophysical Research 109: D04311, doi:10.1029/2003JD003962.

Borrell, P., J.P. Burrows, U. Platt and C. Zehner, 2001. Determining tropospheric concentrations of trace gases from space. ESA Bulletin 107 - August 2001.

Bovensmann, H., J.P. Burrows, M. Buchwitz, J. Frerick, S. Noël, V.V. Rozanov, K.V. Chance and A.P.G. Goede, 1999. SCIAMACHY mission objectives and measurement modes. Journal of the Atmospheric Sciences 56: 127-150.

Bowman, K.W., C.D. Rodgers, S.S. Kulawik, J. Worden, A. Sarkissian, G. Osterman, T. Steck, L. Ming, A. Eldering, M. Shephard, H. Worden, M. Lampel, S. Clough, P. Brown, C. Rinsland, M. Gunson and R. Beer, 2006. Tropospheric emission spectrometer: Retrieval method and error analysis. IEEE Transactions on Geoscience and Remote Sensing 44: 1297-1307.

Boxe, C.S., J.R. Worden, K.W. Bowman, S.S. Kulawik, J.L. Neu, W.C. Ford, G.B. Osterman, R.L. Herman, A. Eldering, D.W. Tarasick, A.M. Thompson, D.C. Doughty, M.R. Hoffmann and S.J. Oltmans, 2010. Validation of northern latitude Tropospheric Emission Spectrometer stare ozone profiles with ARC-IONS sondes during ARCTAS: Sensitivity, bias and error analysis, Atmospheric Chemistry and Physics 10: 9901-9914. doi:10.5194/acp- 10-9901-2010.

Boynard, A., C. Clerbaux, P-F. Coheur, D. Hurtmans, S. Turquety, M. George, J. Hadji-Lazaro, C. Keim and J. Meyer-Arnek, 2009. Measurements of total and tropospheric ozone from IASI: Comparison with correlative satellite, ground-based and ozonesonde observations. Atmospheric Chemistry and Physics 9: 6255-6271. doi:10.5194/acp-9-6255-2009.

Breon, F.M., A. Vermeulen and J. Descloitres, 2011. An evaluation of satellite aerosol products against sunphotometer measurements. Remote Sensing of Environment 115: 3102-3111.

Buchwitz, M., I. Khlystova, H. Bovensmann and J.P. Burrows, 2007. Three years of global carbon monoxide from SCIAMACHY: Comparison with MOPITT and first results related to the detection of CO over cities. Atmospheric Chemistry and Physics 7: 2399-2411.

Bucsela, E.J., E.A. Celarier, M.O. Wenig, J.F. Gleason, J.P. Veefkind, K.F. Boersma and E.J. Brinksma, 2006. Algorithm for NO_2 vertical column retrieval from the ozone monitoring instrument. IEEE Transactions on Geoscience and Remote Sensing 44: 1245-1258.

Burrows, J.P., M. Buchwitz, M. Eisinger, V. Rozanov, M. Weber, A. Richter, and A. Ladstaetter Weissenmayer, 1999. The global ozone monitoring experiment (GOME): mission concept and first scientific results. Journal of the Atmospheric Sciences 56: 151-175.

Burrows, J. P., Borrell, P., and Platt, U. (Eds), 2011. The remote sensing of tropospheric composition from space. Springer, Berlin, Heidelberg. doi:10.1007/978-3-642-14791-3.

Callies, J., E. Corpaccioli, M. Eisinger, A. Hahne and A. Lefebvre, 2000. GOME-2- Metop's second-generation sensor for operational ozone monitoring. European Space Agency Bulletin 102: 28-36.

Chance, K., X. Liu, R. Suleiman, D. Flittner, J. Al-Saadi and S. Janz, 2013. Tropospheric Emissions: Monitoring Of Pollution (TEMPO). IN: Proceedings SPIE 8866, Earth Observing Systems XVIII, 88660D (September 23, 2013). doi:10.1117/12.2024479.

Chen, W-T., R. Kahn, W-H. Li and J. Seinfeld, 2008. Sensitivity of multi-angle imaging to optical and microphysical properties of biomass burning particles. Journal of Geophysical Research 113: D10203. doi:10.1029/ 2007JD009414.

Cheng, T., H. Chen, X. Gu, T. Yu, J. Guo and H. Guo, 2012. The inter-comparison of MODIS, MISR and GOCART aerosol products against AERONET data over China. Journal of Quantitative Spectroscopy and Radiative Transfer 113: 2135-2145.

Clarisse, L., C. Clerbaux, F. Dentener, D. Hurtmans and P-F. Coheur, 2009. Global ammonia distribution derived from infrared satellite observations. Nature Geoscience 2: 479-483.

Clarisse, L., P.F. Coheur, A.J. Prata, D. Hurtmans, A. Razavi, T. Phulpin, J. Hadji-Lazaro and C. Clerbaux, 2008. Tracking and quantifying volcanic SO_2 with IASI, the September 2007 eruption at Jebel at Tair. Atmospheric Chemistry and Physics 8: 7723-7734.

Clarisse, L., Y. R'Honi, P-F. Coheur, D. Hurtmans and C. Clerbaux, 2011. Thermal infrared nadir observations of 24 atmospheric gases. Geophysical Research Letters 38: L10802.

Clarisse, L., M.W. Shephard, F. Dentener, D. Hurtmans, K. Cady-Pereira, F. Karagulian, M. Van Damme, C. Clerbaux and P-F. Coheur, 2010. Satellite monitoring of ammonia: A case study of the San Joaquin Valley. Journal of Geophysical Research 115: D13302.

Clerbaux, C., A. Boynard, L. Clarisse, M. George, J. Hadji-Lazaro, H. Herbin, D. Hurtmans, M. Pommier, A. Razavi, S. Turquety, C. Wespes and P-F. Coheur, 2009. Monitoring of

atmospheric composition using the thermal infrared IASI/ MetOp sounder. Atmospheric Chemistry and Physics 9: 6041-6054.

Clerbaux, C., J.R. Drummond, J-M. Flaud and J. Orphal, 2011. Thermal infrared: Absorption and emission – trace gases and parameters. IN: Burrows, J.P., U. Platt and P. Borrell (Eds.), The Remote Sensing of Tropospheric Composition from Space. Springer Verlag, Heidelberg. pp. 123-152.

Clerbaux, C., J. Hadji-Lazaro, S. Turquety, G. Mégie and P-F. Coheur, 2003. Trace gas measurements from infrared satellite for chemistry and climate applications. Atmospheric Chemistry and Physics 3: 1495-1508.

Connors, V.S., B.B. Gormsen, S. Nolf and H.G. Reichle, 1999. Spaceborne observations of the global distribution of carbon monoxide in the middle troposphere during April and October 1994. Journal of Geophysical Research 104: 21455-21470.

Crevoisier, C., S. Heilliette, A. Chedin, S. Serrar, R. Armante and N.A. Scott, 2004. Mid-tropospheric CO_2 concentration retrieval from AIRS observations in the tropics. Geophysical Research Letters 31. doi: 410.1029/2004gl020141.

Crouse, D.L., P.A. Peters, A. van Donkelaar, M.S. Goldberg, P.J. Villeneuve, O. Brion, S. Khan, D.O Atari, M. Jerrett, C.A. Pope, M. Brauer, J.R. Brook, R.V. Martin, D. Stieb and R.T. Burnett, 2012. Risk of nonaccidental and cardiovascular mortality in relation to long-term exposure to low concentrations of fine particulate matter: A Canadian national-level cohort study. Environmental Health Perspectives 120(5): 708-714.

Damoah, R., N. Spichtinger, C. Forster, P. James, I. Mattis, U. Wandinger, S. Beirle, T. Wagner and A. Stohl, 2004. Around the world in 17 days - hemispheric-scale transport of forest fire smoke from Russia in May 2003. Atmospheric Chemistry and Physics 4: 1311-1321.

de Foy, B.,N.A. Krotkov, N. Bei, S.C. Herndon, L.G. Huey, A-P. Martinez, L.G. Ruiz- Suárez, E.C. Wood, M. Zavala and L.T. Molina, 2009. Hit from both sides: Tracking industrial and volcanic plumes in Mexico City with surface measurements and OMI SO_2 retrievals during the MILAGRO field campaign. Atmospheric Chemistry and Physics 9: 9599-9617.

Deeter, M.N., L.K. Emmons, G.L. Francis, D.P. Edwards, J.C. Gille, J.X. Warner, B. Khattatov, D. Ziskin, J.F. Lamarque, S.P. Ho, V. Yudin, J.L. Attie, D. Packman, J. Chen, D. Mao and J.R. Drummond, 2003. Operational carbon monoxide retrieval algorithm and selected results for the MOPITT instrument. Journal of Geophysical Research 108: 4399. doi:10.1029/ 2002JD003186.

Deeter, M.N., L. K. Emmons, D.P. Edwards, and J.C. Gille, 2004. Vertical resolution and information content of CO profiles retrieved by MOPITT. Geophysical Research Letters 31: L15112. doi:10.1029/2004GL020235.

Deeter, M.N., S. Martínez-Alonso, D.P. Edwards, L.K. Emmons, J.C. Gille, H.M. Worden, J.V. Pittman, B.C. Daube and S.C. Wofsy, 2013. Validation of MOPITT Version 5 thermal-

infrared, near-infrared, and multispectral carbon monoxide profile retrievals for 2000-2011. Journal of Geophysical Research-Atmospheres 118: 6710-6725. doi:10.1002/jgrd.50272.

Deeter, M.N., H.M. Worden, D.P. Edwards, J.C. Gille and A.E. Andrews, 2011. Evaluation of MOPITT retrievals of lower-tropospheric carbon monoxide over the United States. Journal of Geophysical Research 117: D13306. doi:10.1029/2011JD017553.

Di Pierro, M., L. Jaeglé and T.L. Anderson, 2011. Satellite observations of aerosol transport from East Asia to the Arctic: Three case studies. Atmospheric Chemistry and Physics 11: 2225-2243. http://dx.doi.org/10.5194/acp-11-2225-2011.

Dils, B., M. De Maziere, J.F. Müller, T. Blumenstock, M. Buchwitz, R. de Beek, P. Demoulin, P. Duchatelet, H. Fast, C. Frankenberg, A. Gloudemans, D. Griffith, N. Jones, T. Kerzenmacher, I. Kramer, E. Mahieu, J. Mellqvist, R.L. Mittermeier, J. Notholt, C.P. Rinsland, H. Schrijver, D. Smale, A. Strandberg, A.G. Straume, W. Stremme, K. Strong, R. Sussmann, J. Taylor, M. van den Broek, V. Velazco, T. Wagner, T. Warneke, A. Wiacek and S. Wood, 2006. Comparisons between SCIAMACHY and ground-based FTIR data for total columns of CO, CH_4, CO_2 and N_2O. Atmospheric Chemistry and Physics 6: 1953-1976.

Diner, D.J., J.C. Beckert, T.H. Reilly, C.J. Bruegge, J.E. Conel, R.A. Kahn, R.A. Martonchik, T.P. Ackerman, R. Davies, S. Gerstl, H.R. Gordon, J-P. Muller, R. Myneni, P. Sellers, B. Pinty and M. Verstraete, 1998. Multi-angle Imaging Spectro Radiometer (MISR) instrument description and experiment overview. IEEE Transactions on Geoscience and Remote Sensing 36: 1072-1087.

Dirksen, R.J., K.F. Boersma, J. de Laat, P. Stamnes, G.R. van der Werf, M. Val Martin and H.M. Kelder, 2009. An aerosol boomerang: Rapid around-the-world transport of smoke from the December 2006 Australian forest fires observed from space. Journal of Geophysical Research 114, D21201. http://dx.doi.org/10.1029/2009JD012360.

Drummond, J.R. and G.S. Mand, 1996. The measurements of pollution in the troposphere (MOPITT) instrument: Overall performance and calibration requirements. Journal of Atmospheric and Oceanic Technology 13: 314-320.

Dufour G., F. Wittrock, M. Camredon, M. Beekmann, A. Richter, B. Aumont and J.P. Burrows, 2009. SCIAMACHY formaldehyde observations: Constraint for isoprene emission estimates over Europe? Atmospheric Chemistry and Physics 9: 1647-1664.

Dupont, R., B. Pierce, J. Worden, J. Hair, M. Fenn, P. Hamer, M. Natarajan, T. Schaack, A. Lenzen, E. Apel, J. Dibb, G. Diskin, G. Huey, A. Weinheimer, Y. Kondo and D. Knapp, 2012. Attribution and evolution of ozone from Asian wild fires using satellite and aircraft measurements during the ARCTAS campaign. Atmospheric Chemistry and Physics 12: 169-188. doi:10.5194/acp-12-169-2012.

Ebojie, F., C. von Savigny, A. Ladstätter-Weißenmayer, A. Rozanov, M. Weber, K. Eichmann, S. Bötel, N. Rahpoe, H. Bovensmann and J.P. Burrows, 2013. Tropospheric column amount of ozone retrieved from SCIAMACHY limb-nadir-matching

observations. Atmospheric Measurement Techniques Discussions 6: 7811-7865. doi:10.5194/amtd-6-7811-2013.

Emmons, L.K., M.N. Deeter, J.C. Gille, D.P. Edwards, J.L. Attie, J. Warner, D. Ziskin, G. Francis, B. Khattatov, V. Yudin, J.F. Lamarque, S.P. Ho, D. Mao, J.S. Chen, J. Drummond, P. Novelli, G. Sachse, M.T. Coffey, J.W. Hannigan, C. Gerbig, S. Kawakami, Y. Kondo, N. Takegawa, H. Schlager, J. Baehr and H. Zierei, 2004. Validation of Measurements of Pollution in the Troposphere (MOPITT) CO retrievals with aircraft in situ profiles. Journal of Geophysical Research 109: D03309. doi:10.1029/2003JD004101.

Emmons, L.K., G.G. Pfister, D.P. Edwards, J.C. Gille, G. Sachse, D. Blake, S. Wofsy, C. Gerbig, D. Matross and P. Nédélec, 2007. Measurements of Pollution in the Troposphere (MOPITT) validation exercises during summer 2004 field campaigns over North America. Journal of Geophysical Research 112: D12S02. doi:0.1029/ 2006JD007833.

Fioletov, V.E., C.A. McLinden, N. Krotkov, M.D. Moran and K. Yang, 2011. Estimation of SO_2 emissions using OMI retrievals. Geophysical Research Letters 38: L21811. doi:10.1029/2011GL049402.

Fioletov, V.E., C.A. McLinden, N. Krotkov, K. Yang, D. Loyola, P. Valks, N. Theys, M. Van Roozendael, C. Nowlan, K. Chance, X. Liu, C. Lee and R.V. Martin, 2013. Application of OMI, SCIAMACHY, and GOME-2 satellite SO_2 retrievals for detection of large emission sources. Journal of Geophysical Research 118: 11,399-11,418. doi:10.1002/jgrd.50826.

Fishman, J., 1991. Probing planetary pollution from space. Environmental Science and Technology 25: 612-621.

Fishman, J., J. Al-Saadi, P. Bontempi, K. Chance, F. Chavez, M. Chin, P. Coble, C. Davis, P. DiGiacomo, D. Edwards, J. Goes, J. Herman, C. Hu, L.T. Iraci, D. Jacob, C. Jordan, S.R. Kawa, R. Key, X. Liu, S. Lohrenz, A. Mannino, V. Natraj, D. Neil, J. Neu, M. Newchurch, K. Pickering, J. Salisbury, H. Sosik, M. Tzortziou, J. Wang and M. Wang, 2012. Progress Report on NASA's GEO-CAPE Mission: Fulfilling the mandate and meeting the challenges of the Nation's next generation of atmospheric composition and coastal ecosystem measurements: NASA's Geostationary Coastal and Air Pollution Events (GE McLinden O-CAPE) Mission (2011). Bulletin of the American Meteorological Society 93(10): 1547-1566. doi:10.1175/BAMS-D-11-00201.1.

Fishman, J., C.E. Watson, J.C. Larsen and J.A. Logan, 1990. Distribution of tropospheric ozone determined from satellite data. Journal of Geophysical Research 95: 3599-3617.

Franke, K., A. Richter, H. Bovensmann, V. Eyring, P. Jöckel, P. Hoor and J.P. Burrows, 2009. Ship emitted NO_2 in the Indian Ocean: Comparison of model results with satellite data. Atmospheric Chemistry and Physics 9: 7289-7301.

Frankenberg, C., J.F. Meirink, M. van Weele, U. Platt and T. Wagner, 2005. Assessing methane emissions from global space-borne observations. Science 308: 1010-1014.

Fu, D., J. R., Worden, X., Liu, S. S. Kulawik, K. W. Bowman, and V. Natraj, 2013. Characterization of ozone profiles derived from Aura TES and OMI radiances. Atmospheric Chemistry and Physics 13, 3445-3462, doi:10.5194/acp-13-3445-2013.

Gautam, R., N.C. Hsu, T.F. Eck, B.N. Holben, S. Janjai, T. Jantarach, S.C. Tsay and K.M. Lau, 2013. Characterization of aerosols over the Indochina peninsula from satellite-surface observations during biomass burning pre-monsoon season. Atmospheric Environment 78: 51-59. doi:10.1016/j.atmosenv.2012.05.038.

George, M., C. Clerbaux, D. Hurtmans, S. Turquety, P.-F. Coheur, M. Pommier, J. Hadji-Lazaro, D. P. Edwards, H. Worden, M. Luo, C. Rinsland and W. McMillan, 2009. Carbon monoxide distributions from the IASI/METOP mission: evaluation with other space-borne remote sensors. Atmospheric Chemistry and Physics 9: 8317-8330. doi:10.5194/acp-9-8317.

Gloudemans, A.M.S., M.C. Krol, J.F. Meirink, A.T.J. de Laat, G.R. van der Werf, H. Schrijver, M.M.P. van den Broek and I. Aben, 2006. Evidence for long-range transport of carbon monoxide in the Southern Hemisphere from SCIAMACHY observations. Geophysical Research Letters. 33: L16807. doi:10.1029/2006GL026804.

Griggs, M., 1975. Measurements of atmospheric aerosol optical thickness over water using ERS-1 data. Journal of the Air Pollution Control Association 25: 622-626.

Heald, C.L., J.L. Collett, T. Lee, K.B. Benedict, F.M. Schwandner, Y. Li, L. Clarisse, D.R. Hurtmans, M. Van Damme, C. Clerbaux, P-F. Coheur, S. Philip, R.V. Martin and H.O.T. Pye, 2012. Atmospheric ammonia and particulate inorganic nitrogen over the United States. Atmospheric Chemistry and Physics 12: 10295-10312.

Heald, C.L., D.J. Jacob, A.M. Fiore, L.K. Emmons, J.C. Gille, M.N. Deeter, J. Warner, D.P. Edwards, J.H. Crawford, A.J. Hamlin, G.W. Sachse, E.V. Browell, M.A. Avery, S.A. Vay, D.J. Westberg, D.R. Blake, H.B. Singh, S.T. Sandholm, R.W. Talbot and H.E. Fuelberg, 2003. Asian outflow and transpacific transport of carbon monoxide and ozone pollution: An integrated satellite, aircraft and model perspective. Journal of Geophysical Research 108(D24): 4804. doi:10.1029/2003JD003507.

Heald, C.L., D.J. Jacob, D.B.A. Jones, P.I. Palmer, J.A. Logan, D.G. Streets, G.W. Sachse, J.C. Gille, R.N. Hoffman and T. Nehrkorn, 2004. Comparative inverse analysis of satellite (MOPITT) and aircraft (TRACE-P) observations to estimate Asian sources of carbon monoxide. Journal of Geophysical Research 109: D23306. doi:10.1029/2004JD005185.

Heland, J., H. Schlager, A. Richter and J.P. Burrows, 2002. First comparison of tropospheric NO_2 column densities retrieved from GOME measurements and in situ aircraft profile measurements. Geophysical Research Letters 29: 1983. doi:10.1029/2002GL015528.

Herman, J.R. and E.A. Celarier, 1997. Earth surface reflectivity climatology at 340–380 nm from TOMS data. Journal of Geophysical Research 102: 28003-28011.

Herman, M., J.L. Deuzé, A. Marchand, B. Roger and P. Lallart, 2005. Aerosol remote sensing from POLDER/ADEOS over the ocean: Improved retrieval using a non spherical particle model. Journal of Geophysical Research 110: D10S02, 1-12. doi:10.1029/2004JD004798.

Herman, M., A. Lifermann and F. Waquet, 2011. Remote sensing of aerosols by using polarized, directional and spectral measurements within the A-Train: The PARASOL mission. Atmospheric Measurement Techniques Discussions 4: 2037-2069. doi:10.5194/amtd-4-2037-2011.

Heue, K.-P., A. Richter, M. Bruns, J.P. Burrows, C. v. Friedeburg, U. Platt, I. Pundt, P. Wang and T. Wagner, 2005. Validation of SCIAMACHY tropospheric NO_2- columns with AMAXDOAS measurements. Atmospheric Chemistry and Physics 5: 1039-1051.

Hoogen, R., V.V. Rozanov and J.P. Burrows, 1999. Ozone profiles from GOME satellite data: Algorithm description and first validation. Journal of Geophysical Research 104: 8263-8280.

Howell, S.G., A.D. Clarke, S. Freitag, C.S. McNaughton, V. Kapustin, V. Brekovskikh, J-L. Jimenez and M.J. Cubison, 2014. An airborne assessment of atmospheric particulate emissions from the processing of Athabasca oil sands. Atmospheric Chemistry and Physics 14: 5073-5087.

Hsu, N.C., C. Li, N.A. Krotkov, Q. Liang, K. Yang and S-C. Tsay, 2012. Rapid transpacific transport in autumn observed by the A-Train satellites. Journal of Geophysical Research 117: D06312. http://dx.doi.org/10.1029/2011JD016626.

Hsu, N.C., S.C. Tsay, M.D. King and J.R. Herman, 2004. Aerosol properties over bright-reflecting source regions. IEEE Transactions on Geoscience and Remote Sensing 42: 557-569. doi:10.1109/TGRS.2004.824067.

Hsu, N.C., S-C. Tsay, M.D. King and J.R. Herman, 2006. Deep blue retrievals of Asian aerosol properties during ACE-Asia. IEEE Transactions on Geoscience and Remote Sensing 44: 3180-3195. http://dx.doi.org/10.1029/2005JD006549.

Hudson, R.D., J.H. Kim and A.M. Thompson, 1995. On the derivation of tropospheric column ozone from radiances measured by the total ozone mapping spectrometer. Journal of Geophysical Research-Atmospheres 100: 11137-11145.

Hudson, R.D. and A.M. Thompson, 1998. Tropical tropospheric ozone from total ozone mapping spectrometer by a modified residual method. Journal of Geophysical Research-Atmospheres 103: 22129-22145.

Huneeus, N., F. Chevallier and O. Boucher, 2012. Estimating aerosol emissions by assimilating observed aerosol optical depth in a global aerosol model. Atmospheric Chemistry and Physics 12: 4585-4606.

Husar, R.B., 2011. Satellite based measurement of atmospheric aerosol of atmospheric aerosols. IN: Aerosol Measurement: Principles, Techniques, and Applications, Third Edition. Kulkarni, P., P.A. Baron and K. Willeke (Eds). John Wiley & Sons, Inc. pp. 667-678.

Hutchison, K.D., 2003. Applications of MODIS satellite data and products for monitoring air quality in the state of Texas. Atmospheric Environment 37: 2403-2412.

Jacob, D.J., 2006. Inverse modeling techniques. IN: Visconti, G., P. Di Carlo, W. Brune, M. Schoeberl and A. Wahner (Eds.). Observing Systems for Atmospheric Composition. Springer.

Kahn, R.A., B.J. Gaitley, J.V. Martonchik, D.J. Diner, K.A. Crean and B. Holben, 2005. Multiangle imaging spectroradiometer (MISR) global aerosol optical depth validation based on 2 years of coincident aerosol robotic network (AERONET) observations. Journal of Geophysical Research 110: D10S04. doi:10.1029/2004JD004706.

Kahn, R.A., W-H. Li, C. Moroney, D.J. Diner, J.V. Martonchik and E. Fishbein, 2007. Aerosol source plume physical characteristics from space-based multiangle imaging. Journal of Geophysical Research 112: D11205. doi:10.1029/2006JD007647.

Kalashnikova, O.V. and R.A. Kahn, 2006. Ability of multiangle remote sensing observations to identify and distinguish mineral dust types: Part 2. Sensitivity over dark water. Journal of Geophysical Research 111, D11207. doi:10.1029/2005JD006756.

Kalashnikova, O.V. and R.A. Kahn, 2008. Mineral dust plume evolution over the Atlantic from combined MISR/MODIS aerosol retrievals. Journal of Geophysical Research 113: D24204. http://dx.doi.org/10.1029/2008JD010083.

Kaufman, Y.J., D.D. Herring, K.J. Ranson and G.J. Collatz, 1998. Earth Observing System AM1 mission to Earth. IEEE Transactions on Geoscience and Remote Sensing 36(4): 1045-1055.

Kaufman, Y.J., D. Tanré L.A. Remer, E.F. Vermote, A. Chu and B.N. Holben, 1997. Operational remote sensing of tropospheric aerosol over land from EOS moderate resolution imaging spectroradiometer. Journal of Geophysical Research 102 (D14): 17051-17067.

Kim, J.H., R.D. Hudson and A.M. Thompson, 1996. A new method of deriving time-averaged tropospheric column ozone over the tropics using total ozone mapping spectrometer (TOMS) radiances: Intercomparison and analysis using TRACE A data. Journal of Geophysical Research-Atmospheres 101: 24317-24330.

Klenk, K.F., P.K. Bhartia, A.J. Fleig, V.G. Kaveeshwar, R.D. McPeters and P.M. Smith, 1982. Total ozone determination from the backscattered ultraviolet (BUV) experiment. Journal of Applied Meteorology 21: 1672-1684.

Kloog, I., P. Koutrakis, B.A. Coull, H.J. Lee and J. Schwartz, 2011. Assessing temporally and spatially resolved $PM_{2.5}$ exposures for epidemiological studies using satellite aerosol optical depth measurements. Atmospheric Environment 45: 6267-6275.

Kobayashi, H., A. Shimota, K. Kondo, E. Okumura, Y. Kameda, H. Shimoda and T. Ogawa, 1999. Development and evaluation of the interferometric monitor for greenhouse gases: a high throughput Fourier-transform infrared radiometer for nadir Earth observation. Applied Optics 38: 6801-6807.

Koelemeijer, R.B.A., J.F. de Haan and P. Stammes, 2003. A database of spectral surface reflectivity of the Earth in the range 335-772 nm derived from 5.5 years of GOME observations. Journal of Geophysical Research 108: 4070. doi:10.1029/2002JD002429.

Koo, J-H., Y. Wang, T.P. Kurosu, K. Chance, A. Rozanov, A. Richter, S.J. Oltmans, A.M. Thompson, J.W. Hair, M.A. Fenn, A.J. Weinheimer, T.B. Ryerson, S. Solberg, L.G. Huey, J. Liao, J.E. Dibb, J.A. Neuman, J.B. Nowak, R. B. Pierce, M. Natarajan and J. Al-Saadi, 2012. Characteristics of tropospheric ozone depletion events in the Arctic spring: Analysis of the ARCTAS, ARCPAC, and ARCIONS measurements and satellite BrO observations. Atmospheric Chemistry and Physics 12: 9909-9922. doi:10.5194/acp-12-9909-2012.

Kopacz, M., D.J. Jacob, J.A. Fisher, J.A. Logan, L. Zhang, I.A. Megretskaia, R.M. Yantosca, K. Singh, D.K. Henze, J.P. Burrows, M. Buchwitz, I. Khlystova, W.W. McMillan, J.C. Gille, D.P. Edwards, A. Eldering, V. Thouret and P. Nedelec, 2010. Global estimates of CO sources with high resolution by adjoint inversion of multiple satellite datasets (MOPITT, AIRS, SCIAMACHY, TES). Atmospheric Chemistry and Physics 10: 855-876.

Kopacz, M., D.J. Jacob, D.K. Henze, C.L. Heald, D.G. Streets and Q. Zhang, 2009. Comparison of adjoint and analytical Bayesian inversion methods for constraining Asian sources of carbon monoxide using satellite (MOPITT) measurements of CO columns. Journal of Geophysical Research 114: D04305.

Krueger, A.J., 1983. Sighting of El-Chichon sulfur-dioxide clouds with the Nimbus-7 total ozone mapping spectrometer. Science 220: 1377-1379.

Ladstatter-Weißenmayer, A., J. Heland, R. Kormann, R. von Kuhlmann, M.G. Lawrence, J. Meyer-Arnek, A. Richter, F. Wittrock, H. Ziereis and J.P. Burrows, 2003. Transport and build-up of tropospheric trace gases during the MINOS campaign: Comparison of GOME, in situ aircraft measurements and MATCH-MPIC-data. Atmospheric Chemistry and Physics 3: 1887-1902.

Lamsal, L.N., R.V. Martin, A. van Donkelaar, M. Steinbacher, E.A. Celarier, E. Bucsela, E.J. Dunlea and J.P. Pinto, 2008. Ground-level nitrogen dioxide concentrations inferred from the satellite-borne Ozone Monitoring Instrument. Journal of Geophysical Research 113: D16308.

Lamsal, L.N., R.V. Martin, A. Padmanabhan, A. van Donkelaar, Q. Zhang, C.E. Sioris, K. Chance, T.P. Kurosu and M.J. Newchurch, 2011. Application of satellite observations for timely updates to global anthropogenic NOx emission inventories. Geophysical Research Letters 38: L05810. doi:10.1029/2010GL046476.

Lamsal, L.N., R.V. Martin, A. van Donkelaar, E.A. Celarier, E.J. Bucsela, K.F. Boersma, R. Dirksen, C. Luo, and Y. Wang, 2010. Indirect validation of tropospheric nitrogen dioxide retrieved from the OMI satellite instrument: Insight into the seasonal variation of nitrogen oxides at northern midlatitudes. Journal of Geophysical Research 115: D05302. doi:10.1029/2009JD013351.

Lee, C., R.V. Martin, A. van Donkelaar, H. Lee, R.R. Dickerson, J.C. Hains, N. Krotkov, A. Richter, K. Vinnikov and J.J. Schwab, 2011a. SO_2 emissions and lifetimes: Estimates from inverse modeling using in situ and global, space-based (SCIAMACHY and OMI) observations, Journal of Geophysical Research 116: D06304. doi:10.1029/2009JD012123.

Lee, C., A. Richter, M. Weber and J.P. Burrows, 2008. SO_2 retrieval from SCIAMACHY using the weighting function DOAS (WFDOAS) technique: comparison with standard DOAS retrieval. Atmospheric Chemistry and Physics Discussion. 8: 10817-10839.

Lee, H.J., Y. Liu, B.A. Coull, J. Schwartz and P. Koutrakis, 2011b. A novel calibration approach of MODIS AOD data to predict $PM_{2.5}$ concentrations. Atmospheric Chemistry and Physics 11: 7991-8002.

Lee, K.H., Z. Li, Y.J. Kim and A.A. Kokhanovsky, 2009. Aerosol monitoring from satellite observations: a history of three decades. IN: Kim, Y.J., U. Platt, M.B. Gu and H. Iwahashi (Editors). Atmospheric and Biological Environmental Monitoring. Springer, Berlin. pp. 13-38.

Levelt, P.F., E. Hilsenrath, G.W. Leppelmeier, G.H.J. van den Oord, P.K. Bhartia, J. Taminnen, J.F. de Haan and J.P. Veefkind, 2006. Science objectives of the Ozone Monitoring Instrument, IEEE Transactions on Geoscience and Remote Sensing 44(5): 1093-1101.

Levy, R.C., L.A. Remer and O. Dubovik, 2007. Global aerosol optical properties and application to Moderate Resolution Imaging Spectroradiometer aerosol retrieval over land. Journal of Geophysical Research 112: D13210. doi:10.1029/2006JD007815.

Li, F., P. Ginoux and V. Ramaswamy, 2010. Transport of Patagonian dust to Antarctica. Journal of Geophysical Research 115: D18217. http://dx.doi.org/10.1029/2009JD012356.

Li, Z., F. Niu, K.H. Lee, J. Xin, W.M. Hao, B. Nordgren, Y. Wang and P. Wang, 2007. Validation and understanding of MODIS aerosol products using ground-based measurements from the handheld sunphotometer network in China. Journal of Geophysical Research 112: D22S07. doi:10.1029/2007JD008479.

Lim, S.S., A.D. Flaxman, G. Danaei, K. Shibuya, H. Adair-Rohani, M. Amann, H.R. Anderson, K.G. Andrews, M. Aryee, C. Atkinson, L.J. Bacchus and A.N. Bahalim, 2012. A comparative risk assessment of burden of disease and injury attributable to 67 risk factors and risk factor clusters in 21 regions, 1990-2010: A systematic analysis for the Global Burden of Disease Study 2010. Lancet 380: 2224-2260.

Lin, J-T., M.B. McElroy and K.F. Boersma, 2010. Constraint of anthropogenic NOx emissions in China from different sectors: A new methodology using multiple satellite retrievals, Atmospheric Chemistry and Physics 10: 63-78. doi:10.5194/acp-10-63-2010.

Liu, X., K. Chance, C.E. Sioris, T.P. Kurosu, R.J.D. Spurr, R.V. Martin, T.M. Fu, J.A. Logan, D.J. Jacob, P.I. Palmer, M.J. Newchurch, I.A. Megretskaia, R. Chatfield, 2006. First directly-retrieved global distribution of tropospheric column ozone: Comparison with the GEOS-CHEM model. Journal of Geophysical Research 111: D02308. doi:10.1029/2005JD006564.

Liu, X., K. Chance, C.E. Sioris, R.J.D. Spurr, T.P. Kurosu, R.V. Martin and M.J. Newchurch, 2005. Ozone profile and tropospheric ozone retrieval from global ozone monitoring experiment (GOME): Algorithm description and validation. Journal of Geophysical Research 110: D20307. doi:10.1029/2005JD006240.

Liu, Y., K. He, S. Li, Z. Wang, D.C. Christiani and P. Koutrakis, 2012. A statistical model to evaluate the effectiveness of $PM_{2.5}$ emissions control during the Beijing 2008 Olympic Games. Environment International 44: 100-105.

Liu, Y., R.J. Park, D.J. Jacob, Q.B. Li, V. Kilaru and J.A. Sarnat, 2004. Mapping annual mean ground-level $PM_{2.5}$ concentrations using Multiangle Imaging Spectroradiometer aerosol optical thickness over the contiguous United States. Journal of Geophysical Research 109: D22206. doi:10.1029/ 2004JD005025.

Liu, Z., A. Omar, M. Vaughan, J. Hair, C. Kittaka, Y.X. Hu, K. Powell, C. Trepte, D. Winker, C. Hostetler, R. Ferrare and R. Pierce, 2008. CALIPSO LiDAR observations of the optical properties of Saharan dust: a case study of long-range transport. Journal of Geophysical Research 113: D07207. http://dx.doi.org/10.1029/2007JD008878.

Liu, Z., D. Winker, A. Omar, M. Vaughan, C. Trepte, Y. Hu, K.A. Powell, W. Sun and B. Lin, 2011. Effective LiDAR ratios of dense dust layers over North Africa derived from the CALIOP measurements. Journal of Quantitative Spectroscopy and Radiative Transfer 112: 204-213. doi:10.1016/j.jqsrt.2010.05.006.

Lopez, J.P., M. Luo, L.E. Christensen, M. Loewenstein, H. Jost, C.R. Webster and G. Osterman, 2008. TES carbon monoxide validation during two AVE campaigns using the Argus and ALIAS instruments on NASA's WB-57F. Journal of Geophysical Research 113: D16S47. doi:10.1029/2007JD008811.

Loyola, D., J. van Geffen, P. Valks, T. Erbertseder, M. Van Roozendael, W. Thomas, W. Zimmer and K. Wißkirchen, 2008. Satellite-based detection of volcanic sulphur dioxide from recent eruptions in Central and South America. Advances in Geosciences 14: 35-40.

Lu, Z. and D.G. Streets, 2012. Increase in NO_x emissions from Indian thermal power plants during 1996-2010: Unit-based inventories and multi-satellite observations. Environmental Science and Technology 46: 7463-7470.

Luo, M., C. Rinsland, B. Fisher, G. Sachse, G. Diskin, J. Logan, H. Worden, S. Kulawik, G. Osterman, A. Eldering, R. Herman and M. Shephard, 2007. TES carbon monoxide validation with DACOM aircraft measurements during INTEX-B 2006. Journal of Geophysical Research 112: D24S48. doi:10.1029/2007JD008803.

Maignan, F., F-M. Bréon, E. Fédèle and M. Bouvier, 2009. Polarized reflectances of natural surfaces: Spaceborne measurements and analytical modeling. Remote Sensing of Environment. 113: 2642-2650.

Marais, E.A., D.J. Jacob, T.P. Kurosu, K. Chance, J.G. Murphy, C. Reeves, G. Mills, S. Casadio, D.B. Millet, M.P. Barkley, F. Paulot and J. Mao, 2012. Isoprene emissions in Africa inferred from OMI observations of formaldehyde columns. Atmospheric Chemistry and Physics 12/14: 6219-6235.

Martin, R.V., 2008. Satellite remote sensing of surface air quality. Atmospheric Environment. 42: 7823-7843.

Martin, R.V., D.J. Jacob, K. Chance, T.P. Kurosu, P.I. Palmer and M.J. Evans, 2003. Global inventory of nitrogen oxide emissions constrained by space-based observations of NO_2 columns. Journal of Geophysical Research 108 (D17): 4537. doi:10.1029/2003JD003453.

Martin, R.V., D.D. Parrish, T.B. Ryerson and D.K. Nicks, 2004. Evaluation of GOME satellite measurements of tropospheric NO_2 and HCHO using regional data from aircraft campaigns in the southeastern United States. Journal of Geophysical Research 109: D24307. doi:10.1029/2004JD004869.

Martin, R.V., C.E. Sioris, K. Chance, T.B. Ryerson, T.H. Bertram, P.J. Wooldridge, R.C. Cohen, J.A. Neuman, A. Swanson and F.M. Flocke, 2006. Evaluation of space-based constraints on nitrogen oxide emissions with regional aircraft measurements over and downwind of eastern North America. Journal of Geophysical Research 111, D15308. doi:10.1029/2005JD006680.

Martínez-Alonso, S., M.N. Deeter, H.M. Worden, C. Clerbaux, D. Mao and J.C. Gille, 2012. First satellite identification of volcanic carbon monoxide. Geophysical Research Letters 39: L21809.

Martonchik, J.V., D.J. Diner, K. Crean and M. Bull, 2002. Regional aerosol retrieval results from MISR. IEEE Transactions on Geoscience and Remote Sensing 40: 1520-1531.

Martonchik, J.V., D.J. Diner, R. Kahn, M.M. Verstraete, B. Pinty, H.R. Gordon and T.P. Ackerman, 1998. Techniques for the Retrieval of aerosol properties over land ocean using multiangle data. IEEE Transactions on Geoscience and Remote Sensing 36: 1212-1227.

Martonchik, J.V., D.J. Diner, R.A. Kahn, B.J. Gaitley and B.N. Holben, 2004. Comparison of MISR and AERONET aerosol optical depths over desert sites. Geophysical Research Letters 31: L16102. doi:10.1029/2004GL019807.

Matyssek, R., G. Wieser, C. Calfapietra, W. de Vries, P. Dizengremel, D. Ernst, Y. Jolivet, T.N. Mikkelsen, G.M.J. Mohren, D. LeThiec, J-P. Tuovinen, A. Weatherall and E. Paoletti, 2012. Forests under climate change and air pollution: Gaps in understanding and future directions for research. Environmental Pollution 160: 57-65.

McCartney, E.J., 1983. Absorption and emission by atmospheric gases: The physical processes. J. Wiley & Sons, New York.

McCubbin, D.R. and M.A. Delucchi, 1999. The health costs of motor vehicle related air pollution. Journal of Transport, Economics and Policy 33(3): 253-286.

McLinden, C.A., V. Fioletov, K.F. Boersma, N. Krotkov, C.E. Sioris, J.P. Veefkind and K. Yang, 2012. Air quality over the Canadian oil sands: A first assessment using satellite observations. Geophysical Research Letters 39: L04804. doi:10.1029/2011GL050273.

McMillan, W.W., C. Barnet, L. Strow, M.T. Chahine, M.L. McCourt, J.X. Warner, P.C. Novelli, S. Korontzi, E.S. Maddy and S. Datta, 2005. Daily global maps of carbon monoxide from NASA's Atmospheric Infrared Sounder. Geophysical Research Letters 32: L11801. doi:410.1029/2004gl021821.

Mekler, Y., H. Quenzel, G. Ohring and I. Marcus, 1977. Relative atmospheric aerosol content from ERS observations. Journal of Geophysical Research 82: 967-972.

Mi, W., Z. Li, X. Xia, B. Holben, R. Levy, F. Zhao, H. Chen and M Cribb, 2007. Evaluation of the Moderate Resolution Imaging Spectroradiometer aerosol products at two Aerosol Robotic Network stations in China. Journal of Geophysical Research 112: D22S08. doi:10.1029/2007JD008474.

Millet, D.B., D.J. Jacob, K.F. Boersma, T-M. Fu, T.P. Kurosu, K. Chance, C.L. Heald and A. Guenther, 2008. Spatial distribution of isoprene emissions from North America derived from formaldehyde column measurements by the OMI satellite sensor. Journal of Geophysical Research 113: D02307.

Miyazaki, K., H.J. Eskes, K. Sudo, M. Takigawa, M. van Weele and K.F. Boersma, 2012. Simultaneous assimilation of satellite NO_2, O_3, CO, and HNO_3 data for the analysis of tropospheric chemical composition and emissions. Atmospheric Chemistry and Physics 12: 9545-9579.

Molina, M.J., and F.S. Rowland. 1974. Stratospheric sink for chlorofluoromethane: Chlorine atom-catalyzed destruction of ozone. Nature 249:810-812.

Nassar, R., D.B.A. Jones, S.S. Kulawik, J.R. Worden, K.W. Bowman, R.J. Andres, P. Suntharalingam, J.M. Chen, C.A.M. Brenninkmeijer, T.J. Schuck, T.J. Conway and D.E. Worthy, 2011. Inverse modeling of CO_2 sources and sinks using satellite observations of CO_2 from TES and surface flask measurements. Atmospheric Chemistry and Physics 11(2): 6029-6047.

National Research Council (NRC), 2007. Earth science and applications from space: National Imperatives for the Next Decade and Beyond Committee on Earth Science and Applications from Space. National Academy Press, Washington, D.C. A Community Assessment and Strategy for the Future, National Research Council. http://www.nap.edu/catalog/11820.html.

Newell, R.E., Y. Zhu, V.S. Connors, H.G. Reichle, P.C. Novelli and B.B. Gormsen, 1999. Atmospheric processes influencing measured carbon monoxide in the NASA Measurement of Air Pollution From Satellites (MAPS) experiment. Journal of Geophysical Research-Atmospheres 104: 21487-21501.

Nowlan, C.R., X. Liu, K. Chance, Z. Cai, T.P. Kurosu, C. Lee and R.V. Martin, 2011. Retrievals of sulfur dioxide from the Global Ozone Monitoring Experiment 2 (GOME-2) using an optimal estimation approach: Algorithm and initial validation. Journal of Geophysical Research 116: D18301. doi:10.1029/2011JD015808.

Omar, A., D. Winker, C. Kittaka, M. Vaughan, Z. Liu, Y. Hu, C. Trepte, R. Rogers, R. Ferrare, R. Kuehn and C. Hostetler, 2009. The CALIPSO Automated Aerosol Classification and LiDAR Ratio Selection Algorithm. Journal of Atmospheric and Oceanic Technology 26: 1994-2014. doi:10.1175/2009JTECHA1231.1.

Osterman, G.B., S.S. Kulawik, H.M. Worden, N.A. Richards, B.M. Fisher, A. Eldering, M.W. Shephard, L. Froidevaux, G. Labow, M. Luo, R.L. Herman, K.W. Bowman, and A.M. Thompson, 2008. Validation of Tropospheric Emission Spectrometer (TES) measurements of the total, stratospheric, and tropospheric column abundance of ozone. Journal of Geophysical Research-Atmospheres 113: D15S16. doi: 10.1029/2007JD008801.

Palmer, P.I., D.J. Jacob, A.M. Fiore, R.V. Martin, K. Chance and T.P. Kurosu, 2003. Mapping isoprene emissions over North America using formaldehyde column observations from space. Journal of Geophysical Research 108: 4180. doi:10.1029/2002JD002153.

Pan, L., D.P. Edwards, J.C. Gille, M.W. Smith and J.R. Drummond, 1995. Satellite remote sensing of tropospheric CO and CH_4: Forward model studies of the MOPITT instrument. Applied Optics 34: 6976-6988.

Pan, L., J.C. Gille, D.P. Edwards, P.L. Bailey and C.D. Rodgers, 1998. Retrieval of tropospheric carbon monoxide for the MOPITT experiment. Journal of Geophysical Research 103: 32277-32290.

Parkinson, C.L., 2003. Aqua: An Earth-observing satellite mission to examine water and other climate variables. IEEE Transactions on Geoscience and Remote Sensing 41: 2.

Penning de Vries, M.J.M., S. Beirle and T. Wagner, 2009. UV aerosol indices from SCIAMACHY: introducing the SCattering Index (SCI). Atmospheric Chemistry and Physics 9: 9555-9567. doi:10.5194/acp-9-9555-2009.

Pinder, R.W., J.T. Walker, J.O. Bash, K.E. Cady-Pereira, D.K. Henze, M. Luo, G.B. Osterman and M.W. Shephard, 2011. Quantifying spatial and seasonal variability in atmospheric ammonia with in situ and space-based observations. Geophysical Research Letters 38: L04802.

Razavi, A., C. Clerbaux, C. Wespes, L. Clarisse, D. Hurtmans, S. Payan, C. Camy-Peyret and P.F. Coheur, 2009. Characterization of methane retrievals from the IASI space-borne sounder. Atmospheric Chemistry and Physics 9: 7889-7899. doi:10.5194/acp-9-7889-2009.

Razavi, A., F. Karagulian, L. Clarisse, D. Hurtmans, P.F. Coheur, C. Clerbaux, J.F. Muller and T. Stavrakou, 2011. Global distributions of methanol and formic acid retrieved for the first time from the IASI/MetOp thermal infrared sounder. Atmospheric Chemistry and Physics 11: 857-872. doi:10.5194/acp-11-857-2011.

Reichle Jr., H.G., V.S. Connors, J.A. Holland, W.D. Hypes, H.A. Wallio, J.C. Casas, B.B. Gormsen, M. S. Saylor, and W. D. Hesketh, 1986. Middle and upper tropospheric carbon monoxide mixing ratios as measured by a satellite borne remote sensor during November 1981. Journal of Geophysical Research 91, D10, 10865-10,887.

Reichle, H.G., B.E. Anderson, V. Connors, T.C. Denkins, D.A. Forbes, B.B. Gormsen, R.L. Langenfelds, D.O. Neil, S.R. Nolf, P.C. Novelli, N.S. Pougatchev, M.M. Roell and L.P. Steele, 1999. Space shuttle based global CO measurements during April and October 1994, MAPS instrument, data reduction, and data validation. Journal of Geophysical Research 104(17): 21443-21454.

Reichle, H.G., V.E. Conners, J.A. Holland, R.T. Sherril, H.A. Wallio, J.C. Casas, E.P. Condon, B.B. Gormsen and W. Seiler, 1990. The distribution of middle tropospheric carbon monoxide during early 1984. Journal of Geophysical Research 95: 9845-9856.

Remer, L.A., Y.J. Kaufman, D. Tanré, S. Mattoo, D.A. Chu, J.V. Martins, R-R. Li, C. Ichoku, R.C. Levy, R.G. Kleidman, T.F. Eck, E. Vermote and B.N. Holben, 2005. The MODIS aerosol algorithm, products and validation. Journal of the Atmospheric Sciences 62(4): 947-973.

Rinsland, C.P., M. Luo, J.A. Logan, R. Beer, H.M. Worden, S.S. Kulawik, D. Rider, G. Osterman, M. Gunson, A. Eldering, A. Goldman, M.W. Shephard, S.A. Clough, C. Rodgers, M.C. Lampel and L. Chiou, 2006. Nadir measurements of carbon monoxide distributions by the Tropospheric Emission Spectrometer instrument onboard the Aura Spacecraft: Overview of analysis approach and examples of initial results. Geophysical Research Letters 33: L22806. doi:10.1029/2006GL027000.

Rix, M., P. Valks, N. Hao, D. Loyola, H. Schlager, H. Huntrieser, J. Flemming, U. Koehler, U. Schumann and A. Inness, 2012. Volcanic SO_2, BrO and plume height estimations using GOME-2 satellite measurements during the eruption of Eyjafjallajökull in May 2010. Journal of Geophysical Research 117: D00U19.

Rodgers, C.D., 2000. Inverse methods for atmospheric sounding: Theory and practice. World Scientific, Hackensack, New Jersey.

Rothe, K.W., U. Brinkmann and H. Walther, 1974. Applications of tunable dye lasers to air pollution detection: Measurements of atmospheric NO_2 concentrations by differential absorption. Applied Physics 3: 115-119.

Russell, A.R., A.E. Perring, L.C. Valin, E.J. Bucsela, E.C. Browne, K-E. Min, P.J. Wooldridge and R.C. Cohen, 2011. A high spatial resolution retrieval of NO_2 column densities from OMI: Method and evaluation. Atmospheric Chemistry and Physics 11: 8543-8554.

Sandu, A. and T. Chai, 2011. Chemical data assimilation – an overview. Atmosphere 2: 426-463.

Sanghavi, S., J.V. Martonchik, J. Landgraf and U. Platt, 2012. Retrieval of the optical depth and vertical distribution of particulate scatterers in the atmosphere using O_2 A- and B-band SCIAMACHY observations over Kanpur: A case study. Atmospheric Measurement Techniques 5: 1099-1119. doi:10.5194/amt-5-1099-2012.

Schoeberl, M.R., A.R. Douglass, E. Hilsenrath, P.K. Bhartia, R. Beer, J.W. Waters, M.R. Gunson, L. Froidevaux, J.C. Gille, J.J. Barnett, P.F. Levelt and P. DeCola, 2006. Overview of the EOS Aura Mission. IEEE Transactions on Geoscience and Remote Sensing 44(5): 1066-1074.

Schrader S., I.N. Sokolik, B. Vogel, H. Vogel and P. Suppan, 2013. Use of satellite data for air quality applications in northern China. IN: Proceedings SPIE8890, Remote Sensing of Clouds and the Atmosphere XVIII; and Optics in Atmospheric Propagation and Adaptive Systems XVI, 88900G (October 17, 2013). http://dx.doi.org/10.1117/12.2029101.

Shim, C., Y. Wang, Y. Choi, P.I. Palmer, D.S. Abbot and K. Chance, 2005. Constraining global isoprene emissions with Global Ozone Monitoring Experiment (GOME) formaldehyde column measurements. Journal of Geophysical Research 110: D24301.

Sierk, B., A. Richter, A. Rozanov, Ch. Von Savigny, A.M. Schmoltner, M. Buchwitz, H. Bovensmann and J.P. Burrows, 2006. Retrieval and monitoring of atmospheric trace gas concentrations in nadir and limb geometry using the Space-Borne SCIAMACHY Instrument. Environmental Monitoring and Assessment 120: 65-77. doi:10.1007/s10661-005-9049-9.

Stavrakou, T., A. Guenther, A. Razavi, L. Clarisse, C. Clerbaux, P-F. Coheur, D. Hurtmans, F. Karagulian, M. De Mazière, C. Vigouroux, C. Amelynck, N. Schoon, Q. Laffineur, B. Heinesch, M. Aubinet, C. Rinsland and J-F. Müller, 2011. First space-based derivation of the global atmospheric methanol emission fluxes. Atmospheric Chemistry and Physics 11: 4873-4898.

Stavrakou, T. and J.F. Müller, 2006. Grid-based versus big region approach for inverting CO emissions using Measurement of Pollution in the Troposphere (MOPITT) data. Journal of Geophysical Research 111: D15304. doi:10.1029/2005JD006896.

Stohl, A., T. Berg, J.F. Burkhart, A.M. Fjǽraa, C. Forster, A. Herber, Ø. Hov, C. Lunder, W.W. McMillan, S. Oltmans, M. Shiobara, D. Simpson, S. Solberg, K. Stebel, J. Ström, K. Tørseth, R. Treffeisen, K. Virkkunen and K.E. Yttri, 2007. Arctic smoke – record high air pollution levels in the European Arctic due to agricultural fires in Eastern Europe in spring 2006. Atmospheric Chemistry and Physics 7: 511-534. doi:10.5194/acp-7-511.

Stowe, L.L., H. Jacobowitz, G. Ohring, K.R. Knapp and N.R. Nalli, 2002. The Advanced Very High Resolution Radiometer (AVHRR) Pathfinder Atmosphere (PATMOS) climate dataset: Initial analyses and evaluations. Journal of Climate 15: 1243-1260.

Streets, D.G., T.C. Bond, G.R. Carmichael, S.D. Fernandes, Q. Fu, D. He, Z. Klimont, S.M. Nelson, N.Y. Tsai, M.Q. Wang, J.H. Woo and K.F. Yarber, 2003. An inventory of 20 gaseous and primary aerosol emissions in Asia in the year 2000. Journal of Geophysical Research 108: 8809. doi:10.1029/2002jd003093.

Streets, D.G., T. Canty, G.R. Carmichael, B. de Foy, R.R. Dickerson, B.N. Duncan, D.P. Edwards, J.A. Haynes, D.K. Henze, M.R. Houyoux, D.J. Jacob, N.A. Krotkov, L.N. Lamsal, Y. Liu, Z. Lu, R.V. Martin, G.G. Pfister, R.W. Pinder, R.J. Salawitch and K.J. Wecht, 2013. Emissions estimation from satellite retrievals: A review of current capability. Atmospheric Environment 77: 1011-1042.

Suleiman, R.M., K. Chance, X Liu and T.P. Kurosu, 2013. OMI BrO measurements: Operational data analysis algorithm and initial validation. American Geophysical Union, Fall Meeting 2013, abstract #V43B-2885.

Tan, K.C., H.S. Lim and M.Z. Mat Jafri, 2013. Relationship between ozone and the air pollutants in Peninsular Malaysia for 200 retrieved from SCIAMACHY. IN: AIP Conference Proceedings 1528, 151. doi:10.1063/1.4803586.

Tanré, D., F.M. Bréon, J.L. Deuzé, O. Dubovik, F. Ducos, P. François, P. Goloub, M. Herman, A. Lifermann and F. Waquet, 2011. Remote sensing of aerosols by using polarized, directional and spectral measurements within the A-Train: The PARASOL mission. Atmospheric Measurement Techniques Discussions 4: 2037-2069. doi:10.5194/amtd-4-2037-2011.

Tanré, D., Y.J. Kaufman, M. Herman and S. Mattoo, 1997. Remote sensing of aerosol properties over oceans using the MODIS/EOS spectral radiances. Journal of Geophysical Research 102(D14): 16971-16988.

Tesche, M., A. Ansmann, D. Muller, D. Althausen, R. Engelmann, V. Freudenthaler and S. Groß, 2009. Vertically resolved separa- tion of dust and smoke over Cape Verde using multiwavelength Raman and polarization LiDARs during Saharan Mineral Dust Experiment 2008. Journal of Geophysical Research 114: D13202.

Torres, O., P.K. Bhartia, J.R. Herman, A. Sinyuk and B. Holben, 2002. A long term record of aerosol optical thickness from TOMS observations and comparison to AERONET measurements. Journal of the Atmospheric Sciences 59: 398-413.

Torres, O., A. Tanskanen, B. Veihelmann, C. Ahn, R. Braak, P.K. Bhartia, J.P. Veefkind and P.F. Levelt, 2007. Aerosols and surface UV products from OMI observations: An overview. Journal of Geophysical Research 112: D24S47. doi:10.1029/2007JD008809.

Turner, M.C., C.D. Krewski, C.A. Pope, III, Y. Chen, S.M. Gapstur and M.J. Thun, 2011. Long-term ambient fine particulate matter air pollution and lung cancer in a large cohort of never-smokers. American Journal of Respiratory and Critical Care Medicine 184(12): 1374-1381.

Turquety, S., J. Hadji-Lazaro, C. Clerbaux, D.A. Hauglustaine, S.A. Clough, V. Casse´, P. Schlüssel and G. Mégie, 2004. Operational trace gas retrieval algorithm for the Infrared Atmospheric Sounding Interferometer. Journal of Geophysical Research 109: D21301. doi:10.1029/2004JD004821.

Uno, I., K. Eguchi, K. Yumimoto, Z. Liu, Y. Hara, N. Sugimoto, A. Shimizu and T. Takemura, 2011. Large Asian dust layers continuously reached North America in April (2010). Atmospheric Chemistry and Physics 11: 7333-7341. http://dx.doi.org/10.5194/acp-11-7333-2011.

Uno, I., K. Eguchi, K. Yumimoto, T. Takemura, A. Shimizu, M. Uematsu, Z. Liu, Z. Wang, Y. Hara and N. Sugimoto, 2009. Asian dust transported one full circuit around the globe. Nature Geoscience 2: 557-560. http://dx.doi.org/10.1038/ngeo583.

van der Werf, G.R., J.T. Randerson, L. Giglio, G.J. Collatz, P.S. Kasibhatla and A.F. Arellano Jr., 2006. Interannual variability in global biomass burning emissions from 1997 to 2004, Atmospheric Chemistry and Physics 6 (11): 3423-3441. http://www.atmos-chem-phys.net/6/3423/2006/acp-6-3423-2006.pdf

van Donkelaar, A., R.V. Martin, M. Brauer, R. Kahn, R. Levy, C. Verduzco and P.J. Villeneuve, 2010. Global estimates of ambient fine particulate matter concentrations from satellite-based

aerosol optical depth: Development and application. Environmental Health Perspectives 118: 847-855.

van Donkelaar, A., R.V. Martin, R.C. Levy, M. da Silva, M. Krzyzanowski, N.E. Chubarova, E. Semutnikova and A.J. Cohen, 2011. Satellite-derived estimates of ground-level fine particulate matter during extreme events: A case study of the Moscow fires in 2010. Atmospheric Environment 45: 6225-6232.

van Donkelaar, A., R.V. Martin, R.J.D. Spurr, E. Drury, L.A. Remer, R.C. Levy and J. Wang, 2013. Optimal estimation for global ground-level fine particulate matter concentrations. Journal of Geophysical Research 118: 5621-5636. doi:10.1002/jgrd.50479.

Veefkind, J.P., I. Abenb, K. McMullanc, H. Försterd, J. de Vriese, G. Otterf, J. Claasa, H.J. Eskesa, J.F. de Haana, Q. Kleipoola, M. van Weelea, O. Hasekampb, R. Hoogeveenb, J. Landgrafb, R. Snelb, P. Tolb, P. Ingmannc, R. Voorse, B. Kruizingaf, R. Vinkf, H. Visserf and P.F. Leveltа, 2012. TROPOMI on the ESA Sentinel-5 Precursor: A GMES mission for global observations of the atmospheric composition for climate, air quality and ozone layer applications. Remote Sensing of Environment 120: 70-83.

Veihelmann, B., P.F. Levelt, P. Stammes and J.P. Veefkind, 2007. Aerosol Information Content in OMI Spectral Reflectance Measurements. Atmospheric Chemistry and Physics 7: 3115-3127.

Villeneuve, P.J., M.S. Goldberg, R.T. Burnett, A. van Donkelaar, H. Chen and R.V. Martin, 2011. Associations between cigarette smoking, obesity, sociodemographic characteristics, and remote sensing derived estimates of ambient $PM_{2.5}$: Results from a Canadian population-based survey. Journal of Occupational and Environmental Medicine 68(12): 920-7.

Voulgarakis, A., P.J. Telford, A.M. Aghedo, P. Braesicke, G. Faluvegi, N.L. Abraham, K.W. Bowman, J.A. Pyle and D.T. Shindell, 2011. Global multi-year O_3-CO correlation patterns from models and TES satellite observations. Atmospheric Chemistry and Physics 11: 5,819-5,838. doi:10.5194/acp-11-5819-2011.

Wald, L. and J.M. Baleynaud, 1999. Observing air quality over the city of Nantes by means of Landsat thermal infrared data. International Journal of Remote Sensing 20(5): 947-959.

Walker, J.C., E. Carboni, A. Dudhia and R.G. Grainger, 2012. Improved detection of sulphur dioxide in volcanic plumes using satellite-based hyperspectral infrared measurements: Application to the Eyjafjallajökull 2010 eruption. Journal of Geophysical Research 117: D00U16. doi:10.1029/2011JD016810.

Wang, J., S.A. Christopher, U.S. Nair, J.S. Reid, E.M. Prins, J. Szykman and J.L. Hand, 2006. Mesoscale modeling of Central American smoke transport to the United States: 1. "Top-down" assessment of emission strength and diurnal variation impacts. Journal of Geophysical Research 111: D05S17. doi:10.1029/2005JD006416.

Wang, J., X. Xu, D.K. Henze, J. Zeng, Q. Ji, S-C. Tsay and J. Huang, 2012. Top-down estimate of dust emissions through integration of MODIS and MISR aerosol retrievals with the GEOS-Chem adjoint model. Geophysical Research Letters 39: L08802. doi:10.1029/2012GL051136.

Warner, J., M.M. Comer, C.D. Barnet, W.W. McMillan, W. Wolf, E. Maddy and G. Sachse, 2007. A comparison of satellite tropospheric carbon monoxide measurements from AIRS and MOPITT during INTEX-A. Journal of Geophysical Research 112: D12S17. doi:10.1029/2006JD007925.

Wells, K.C., D.B. Millet, L. Hu, K.E. Cady-Pereira, Y. Xiao, M.W. Shephard, C.L. Clerbaux, L. Clarisse, P-F. Coheur, E.C. Apel, J. de Gouw, C. Warneke, H.B. Singh, A.H. Goldstein and B.C. Sive, 2012. Tropospheric methanol observations from space: retrieval evaluation and constraints on the seasonality of biogenic emissions. Atmospheric Chemistry and Physics 12: 5,897-5,912. doi:10.5194/acp-12-5897-2012.

Wespes, C., L. Emmons, D.P. Edwards, J. Hannigan, D. Hurtmans, M. Saunois, P-F. Coheur, C. Clerbaux, M.T. Coffey, R.L. Batchelor, R. Lindenmaier, K. Strong, A.J. Weinheimer, J.B. Nowak, T.B. Ryerson, J.D. Crounse and P.O. Wennberg, 2012. Analysis of ozone and nitric acid in spring and summer Arctic pollution using aircraft, ground-based, satellite observations and MOZART-4 model: Source attribution and partitioning. Atmospheric Chemistry and Physics 12: 237-259. doi:10.5194/acp-12-237-2012.

Winker, D., Z. Liu, A. Omar, J. Tackett and D. Fairlie, 2012. CALIOP observations of the transport of ash from the Eyjafjallajokull volcano in April 2010. Journal of Geophysical Research 117: D00U15. http://dx.doi.org/10.1029/2011JD016499.

Winker, D.M., Pelon, J., J. A. Jr Coakley, S. A. Ackerman, R. J. Charlson, P. R. Colarco, P. Flamant, Q. Fu, R. M. Hoff, C. Kittaka, T. L. Kubar, H. Le Treut, M. P. McCormick, G. Megie, L. Poole, K. Powell, C. Trepte, M. A. Vaughan, B. A. Wielicki, 2010. The CALIPSO mission: A global 3D view of aerosols and clouds. Bulletin of the American Meteorological Society 91: 1,211-1,229.

Winker, D.M. and M.T. Osborn, 1992. Preliminary analysis of observations of the Pinatubo volcanic plume with a polarization-sensitive LiDAR. Geophysical Research Letters 19(2): 171-174. http://dx.doi.org/10.1029/91GL02866.

Winker, D.M., M.A. Vaughan, A. Omar, Y. Hu, K.A. Powell, Z. Liu, W.H. Hunt and S.A. Young, 2009. Overview of the CALIPSO mission and CALIOP data processing algorithms. Journal of Atmospheric and Oceanic Technology 26: 2310-2323.

Wittrock, F., A. Richter, H. Oetjen, J.P. Burrows, M. Kanakidou, S. Myriokefalitakis, R. Volkamer, S. Beirle, U. Platt and T. Wagner, 2006. Simultaneous global observations of glyoxal and formaldehyde from space. Geophysical Research Letters 33: L16804. doi:10.1029/2006GL026310.

Wong, M.S., M.I. Shahzad, J.E. Nichol, K.H. Lee and P.W. Chan, 2013. Validation of MODIS, MISR, OMI, and CALIPSO aerosol optical thickness using ground based sunphotometers in Hong Kong. International Journal of Remote Sensing 34: 3897-3918. doi:10.1080/01431161.2012.72073.

Worden, H.M., M.N. Deeter, D.P. Edwards, J.C. Gille, J.R. Drummond and P.P. Nedelec, 2010. Observations of near-surface carbon monoxide from space using MOPITT multispectral retrievals. Journal of Geophysical Research 115, D18314. doi:10.1029/2010JD014242.

Worden, H.M., M.N. Deeter, C. Frankenberg, M. George, F. Nichitiu, J. Worden, I. Aben, K.W. Bowman, C. Clerbaux, P-F. Coheur, A.T.J. de Laat, R. Detweiler, J.R. Drummond, D.P. Edwards, J.C. Gille, D. Hurtmans, M. Luo, S. Martínez-Alonso, S. Massie, G. Pfister and J.X. Warner, 2013. Decadal record of satellite carbon monoxide observations. Atmospheric Chemistry and Physics 13: 837-850.

Worden, H.M., J.A. Logan, J.R. Worden, R. Beer, K. Bowman, S.A. Clough, A. Eldering, B.M. Fisher, M.R. Gunson, R.L. Herman, M.C. Lampel, M. Luo, I.A. Megretskaia, G.B. Osterman and M.W. Shephard, 2007. Comparisons of Tropospheric Emission Spectrometer (TES) ozone profiles to ozonesondes: Methods and initial results. Journal of Geophysical Research 112: D03309. doi:10.1029/2006JD007258.

Worden, J., S.S. Kulawik, M.W. Shephard, S.A. Clough, H. Worden, K. Bowman and A. Goldman, 2004. Predicted errors of tropospheric emission spectrometer nadir retrievals from spectral window selection. Journal of Geophysical Research 109: D09308. doi:10.1029/2004JD004522.

Wright D., L. Grego and L. Gronlund, 2005. The physics of space security: A reference manual. American Academy of Arts and Sciences, Cambridge, Massachusetts. http://ucsusa.org/assets/documents/nwgs/physics-space-security.pdf.

Xiong, X., C. Barnet, E. Maddy, J. Wei, X. Liu and T.S. Pagano, 2010. Seven years' observation of mid-upper tropospheric methane from Atmospheric Infrared Sounder. Remote Sensing 2: 2509-2530.

Xiong, X., S. Houweling, J. Wei, E. Maddy, F. Sun and C. Barnet, 2009. Methane plume over south Asia during the monsoon season: satellite observation and model simulation. Atmospheric Chemistry and Physics 9: 783-794.

Xu, X., J. Wang, D.K. Henze, W. Qu and M. Kopacz, 2013. Constraints on aerosol sources using GEOSChem adjoint and MODIS radiances, and evaluation with multisensor (OMI, MISR) data. Journal of Geophysical Research 118: 6396-6413. doi:10.1002/jgrd.50515.

Yang, W., A. Marshak, T. Várnai, O.V. Kalashnikova and A.B. Kostinski, 2012. CALIPSO observations of transatlantic dust: vertical stratification and effect of clouds. Atmospheric Chemistry and Physics 12: 11339-11354. doi:10.5194/acp-12-11339-2012.

Yu, H., L.A. Remer, M. Chin, H. Bian, R. Kleidman and T. Diehl, 2008. A satellite- based assessment of trans-Pacific transport of pollution aerosol. Journal of Geophysical Research 113: D14S12.

Yu, H., L.A. Remer, M. Chin, H. Bian, Q. Tan, T. Yuan and Y. Zhang, 2012. Aerosols from overseas rival domestic emissions over North America. Science 337: 566-569.

Zhang, L., D.J. Jacob, K.F. Boersma, D.A. Jaffe, J.R. Olson, K.W. Bowman, J.R. Worden, A.M. Thompson, M.A. Avery and R.C. Cohen, 2008. Transpacific transport of ozone pollution and the effect of recent Asian emission increases on air quality in North America: an integrated analysis using satellite, aircraft, ozonesonde, and surface observations. Atmospheric Chemistry and Physics 8: 6117-6136.

Zhang, H., R.M. Hoff and J.A. Engel-Cox, 2009. The relation between Moderate Resolution Imaging Spectroradiometer (MODIS) aerosol optical depth and $PM_{2.5}$ over the United States: A geographical comparison by EPA regions. Journal of the Air & Waste Management Association 59: 1358-1369.

Zhao, C., L. Peng, X.X. Tie, Y. Lin, C. Li, X. Zheng and Y. Fang, 2007. A high CO episode of long-range transport detected by MOPITT. Water, Air, & Soil Pollution 178: 207-216. doi:10.1007/sl11270-006-9191-1.

Zhao, Q., W. Gao, W. Xiang, R. Shi, C. Liu, T. Zhai, H.A. Huang, L.E. Gumley and K. Strabala, 2013. Analysis of air quality variability in Shanghai using AOD and API data in the recent decade. Frontiers of Earth Science 7(2): 159-168.

Zhao, Y., L. Duan, J. Xing, T. Larssen, C.P. Nielsen and J. Hao, 2009. Soil acidification in China: Is controlling SO_2 emissions enough? Environmental Science and Technology 43(21): 8021-8026.

Zhu, L., D.K. Henze, K.E. Cady-Pereira, M.W. Shephard, M. Luo, R.W. Pinder, J.O. Bash and G-R. Jeong, 2013. Constraining U.S. ammonia emissions using TES remote sensing observations and the GEOS-Chem adjoint model. Journal of Geophysical Research 118: 3355-3368.

7 GLOSSARY

7.1 Terms

Active Remote Sensing

A system that emits its own radiation from the active remote sensors and detects back-scattered radiation from the target.

Aerosol

Solid or liquid particles suspended in air or other gaseous environment.

Air Mass Factor (AMF)

The ratio of the slant column to the vertical column.

Geospatial

Relating to or denoting data that is associated with a particular location.

Ground Track

The path on the earth's surface below an aircraft, or satellite.

Inclination Angle

The angle between the equatorial plane and the orbital plane.

Limb Geometry

In this geometry light scattered from the Earth's edge is analysed by sampling the atmosphere tangentially.

Mixing Ratio

The ratio of the number density of the gas to the total number density of the atmosphere.

Nadir Geometry

Refers to atmospheric volume observations directly beneath the instrument (i.e., the spacecraft).

Negative Bias

The persistent negative difference between two fields.

Occultation

A system of observing the light of the rising or setting sun, moon, or stars through the atmosphere at different tangent altitudes.

Oversampling

The process of averaging observations from a large number of satellite overpasses, each at a slightly different location to get better spatial resolution.

Passive Remote Sensing

A system that measures the reflected and emitted electromagnetic radiation that is coming from naturally available passive sensors (e.g., the sun), after it has passed through the atmosphere.

Polar Orbit

An orbit that has an inclination near 90 degrees, so a satellite passes over both poles of the body being orbited on every revolution.

Positive Bias

The persistent positive difference between two fields.

Retrieval

The inferred concentration of chemical species from the observed radiation.

Slant Column Density

The trace gas concentration integrated along the atmospheric light paths.

Solar Back Scatter

The process by which electromagnetic radiation interacts with and is redirected by the molecules of the atmosphere, ocean, or land surface.

Spatial Resolution

The smallest area on the ground (pixel) that can be resolved by satellite sensor.

Spectral Region

Refers to a finite segment of wavelengths in the electromagnetic spectrum.

Stratosphere
The region of the atmosphere extending from the top of the troposphere (the tropopause), at heights of approximately 8 km at the poles to 15 km at the equator, to the base of the mesosphere (the stratopause), at a height of roughly 50 km.

Sun-synchronous

Describes the orbit of a satellite that crosses the equator and each latitude at a fixed local time each day.

Swath Width

The width of the area observed by a satellite as it orbits the Earth.

Temporal Resolution

Refers to the time needed to revisit and acquire data for the exact same location.

Time Curtain

The contour plot that has x axis as time, y axis as an altitude, and z axis as the measured quantity.

Troposphere

The lower part of the atmosphere, to a height varying from about 8 km at the poles to 15 km at the equator, where temperature generally decreases with altitude, clouds form, precipitation occurs, and convection currents are active.

7.2   List of Acronyms

A	Averaging kernel
AAI	Absorbing Aerosol Index
AAOD	Absorbing Aerosol Optical Depth
ADEOS	Advanced Earth Observing System
AERONET	Aerosol Robotic Network
AIRS	Atmospheric Infrared Sounder
AMF	Air Mass Factor
AOD	Aerosol Optical Depth
API	Air Pollution Index

ARCTAS	Arctic Research of the Composition of the Troposphere from Aircraft and Satellites
AVHRR	Advanced Very High Resolution Radiometer
BUV	Backscattered Ultraviolet
CALIOP	Cloud-Aerosol LiDAR with Orthogonal Polarization
CALIPSO	Cloud Aerosol LiDAR and Infrared Pathfinder Satellite Observations
CASA	Clean Air Strategic Alliance
CTM	Chemical Transport Model
DDV	Dense Dark Vegetation
DOAS	Differential Optical Absorption Spectroscopy
DOFS	Degrees Of Freedom for Signal
DU	Dobson Units
EI	Emissions Inventories
ENVISAT	Environmental Satellite
EOS	Earth Observing System
ERTS	Earth Resources Technology Satellite
ESA	European Space Agency
EUMETSAT	European Organization for the Exploitation of Meteorological Satellites
FM	Fine Mode
FMF	Fine Mode Fraction
FRP	Fire Radiative Power
FTIR	Fourier Transform Infrared Spectroscopy
FTS	Fourier Transform Spectrometer
GDAS	Global Data Assimilation System
GEO	Geo-Stationary Orbits
GEO-CAPE	Geostationary Coastal and Air Pollution Events
GOME	Global Ozone Monitoring Experiment
HIRDLS	High Resolution Dynamics Limb Sounder
HYSPLIT	Hybrid Single Particle Lagrangian Integrated Trajectory

IAGOS	In service Aircraft for Global Observing System
IASI	Infrared Atmospheric Sounding Interferometer
KARI	Korea Aerospace Research Institute
LANCE	Land Atmosphere Near-real time Capability for EOS
LEO	Low Earth Orbits
MAPS	Measurements of Atmospheric Pollution from Satellites
MISR	Multi-angle Imaging SpectroRadiometer
MLS	Microwave Limb Sounder
MODIS	Moderate Resolution Imaging Spectroradiometer
MOPITT	Measurements of Pollution in the Troposphere
MSS	Multi Spectral Scanner
NASA	National Aeronautics and Space Administration
NCAR	National Center for Atmospheric Research
NCEP	National Centers for Environmental Prediction
NIR	Near-Infrared
NOAA	National Oceanic and Atmospheric Administration
NRC	National Research Council
OMI	Ozone Monitoring Instrument
OSRIN	Oil Sands Research and Information Network
PARASOL	Polarization & Anisotropy of Reflectances for Atmospheric Sciences coupled with Observations from a LiDAR
PBL	Planetary Boundary Layer
POLDER	Polarization and Directionality of the Earth's Reflectances
RAQM	Real-time Air Quality Modeling System
SCIAMACHY	SCanning Imaging Absorption SpectroMeter for Atmospheric CHartographY
SEE	School of Energy and the Environment
SERS	Second European Research Satellite
TEMPO	Tropospheric Emissions: Monitoring of Pollution
TES	Tropospheric Emission Spectrometer
TIR	Thermal Infrared

TOMS	Total Ozone Mapping Spectrometer
TROPOMI	TROPOspheric Monitoring Instrument
UV	Ultra Violet
Vis	Visible

7.3 Aerosols, Gases and Pollutants

BrO	Hypobromite
CFC	Chlorofluorocarbons
C_2H_2	Acetylene
C_3H_6	Cyclopropane
C_4H_4O	Furan
CH_3OH	Methanol
CH_4	Methane
CO	Carbon monoxide
CO_2	Carbon dioxide
H_2O	Water
HCl	Hydrochloric acid
HCHO	Formaldehyde
HCOOH	Formic acid
HF	Hydroflouric acid
HNO_3	Nitric acid
N_2	Nitrogen
N_2O	Nitrous oxide
$(NH_4)_2SO_4$	Ammonium sulphate
NO_2	Nitrogen dioxide
O_3	Ozone
OClO	Chlorine dioxide
OCS	Carbonyl sulfide
PAN	Peroxyacyl nitrates
PM	Particulate Matter

PM$_{2.5}$	The fine particulate matter with aerodynamic diameter less than 2.5 μm
SO$_2$	Sulphur dioxide
VOC	Volatile Organic Carbon

APPENDIX 1: Spatial and Temporal Variation of CO Over Alberta Using Measurements From Satellite, Aircrafts, and Ground Stations

Heba S Marey[1,2], Zaher Hashisho[1], Long Fu[3] and John Gille[4]

[1] University of Alberta, Department of Civil and Environmental Engineering, Edmonton, Alberta, Canada

[2] Alexandria University, Institute of Graduate Studies and Research, Alexandria, Egypt.

[3] Alberta Environment and Sustainable Resource Development, Environmental Monitoring, Alberta, Canada

[4] National Center for Atmospheric Research, Boulder, Colorado, USA.

A similar version of this study will be submitted for journal publication.

Alberta is Canada's largest oil producer and its oil sand deposits comprise 30% of the world's oil reserves. The process of bitumen extraction and upgrading releases trace gases and aerosols to the atmosphere. In this study we present satellite-based analysis to explore, for the first time, various contributing factors that affect tropospheric carbon monoxide (CO) levels over Alberta. The multispectral products that use both near-infrared (NIR) and thermal-infrared (TIR) radiances for CO retrieval from Measurements of Pollution in the Troposphere (MOPITT) are examined for the 13 year period from 2000 to 2012. The Moderate Resolution Imaging Spectroradiometer (MODIS) thermal anomaly product from 2001 to 2012 is employed to investigate the seasonal and temporal variations of forest fires. Additionally, in-situ CO measurements at industrial and urban sites are compared to satellite data. Furthermore, the available MOZAIC/IAGOS aircraft CO profiles (April 2009 to December 2011) are used to validate MOPITT CO data.

The climatological time curtain plot and spatial maps for CO over northern Alberta indicate the signatures of transported CO for two distinct biomass burning seasons, summer and spring. Distinct seasonal patterns of CO at the urban sites (Edmonton and Calgary cities) point to the strong influence of traffic. Meteorological parameters play an important role on the CO spatial distribution at various pressure levels. Northern Alberta shows stronger upward lifting motion which leads to pronounced CO total column values while the poor dispersion in central and south Alberta exacerbates the surface CO pollution. Inter-annual variations of satellite data depict a slightly decreasing trend for both regions while the decline trend is more evident from ground observations, especially at the urban sites.

MOPITT CO vertical averages and MOZAIC/IAGOS aircraft profiles were in good agreement within the standard deviations at all pressure levels. There is consistency between the time evolutions of high CO episodes, monitored by satellite and ground measurements, and the fire frequency peak time which implies that biomass burning affects tropospheric CO distribution in northern Alberta.

These findings have further demonstrated the potential use of the MOPITT V5 multispectral (NIR+TIR) product for assessing a complicated surface process.

INTRODUCTION

Canada's crude oil reserves are the world's 3rd largest after Saudi Arabia and Venezuela, and Canada is currently the world's 7th largest producer of crude oil (Canadian Association of Petroleum Producers 2012). Alberta is Canada's largest oil producer and its oil sands deposits comprise 30% of the world's oil reserves (Kean 2009). Alberta's oil sands deposits are located in three regions: Athabasca, Peace River and Cold Lake. The Athabasca oil sands region (AOSR) (Figure 1) contains most of the oil sands reserves. About 20% of the deposits in the Athabasca region are shallow (<75 m deep) and hence can be surface mined.

Figure 1.   Alberta's oil sands deposits in the Athabasca, Peace River and Cold Lake regions (Percy 2013).

The bitumen contained within the sand is extremely heavy crude oil, requiring heat or solvents to extract it from the sand (Alberta Environment 2012). Processing mined bitumen utilizes hot water and caustic for extraction; the process releases SO_2, H_2S and light hydrocarbons as well as CO_2 and CO (Strausz et al. 1977). After extraction, bitumen is separated from the water and solids using solvents/diluents such as naphtha (Siddique et al. 2007) and paraffins (Siddique et al. 2006) which are also used to decrease bitumen's viscosity. Deeper deposits are not recoverable by surface mining so in-situ recovery methods such as steam injection are used.

The rapid expansion of oil sands developments, and massive energy requirements (NEB 2013) to extract and upgrade the bitumen, lead to numerous environmental concerns, particularly for air quality (Timoney and Lee 2009) and hence an environmental monitoring program that measures the ambient air quality is needed. Air monitoring in Alberta is carried out through airshed associations that were launched as non-profit societies under the umbrella of the Clean Air Strategic Alliance (CASA). Air quality in the AOSR is monitored locally by the Wood Buffalo Environmental Association (WBEA), which is a multi-stakeholder organization (Wood Buffalo Environmental Association 2013).

In addition to the existing continuous air quality monitoring network in Alberta, independent studies were conducted to investigate the impact of the oil sands mining operations on the air quality over Alberta (e.g., Bytnerowicz et al. 2010, Howell et al. 2014, Jacob et al. 2010, Simpson et al. 2010). Recent studies of aerosol and trace gas emissions were carried out in summer 2008 when the NASA DC-8 and P-3B research aircraft were deployed at the Canadian Forces Base Cold Lake (Jacob et al. 2010). Their work reported significantly elevated levels of trace gases (CO_2, CH_4, CO, NO, NO_2, NOy, SO_2 and 53 VOCs) above background (Simpson et al. 2010). However, these data are limited in spatial coverage as they reflect local air quality and cannot provide information about the overall regional air quality.

A complementary approach to surface and aircraft measurements is satellite-based monitoring which can provide large spatial coverage and make measurements over extended periods of time, allowing the study of the impact of intense emission sources on regional and global scale air quality. Over the last decade, satellite remote sensing of trace gases and aerosols for air quality applications has progressed (Martin 2008). Despite the emerging importance of using satellites in air quality applications, there was no research using them over Alberta until 2012, when McLinden et al. (2012) employed the Ozone Monitoring Instrument (OMI) for NO_2 and SO_2 assessment over the AOSR. They presented high-resolution maps that revealed distinct increases for both species over the area of intensive surface mining compared with background levels. In addition, they showed that NO_2 was increasing at a rate of 11%/year which is generally consistent with the annual increase of bitumen production. Accordingly, further study to characterize more trace gases and aerosols that are emitted from various natural and anthropogenic sources in Alberta is required.

Beside oil sands operations, Alberta has other anthropogenic sources, such as combustion of fossil fuels and various industrial processes which emitted about 432,277 tonnes of CO in 2011(Environment Canada 2011). Additionally, natural emissions such as boreal forest fires are a major source of CO. Boreal forest fires in summer influence the carbon cycle (Preston and Schmidt 2006), climate (Amiro et al. 2001), and air quality of the Arctic atmosphere (Colarco et al. 2004). The fire frequency at high latitudes (>55∘ N), is expected to increase (Gillett et al. 2004, Girardin 2007) as a result of global warming (Flannigan et al. 2005, Stocks et al. 1998) which is accompanied by increased dryness and temperature (Marlon et al. 2008).

One of the most important trace gases emitted from anthropogenic pollution and biomass burning is CO. CO can also be produced from photochemical oxidation of CH_4 and non-methane hydrocarbons (Duncan et al. 2007, Novelli et al. 1998). CO plays a critical role in the

tropospheric chemistry where it is the dominant sink of the hydroxyl radical (OH), which is the major oxidizing agent in the troposphere. It has also significant impacts on regional air quality where it can be a precursor to photochemical ozone smog in areas with sufficient NO_x (Ridley et al. 1992). Additionally, CO was recognized as an important indirect greenhouse gas that could have an effect on global climate (Daniel and Solomon 1998).

With a relatively long life-time (the global average CO lifetime is about 2 months), CO is an excellent tracer for tropospheric transport processes (Pétron et al. 2004) and plumes from strong emission sources that are extending great distances. Fortunately, CO is one of the few tropospheric gases that can be successfully monitored from space at the present time. It can be measured by the Measurements of Pollution in the Troposphere (MOPITT) instrument which has global data from 2000 till now. This long term record of MOPITT data allows investigating the inter-annual and spatial variability of tropospheric CO air quality.

The current study aims to address the general features of the overall CO loading over Alberta using MOPITT data. Major source contributions of CO and their impacts on temporal and spatial variability will be examined through the use of MOPITT and Moderate Resolution Imaging Spectroradiometer (MODIS) sensors, meteorology and ground level measurements. This work is the first study to explore various contributing factors that affect tropospheric CO levels over Alberta using satellite remote sensing observations. The data and methods used in the study are described briefly. Climatological spatial distribution and time-altitude profiles of MOPITT CO over Alberta are presented and compared with aircraft CO profiles and ground-level measurements. Contribution of forest fires to CO levels in the AOSR are analysed using MODIS fire counts analysis.

DATA AND METHODS

This study uses data from two satellite instruments, MODIS (available from https://earthdata.nasa.gov/data/near-real-time-data/firms) and MOPITT V5J (available from ftp://l5eil01.larc.nasa.gov/MOPITT/MOP02J.005) coupled with ground measurement data (available from http://www.casadata.org/). Fort McMurray, Edmonton, and Calgary are chosen for analysis where the former represents an industrial region and the latter two represent urban regions. The boundaries of the study areas are:

Fort McMurray	56.0 to 58.0N	112.0 to 110.0W
Edmonton	52.0 to 54.0N	114.0 to 112.0W
Calgary	50.0 to 52.0N	115.0 to 113.0W

Satellite Data

MOPITT

The MOPITT instrument on board the Terra spacecraft is specifically designed to measure CO and CH_4 columns (Drummond 1992). It takes about 3 days for near-complete global coverage with a horizontal resolution of 22 km $\times$ 22 km at nadir (Deeter et al. 2003). MOPITT has a

unique feature, compared to other tropospheric CO satellite instruments, as it measure CO simultaneously in both the thermal infrared (TIR) band (4.7 µm) and the near-infrared (NIR) band (2.3 µm). The NIR observations mainly provide information about the CO total column whereas TIR radiances are often most sensitive to CO in the middle and upper-troposphere.

In this study we used the MOPITT multispectral product that exploits both channels (TIR+ NIR) which has been shown to have higher sensitivity to CO in the lower troposphere (Deeter et al. 2011, 2012, Jiang et al. 2013, Worden et al. 2010). MOPITT V5 data have been recently validated using in situ CO profiles measured from aircrafts (Deeter et al. 2013). Only daytime MOPITT retrievals were used in this study because they have better information content than nighttime data (Deeter et al. 2010).

MODIS Thermal Anomaly Products

MODIS sensors are located on the Terra and Aqua satellite platforms. They were designed to offer a broad range of information about land, oceanic, and atmospheric conditions (Kaufman et al. 1998a, Masuoka et al. 1998). They detect fires globally on a daily basis at 1 km spatial resolution. The fire detection algorithm has been described by Kaufman et al. (1998b) and Giglio et al. (2003).

In this study we used the Collection 5.1 Terra and Aqua MODIS MOD1/MYD14 product from November 2000 (Terra) and July 2002 (Aqua) through December 2012. Each fire pixel is associated with a confidence limit parameter to specify the quality of the data which ranges from 0% to 100% (Giglio 2007). The threshold limit for fire pixel confidence that is used in this study is 20%. We used the MODIS fire data in shape file format to use them in geographic information system (GIS) maps. Data were obtained from the Land Atmosphere Near-real time Capability for EOS (LANCE) system operated by the NASA/GSFC/Earth Science Data.

CASA Ground Measurements

CASA Data Warehouse is a central repository for ambient air quality data collected in Alberta. In-situ measurements of surface CO are recorded at nine monitoring stations. CO is monitored continuously either by non-dispersive infrared photometry or gas filter correlation (Alberta Environment 2013).

MOZAIC/IAGOS (In service Aircraft for Global Observing System) Aircraft Measurements

IAGOS (formerly MOZAIC) instruments, used onboard commercial aircraft since August 1994, aim to sample tropospheric gases with high vertical resolution over about 50 airports (Marenco et al. 1998). CO has been monitored since 2001 using the infrared CO analyzer (Model 48CTL from Thermo Environmental Instruments, USA) with a precision of ±5 ppbv (Nedelec et al. 2003). Data are available at http://www.iagos.org.

Meteorological Data and HYSPLIT Trajectories

The HYSPLIT (Hybrid Single-Particle Lagrangian Integrated Trajectory) model Version 4 was used to generate air mass backward trajectories. It is the latest version of an integrated system for computing air parcel trajectories, dispersion and deposition simulations. The model calculates the trajectories using the Global Data Assimilation System (GDAS) meteorological dataset which has been operated by National Centers for Environmental Prediction (NCEP) (Draxler and Rolph 2013, Rolph 2013). Trajectory calculation is conducted by time integration of the position of an air parcel as it is transported by the 3-D winds (Draxler and Hess 1998). Data of mean monthly omega for the study period were taken from the National Oceanic and Atmospheric Administration (NOAA) Climate Data Assimilation System I, based on the National Centers for Environmental Prediction/National Center for Atmospheric Research (NCEP/NCAR) Reanalysis Project. The NCEP/NCAR global re-analysis meteorological dataset is described in detail by Kalnay et al. (1996).

RESULTS AND DISCUSSION

Climatological Spatial Distribution of MOPITT CO over Alberta

Figure 2 shows the seasonally averaged distribution of MOPITT CO total column measurements over Alberta for the period March 2000 to December 2012. The symbols F, E and C represent Fort McMurray, Edmonton and Calgary, respectively. Data are gridded at 0.25 x 0.25 degree resolution.

High CO loadings extended from the North East to North West of Alberta in all seasons except in winter (December to February) where the spatial variations are less prominent. Maximum variations around Fort McMurray are more remarkable in the spring (March to May) where the CO total column ranges are 2.5 to 2.75 • 10^{18} and 2.0 to 2.25 • 10^{18} molecules cm^{-2}, respectively. Additionally, it is apparent that summer (June to August) and fall (September to November) seasons displayed minimum CO loading, especially in the center and south of Alberta.

The spatial distributions of CO mixing ratios at the surface level (Figure 3) reveal distinct enhancements, covering south east Alberta in winter with CO mixing ratios of 180 to 200 ppb. While in the spring, the CO mixing ratios are generally high in the whole province. Thus, the spatial distributions of surface CO in spring and winter have a different pattern than CO total column (Figure 2) for the same period. However, summer season demonstrated relatively high surface CO concentrations (140 to160 ppb) north of Fort McMurray, although it shows minimum levels for the rest of Alberta, while fall season illustrates similar spatial distribution.
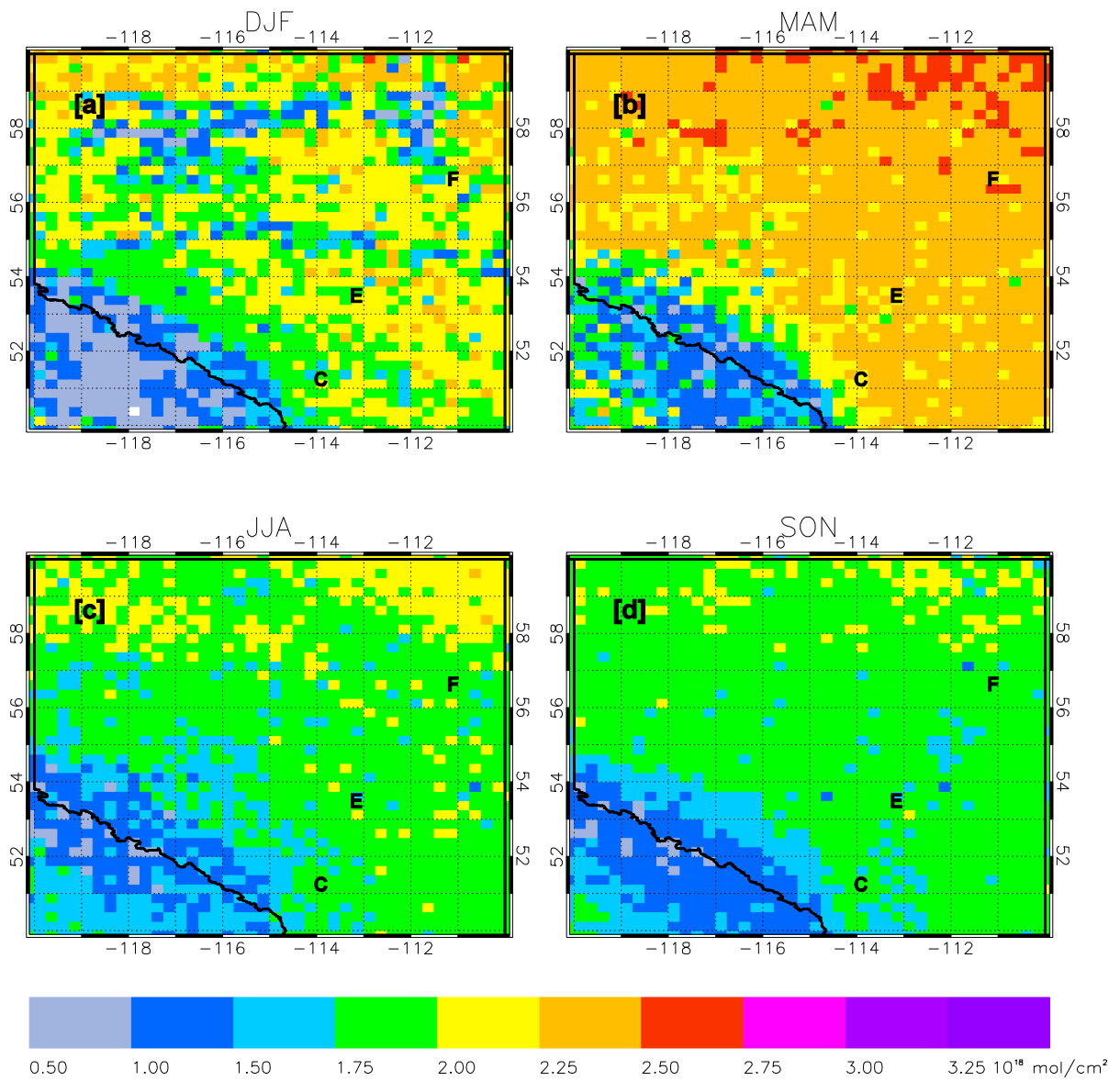
Figure 2.   The MOPITT daytime CO total column measurements over Alberta for the period
            March 2000 to December 2012 in (a) winter, (b) spring, (c) summer and (d) fall.
            The symbols F, E and C represent Fort McMurray, Edmonton Calgary, respectively.
   Data are gridded at 0.25 x 0.25 degree resolution.
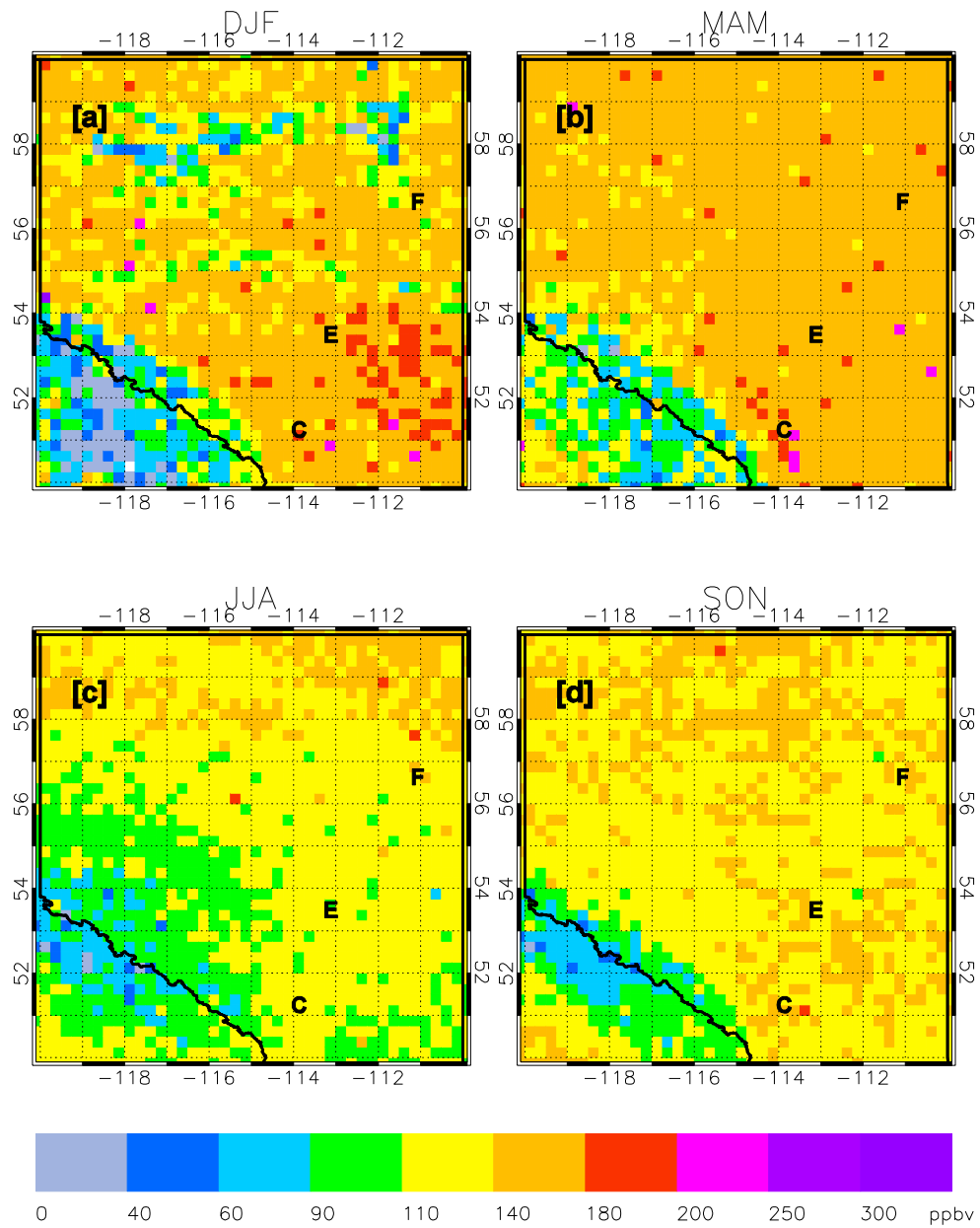
Figure 3.   MOPITT daytime CO mixing ratios at the surface level over Alberta for the period March 2000 to December 2012 in (a) winter, (b) spring, (c) summer and (d) fall. The symbols F, E and C represent Fort McMurray, Edmonton and Calgary, respectively. Data are gridded at 0.25 x 0.25 degree resolution.

73

To assist in the interpretation of the results, the vertical velocity (Omega) which is defined as change of pressure with time is analyzed. The spatial distributions of Omega (dp/dt) at pressure level 850 mb for four seasons are depicted in Figure 4. They demonstrate upward movements of air mass in the northeast and southwest areas of Alberta as indicated by negative values. This suggests that the CO emissions are uplifted raising the CO total column values in the north area. Conversely, downward movements (positive values) are recorded in the central and south east areas of Alberta allowing subsidence of CO emissions as conditions are favorable. Therefore, there is a general consistency between the climatological maps of Omega and the CO spatial distributions where the CO total columns shows remarkable enhancements in the north while there are elevated surface CO values in the south. This highlights the important role of meteorological parameters in ambient air quality.

The southwestern area of Alberta exhibits minimum CO levels, which are less than 1.5 molecule/cm^2 and 60 ppb for CO total column (Figure 2) and surface concentration (Figure 3), respectively. Alberta has a varied topography, from mountain peaks along the western border, to lowland areas in northeastern Alberta. It follows, then, that topographical features influence air quality – mountainous regions with little population contribute to background conditions of CO resulting in the lowest CO concentrations in the southwest area of Alberta.

The main sources of CO in the atmosphere are combustion processes and photochemical oxidation of hydrocarbons (Duncan et al. 2007, Novelli et al. 1998). Hence, it is assumed that CO spatial variations in northern Alberta are associated with oil sands industrial activities. It is reported that the oil sands industry consumption of natural gas was 17 x 10^6 m^3/day in 2003 and is expected to increase to 40 to 45 million m^3/day in 2015 (National Energy Board 2013).

Extracted bitumen is upgraded at mine sites north of Fort McMurray as well as at downstream industrial centres such as the industrial heartland in Fort Saskatchewan (north east Edmonton). A small fraction of diluent (mainly aromatic and aliphatic hydrocarbons) used in bitumen extraction and transport is emitted to the atmosphere (Siddique et al. 2006, 2007). As reported in earlier studies, the measured CO on July 10, 2008, as part of Arctic Research of the Composition of the Troposphere from Aircraft and Satellites (ARCTAS) mission, showed a strong correlation with alkanes, aromatics and cycloalkanes that are associated with direct emissions from the oil sands and/or diluent (Simpson et al. 2010). Furthermore, the timing, distribution of other sporadic sources such as fires, and the effects of large-scale transport have a substantial influence on the spatial discrepancies of CO.
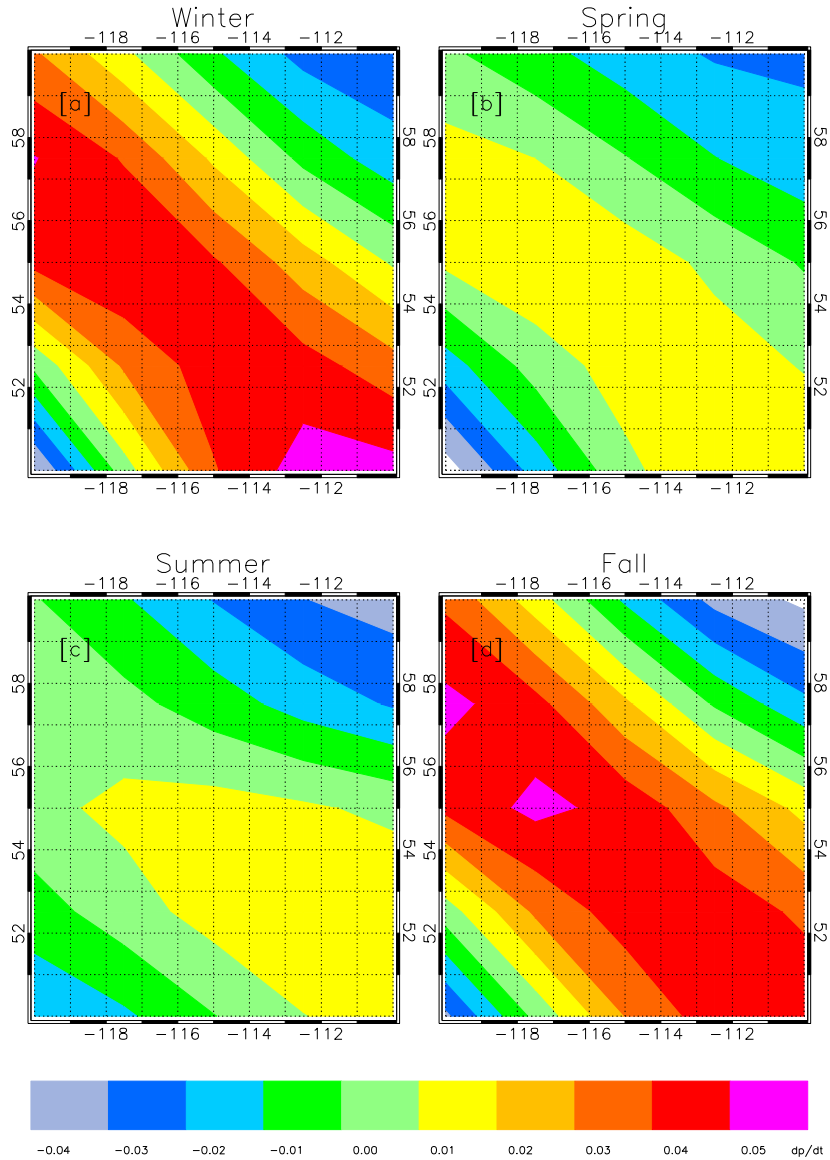
Figure 4. Spatial distributions of Omega at pressure level 850 mb for the period from 2000 to 2012 in winter (a), spring (b), summer (c), and fall (d).

Time-Altitude MOPITT CO

To gain further insight about the impact of various emission sources on CO levels, temporal climatology of 13 years for Fort McMurray, Edmonton, and Calgary areas are calculated. The monthly mean CO profiles using all the available MOPITT data between March 2000 and December 2012 are used for altitude/month contours for the two regions (Figure 5). The vertical profiles of MOPITT CO are retrieved on only 10 altitude levels (surface, 900, 800, 700, 600, 500, 400, 300, 200, 100 hPa), so levels in between have been linearly interpolated. Generally,

75

the regions demonstrate the same profile structure where CO mixing ratios are higher at low altitudes (high pressure) than high altitudes (low pressure).
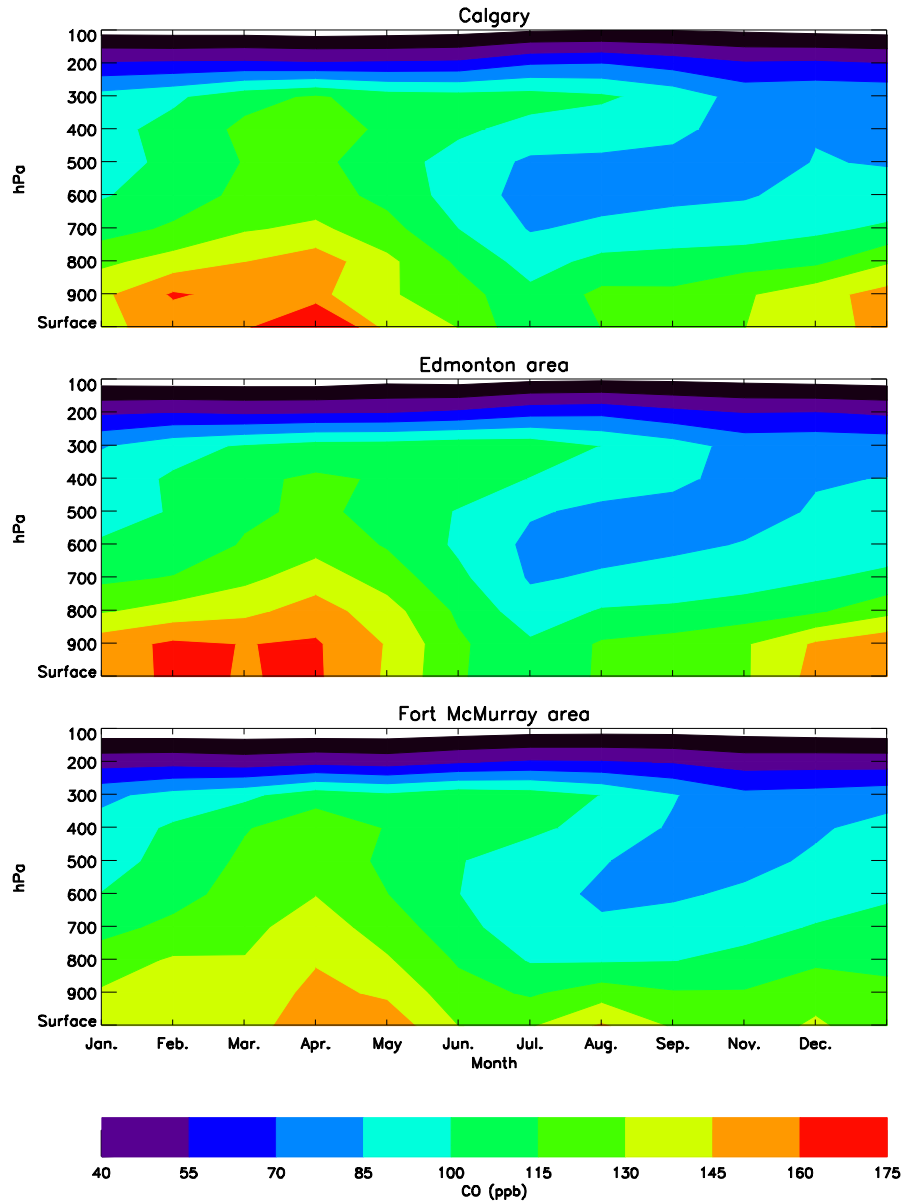

Figure 5.   Climatological MOPITT CO profiles for the period March 2000 to December 2012 over Calgary, Edmonton, and Fort McMurray area.

At Edmonton and Calgary, vertical CO profile exhibits significant elevated levels in winter and spring, occurring in February and April with maximum mixing ratios of 160 to 175 ppb at low

altitude levels (≤ 800 hPa), while it shows minimum mixing ratios in summer. This pattern is consistent with the general seasonal cycle of CO in the Northern Hemisphere. Edwards et al. (2004) analyzed CO variability from the Terra MOPITT satellite in the Northern Hemisphere and their results showed peak values in the early spring due to fossil fuel burning for heating and increased power requirements. The wintertime CO emissions persist for several weeks after the emissions themselves have ceased causing high CO concentrations which are detected in early spring. In fact, the seasonal cycle of CO loading is driven primarily by the balance of photochemical production and destruction of hydroxyl radical (OH) (Novelli et al. 1998). During the summer months under conditions of high solar illumination, OH is produced mainly through O_3 photolysis and subsequent reaction with H_2O which accounts for strongest sink of CO in summer. Thus the main (90%) CO loss is caused by OH oxidation, followed by dry deposition (Thompson 1992).

Although both Calgary and Edmonton represent urban pollution, Calgary CO concentrations show lower values in winter, especially in January (Figure 5). Different air masses and weather systems influence Alberta, and it is likely that these have a significant impact on air quality. Southwestern Alberta has a complex and non-uniform spatial pattern of chinook frequency in winter which is associated with warmer temperatures and strong westerly winds that carry cleaner air from the mountains and may contribute to pollution dilution (Cullen and Marshall 2011). Additionally, Calgary has less industrial development than Edmonton.

The seasonality at Fort McMurray is less pronounced, where there is a marked increase of CO loading in summer, especially at low altitude levels (≤ 800 hPa). However, because the OH loading is higher in summer than the springtime, the CO peak does not persist long and declines rapidly. Simpson et al. (2011) calculated backward trajectories for ten days starting on July 10, 2008 over the Athabasca surface mines (northeast Alberta) as part of the summer deployment of the ARCTAS field mission. The aircraft flew over both boreal forest and industrial land including tailings ponds and upgrader facilities. Then the aircraft flew in a clean air area south of the oil sands. The ten-day backward trajectories of the area to the south (by one degree) of the oil sands and clean areas revealed that the air masses are transported at the aircraft's pressure level from the west and not from oil sands mines to the north. Consequently, summer CO increments can be attributed to other sporadic sources such as forest fires. Thus, the forest fire emissions will be discussed in the MODIS Fire Counts section Furthermore, the winter/spring levels over Fort McMurray start to peak late in April and May with maximum mixing ratios of 145 to 160 ppb (≤ 800 hPa). Figure 5 illustrates higher CO mixing ratios at low altitude levels (≤ 800 hPa) over Edmonton and Calgary than the Fort McMurray area, especially in winter and spring which point out to the significance of the non-industrial sources (e.g., vehicle and heating emissions). CO emissions from mobile sources (e.g., transportation emissions) over Alberta in 2011 were about 900 thousand tonnes, which is about 60% of the total CO emissions (1.5 million tonnes) (Environment Canada 2011).

For all locations, CO mixing ratios in spring exhibit greater values at higher altitudes (>700 hPa) compared to other seasons. This could be attributed to seasonal variations in deep convection, which lofts surface emissions into the upper troposphere (e.g., Duncan et al. 2007, Jiang et al.

2007, Liu et al. 2010, Livesey et al. 2013). This is further confirmed by monthly Omega averages (2000 to 2012) at 700 hPa (Figure 6) which indicate that the vertical mixing is more pronounced in May and June when Omega averages range from -0.02 to -0.01.
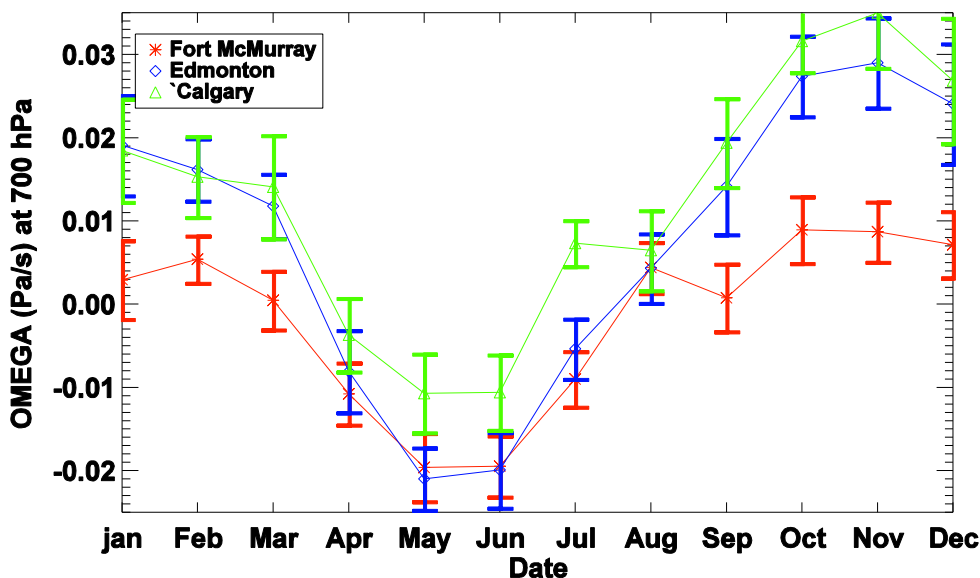

Figure 6.   Omega averages at 700 hPa from 2000 to 2012.

Although CO mixing ratios over Edmonton and Calgary areas are higher at lower altitudes, the CO total column data for all regions are comparable (not shown). This indicates that northern Alberta is affected more by CO plumes transported vertically above the planetary boundary layer (PBL) whereas cities such as Edmonton and Calgary are more influenced by local emissions confined in the PBL.

Figure 7 shows the 11 year inter-annual variation of monthly averaged CO mixing ratios (ppb) as measured by MOPITT from January 2002 to December 2012 at the ten pressure levels over Fort McMurray, Edmonton and Calgary. The first two years are not considered for inter-annual analysis since this period (referred to as phase 1) corresponded to times when the instrument was experiencing problems, such instrument cooler failure which might affect the retrieval validity. Accordingly, different channels and a different retrieval configuration called mission phase 2, are used to get the information (Emmons et al. 2004). The annual mean for each year is calculated and then subtracted from monthly averages of that year to show inter-annual variation. The white intervals indicate missing data due calibration events, instrument problem or the pressure at that location is less than MOPITT pressure level.
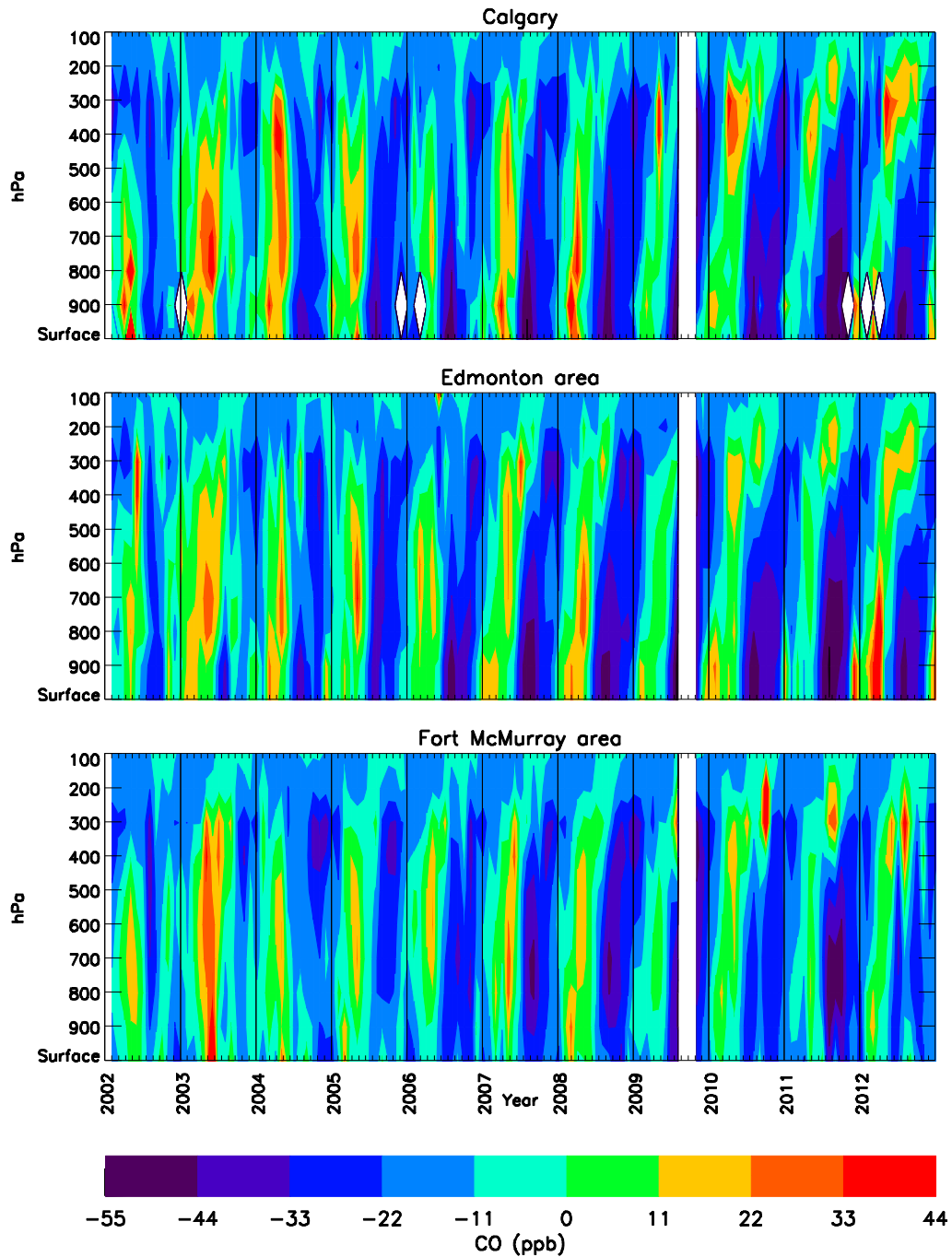
Figure 7.   The 11 year inter-annual variation monthly averaged daytime MOPITT CO mixing
ratios (ppb) as measured by MOPITT from January 2002 to December 2012 over
Calgary, Edmonton, and Fort McMurray areas.

Strong seasonal cycles are seen over all regions through all the years with maximum values in springtime. The degree of repeatable seasonal variability varies by year and region where it is more pronounced over Edmonton and Calgary areas. However, Fort McMurray data (Figure 7) show highest inter-annual variation where for example the CO loading during the winter-spring of 2003 was considerably greater than that of the next winter seasons. The upstream oil and gas emissions in Alberta peaked in 2000 (Alberta Environment 2008) and this increment could affect CO levels especially around Fort McMurray (Figure 7). CO emission trends from 2000 to 2011 for anthropogenic sources over Canada reached a maximum value in 2000 of about 11 million tonnes (Environment Canada 2011).

The monthly average time series from 2002 to 2012 of CO mixing ratios over Fort McMurray area displays a secondary peak in summer while its magnitude varies from year to year. Summer CO episodes over Fort McMurray area could be a signature of polluted air parcels coming from biomass burning emissions (e.g., forest fires). Accordingly, the impact of forest fire on CO levels is examined in the MODIS Fire Counts section. Furthermore, CO mixing ratios of Edmonton and Calgary areas at lower altitudes are higher than Fort McMurray area during the entire period except 2000. This result indicates the significance of the anthropogenic local urban sources (e.g., transportation) compared to the industrial sources (oil sand activities).

The inter-annual variation of CO total column is calculated in the same way as CO profiles (mentioned above) (Figure 8). To investigate whether there is a trend a linear regression analysis was performed to fit the observations of the monthly CO total column for Fort McMurray, Edmonton and Calgary areas. A slightly decreasing trend is identified for all regions with a rate of -1%. The seasonal variation is evident each year with small inter-annual variability. However, Calgary and Fort McMurray show higher spring values in 2002 and 2003, respectively. The striking feature in 2012 is the presence of an air pollution episode in the Edmonton and Fort McMurray areas in summer which is reflected by the highest, among all summers, CO total column ($2.6 \cdot 10^{18}$ molecules cm^{-2}) value in July. Thus a case study of summer 2012 is analyzed.
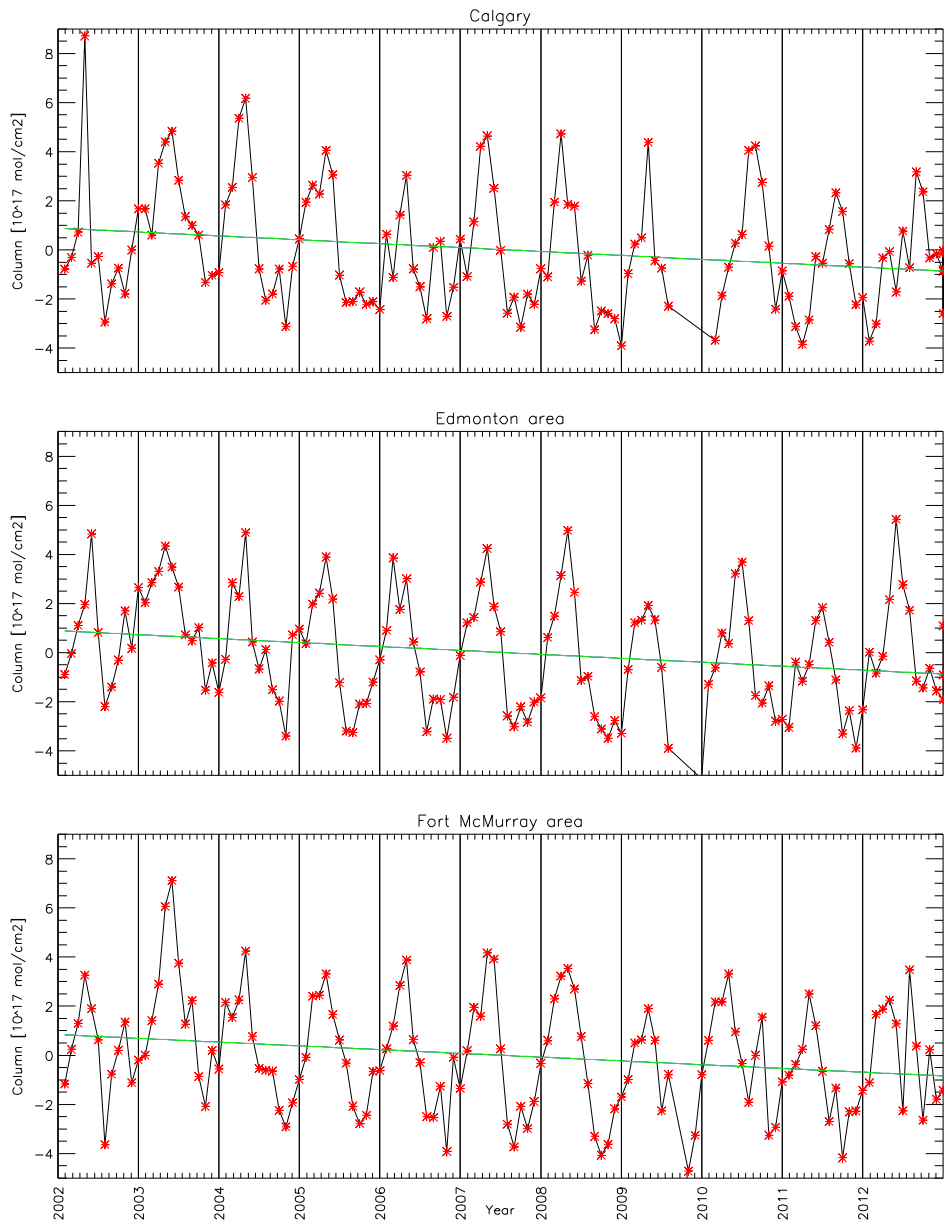
Figure 8. The 11 year inter-annual variations monthly averaged daytime MOPITT CO total column measurements for the period January 2002 to December 2012 over Calgary, Edmonton, and Fort McMurray areas.

Comparison with MOZAIC/IAGOS Aircraft CO Profiles

To verify MOPITT measurements, profiles of CO MOZAIC/IAGOS aircraft on descent to or ascent from Calgary airport are exploited for comparisons. The available aircraft data are between April 2009 and December 2011 with a total of 186 profiles. Because of MOPITT's temporal resolution of 2 to 3 days and the blockage of clouds, there are missing data in daily CO profiles and hence only the matching MOPITT and aircraft profiles in time and location are utilized. For comparison, MOZAIC/IAGOS profiles are first interpolated to the pressure level of the corresponding MOPITT retrievals.

Since the MOPITT retrieval derives CO concentration profiles by convolution of its radiometric observations with *a priori* estimates of the vertical profile of atmospheric CO, the sensitivity of the retrievals to the actual concentration profiles must be considered when conducting quantitative comparison to independent measurements (Emmons et al. 2004, 2007). The sensitivity of the MOPITT measurements to the true CO profile is represented by averaging kernels (Deeter et al. 2003). Accordingly, the interpolated aircraft profile is transformed by applying the averaging kernel and *a priori* profile associated with the corresponding MOPITT retrieval using equation 1 (Emmons et al. 2009). The transformed profiles (x_{ret}) are denoted as MOZAIC/IAGOS (AK), and then they are averaged and plotted with corresponding MOPITT retrieved vertical profiles of CO as illustrated in Figure 9a.

$$x_{ret} = \mathbf{A}x + (\mathbf{I} - \mathbf{A})x_a$$

where $\mathbf{x_a}$ is the *a priori* CO profile, $\mathbf{A}$ is the averaging kernel, and $\mathbf{x}$ is the in situ CO profile.

Both aircraft and MOPITT measurements show that CO mixing ratios below 700 hPa are higher than those above 700 hPa. The vertical distributions and gradients of aircraft and MOPITT CO mixing ratios are in good agreement where their averages values match fairly well within the standard deviations at all pressure levels. However, MOPITT averages generally have positive bias in the upper troposphere where the largest differences are seen below 400 mb. Nevertheless, the comparison demonstrates the potential of using multispectral MOPITT CO data in estimating surface air quality (Deeter et al. 2011, Worden et al. 2010). The seasonal profiles of the available MOZAIC/IAGOS data are computed and displayed in Figure 9b. They illustrate higher concentrations in winter for all altitudes and minimum values in summer. Additionally, spring measurements exhibited relatively high mixing ratios above ~2 km. Thus the seasonal variation results are generally consistent with MOPITT results over Calgary except that MOPITT shows the maximum in spring rather than winter. This discrepancy suggests that winter surface emissions are more entrained in the boundary layer which exacerbates the local surface pollution, resulting in high concentrations in winter. As MOPITT's sensitivity to CO is relatively low in the boundary layer (Deeter et al. 2007) surface emission may not be captured very well. Since the meteorological conditions in spring favor lofting the emissions up (warm air has lower density), the retrieved MOPITT signal at mid-troposphere can capture the enhanced CO where its sensitivity is better (Hyer et al. 2007). As a result MOPITT data record the

seasonal peak in spring rather than winter. This finding suggests the significant influence of transported emissions on CO levels. The surface seasonal variations of CO are further confirmed by analysis of ground level measurements in the next section.
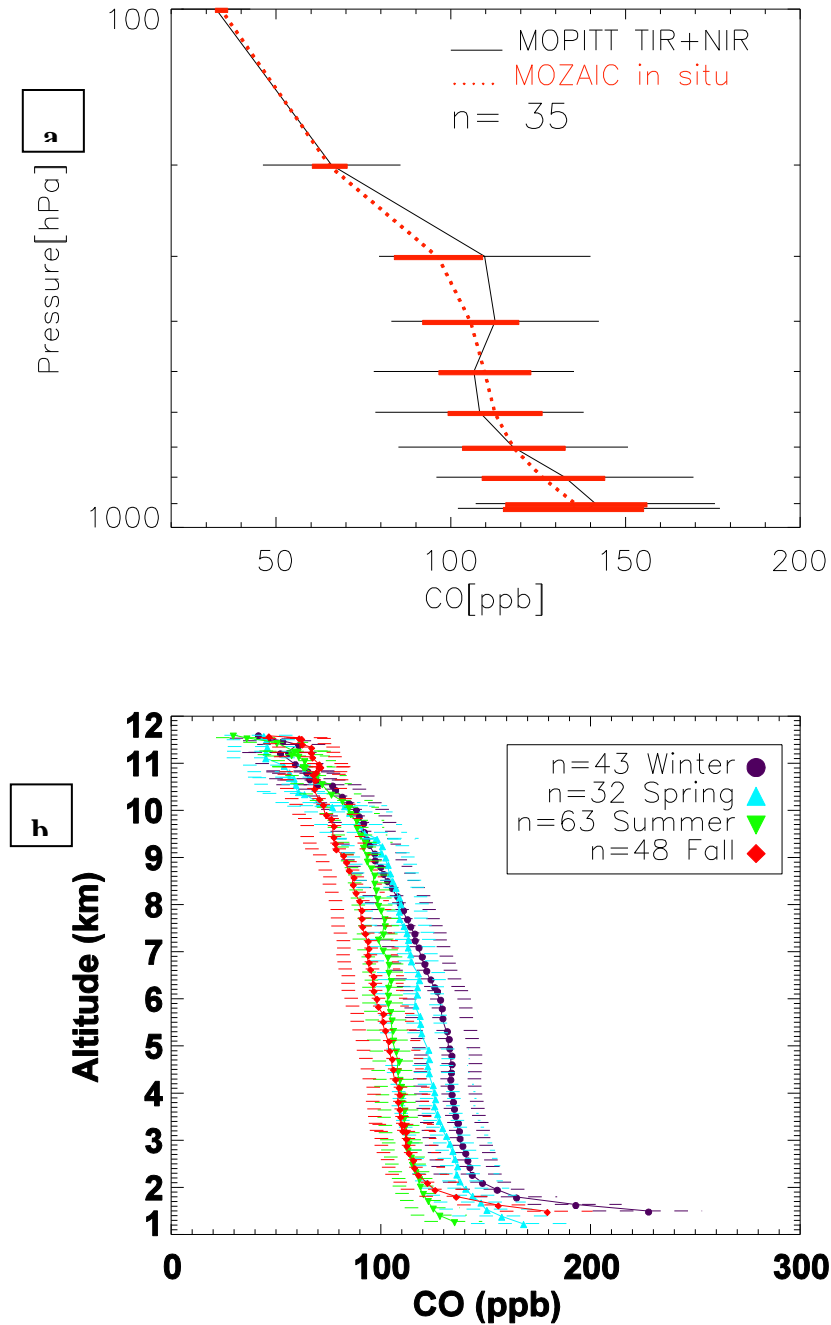

Figure 9.   MOZAIC/IAGOS (AK) and the corresponding MOPITT CO profiles (a) and MOZAIC/IAGOS seasonal averages CO profiles, the horizontal bars are standard errors.

Comparison with Ground Measurements

The in-situ ground measurements are more sensitive to the boundary layer than the MOPITT CO, where earlier studies of the averaging kernels indicated that there are effectively two independent pieces of information in the vertical profiles retrieved by MOPITT with more sensitivity to the middle troposphere. MOPITT retrieval does not have more than two pieces of information where the DFS values ranges from 1.4 to 2.0 (Deeter et al. 2007, Worden et al. 2010).

In this section we consider analysis of surface CO recorded at nine monitoring stations. The elevation, exact location, starting date, and the status are presented in Table 1. The selected stations represent various anthropogenic sources of CO where Fort McMurray-Athabasca Valley is an industrial town and the other stations are main urban sites (Edmonton and Calgary). The monthly-averaged time series of CO mixing ratio (ppb) at these stations are computed from 2000 to 2012 for comparison with MOPITT CO surface variability (Figure 10). The availability of CASA data differs among the stations as shown in Table 1. The MOPITT data are centred at each location in a one degree grid box.

Table 1 Location, elevation and starting date of selected CASA monitoring stations

| Name of the station	Longitude	Latitude	Elevation	Starting date
Calgary Central 2	51.046944	-114.074722	1051.0	01/04/2008
Calgary Central	51.0471506	-114.0731477	1051.0	01/05/1979
Calgary East	51.009444	-114.025278	1028.0	01/08/1974
Calgary Northwest	51.079167	-114.141944	1106.0	01/08/1974
Fort McMurray-Athabasca Valley	56.732778	-111.390278	260.0	01/12/1997
Edmonton Central	53.544453	-113.498842	663.0	03/12/1976
Edmonton East	53.548139	-113.368194	679.0	01/10/1972
Edmonton Northwest	53.594167	-113.54	679.0	12/07/1973
Edmonton South	53.500139	-113.526056	681.0	21/09/2005
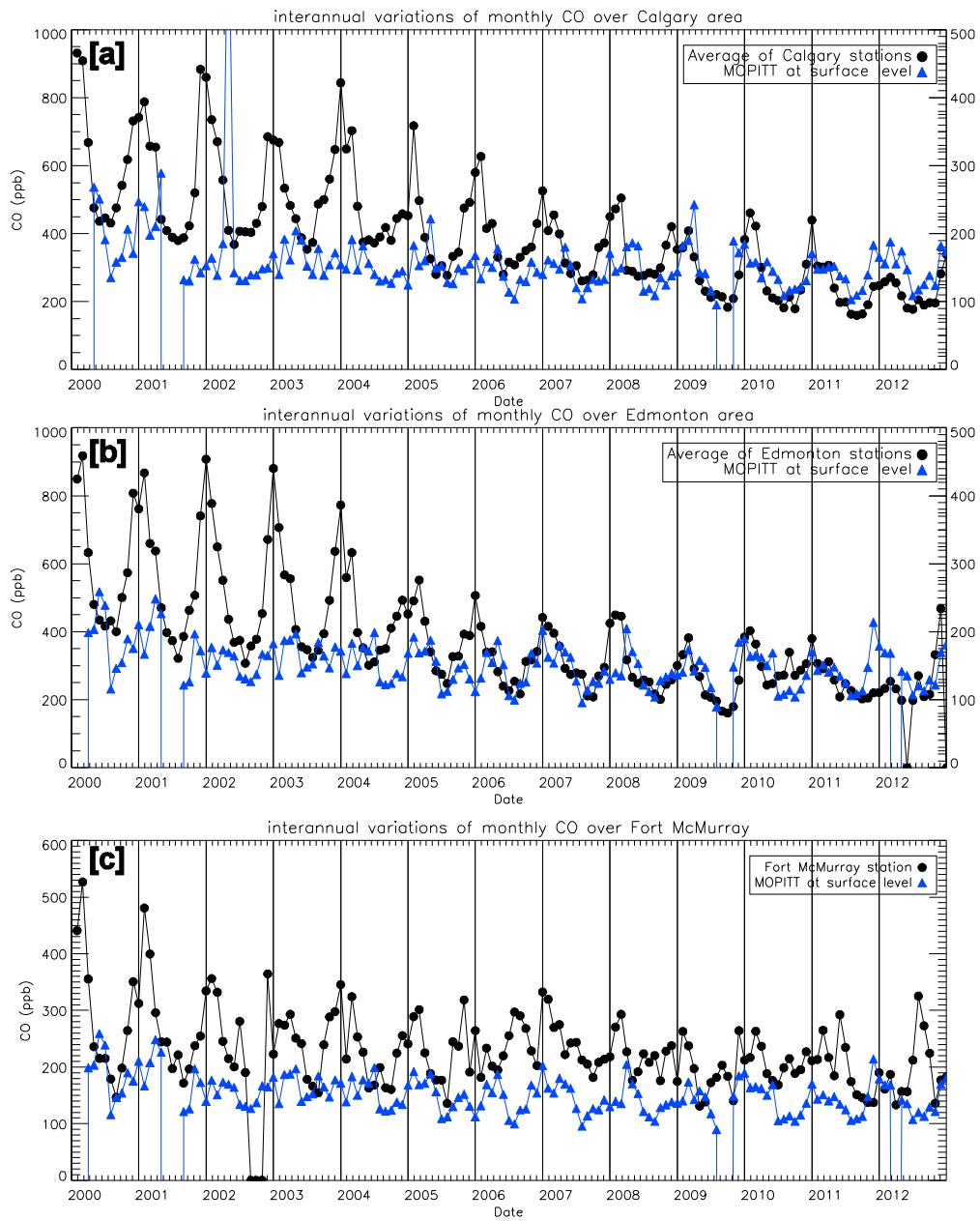
Figure 10. CASA CO in-situ measurements (left axis) and MOPITT CO at surface level (right axis) at (a) Calgary, (b) Edmonton and (c) Athabasca Valley.

The CO temporal data from all stations reveal distinct inter-annual variations with a significant decline trend. The trend is more recognizable over Edmonton and Calgary (Figure 10a and 10b) than Fort McMurray (Figure 10c) where their maximum declining rates are 4.4, 5.7 and 0.6, respectively. Furthermore, the CO levels are much higher at the urban stations than the industrial one where their maximum concentrations are about 1,000 ppb and 500 ppb, respectively. Additionally, it is apparent that the first 7 years (2000 to 2006) have larger inter-annual variations than the next years (2006 to 2012), especially over Edmonton and Calgary. In other words, the decreasing rate in the last 6 years is not as significant as the first years which reflect the influence of improvement in vehicle carbon monoxide emissions (Alberta Environment 2008).

Moreover, for each city, there are discrepancies in the CO concentrations among different locations, where the central and east Calgary and central and northwest Edmonton stations exhibited greatest values (not shown). This increase could be attributed to high traffic or industrial load at these locations which imply the substantial impact of these emissions sources on ambient CO levels. This finding is consistent with the results of Simpson et al. (2010) that showed relatively low emitted levels of CO throughout the mining operations, suggesting efficient combustion, although the CO concentrations were 48% greater than the local background. Compared to MOPITT, the spatial and the temporal variations of surface CO mixing ratios also experienced higher values over Edmonton than Fort McMurray.

The seasonal cycle of CO is evident for all years at all stations where it is characterized by a maximum in winter (December and January) and a minimum in summer (Figure 10). MOPITT CO surface data capture monthly variation in ground data except at Fort McMurray in 2006. However, the magnitude of MOPPIT CO surface data is less than ground data which could be because MOPITT surface values are the layer average from the surface to the next level (e.g., 900 hPa) as well as MOPITT surface sensitivity. Seasonal variations at Fort McMurray (Athabasca Valley station) (Figure 10c) are different for the whole study period with a secondary peak in summer which is more pronounced in some years such as 2012. Interestingly, the summer 2012 peak value exceeds the winter values of the same year, where monthly CO mixing in July 2012 was more than 300 ppb. Although MOPITT temporal resolution is about 3 days (Liu et al. 2005), the same observation is detected by MOPITT CO total column where the monthly July average in 2012 over Fort McMurray area was ~ 2.6 • 10^{18} molecules cm^{-2}. This implies the substantial impact of a non-industrial source such as forest fires, on air quality. Consequently, it is essential to analyze biomass burning over Alberta which is one of the major sources of CO (Morris et al. 2006).

MODIS Fire Counts

To assess the impact of forest fires on CO levels, the MODIS thermal anomaly product was analyzed for 12 years (2001 to 2012). GIS maps were used to display the spatial distributions of active fire points using ArcGIS software version 10.1.

Figure 11 illustrates the seasonal variations of fire counts for the study period over Alberta. A significant number of fires occur during summer (June to August) in northern areas of Alberta

extending from west to east. In the spring (February to April), large forest fires are spatially clustered in the area north of Fort McMurray as well as in central Alberta. In winter (December to February) and fall (September to November) seasons, most of the fire locations are distributed in the west and northwest areas of Alberta, especially in the fall season.

Temporal analysis of fire count monthly averages for the entire period (2001 to 2012) demonstrates that July, June and May comprise more than 75% of the total fire occurrence where their relative frequencies are 28%, 24%, and 18%, respectively (Figure 12a). Thus, the period of May to July is recognized to be the main biomass burning season where the largest fires occur in Northern Alberta. High pressure subsidence (a slow, sinking motion of high level air occurring in high pressure areas) and dry conditions were identified as the dominant meteorological conditions in this period which cause fires where the subsiding air is warmed by compression and becomes more stable (Skinner et al. 2002, Soja et al. 2007).

Inter-annual variations of seasonal fire frequency (Figure 12b) indicate a large variability with an ascending trend where the total number of fire counts over Alberta increased from 1,959 in 2001 to 10,608 in 2012. A very distinct increase in fire frequency is observed in summer with peak number in 2012. Additionally, 2011 had more than 5,500 fires in spring and in summer. The overall pattern of fires is largely consistent with the seasonal and temporal variations of MOPITT CO values of northern Alberta as well as the ground level in situ measurements at Fort McMurray station. Therefore, it is suggested that the high CO concentrations that emerge each summer in the area around Fort McMurray (northern Alberta) are mainly caused by the biomass burning of boreal forest fires. Earlier studies pointed out the significance of biomass burning on air quality, where it accounts for about 30% of the global total CO sources (Galanter et al. 2000).
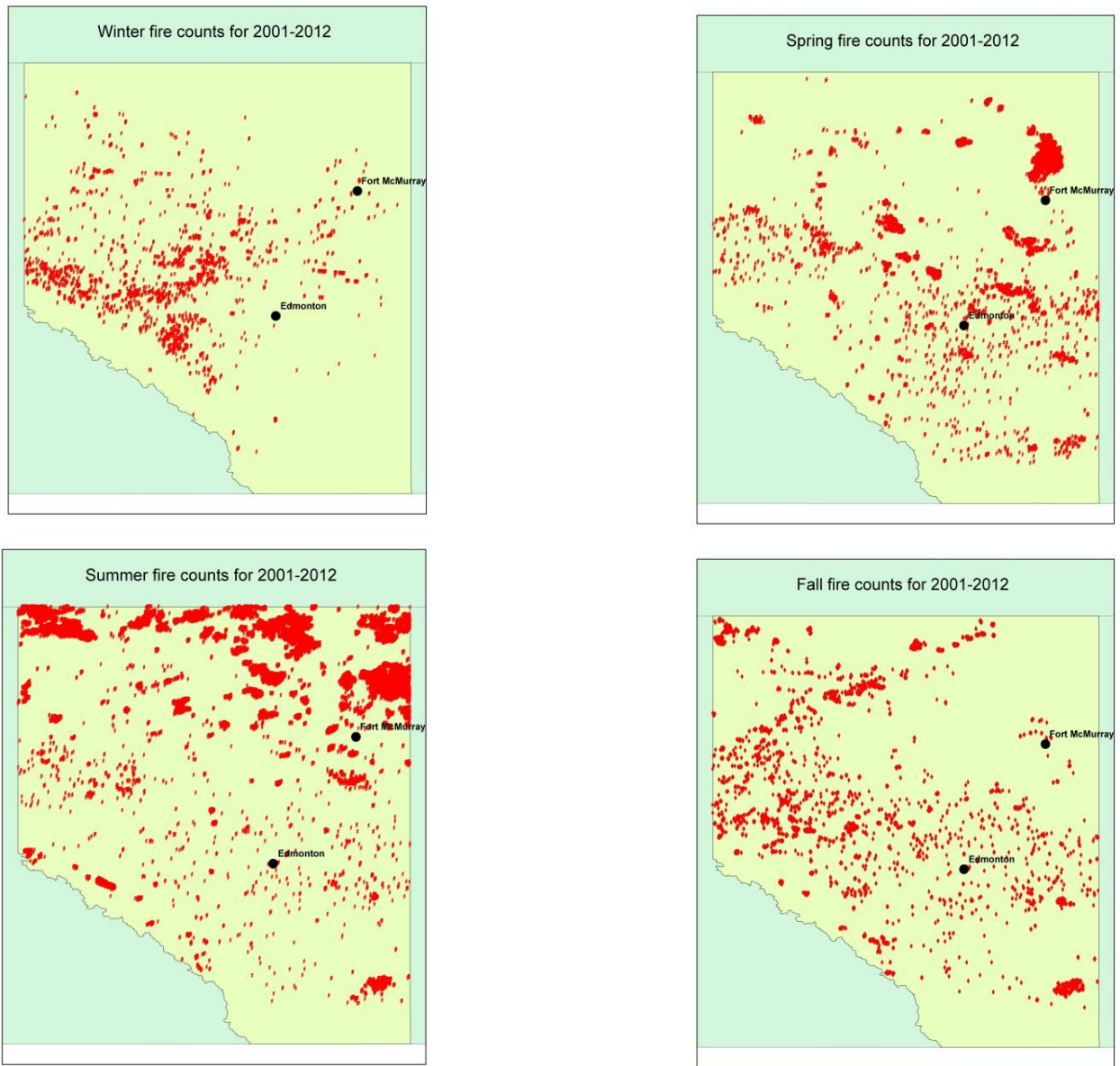
Figure 11. Seasonal variations of MODIS fire counts for the study period (2001-2012) over Alberta.
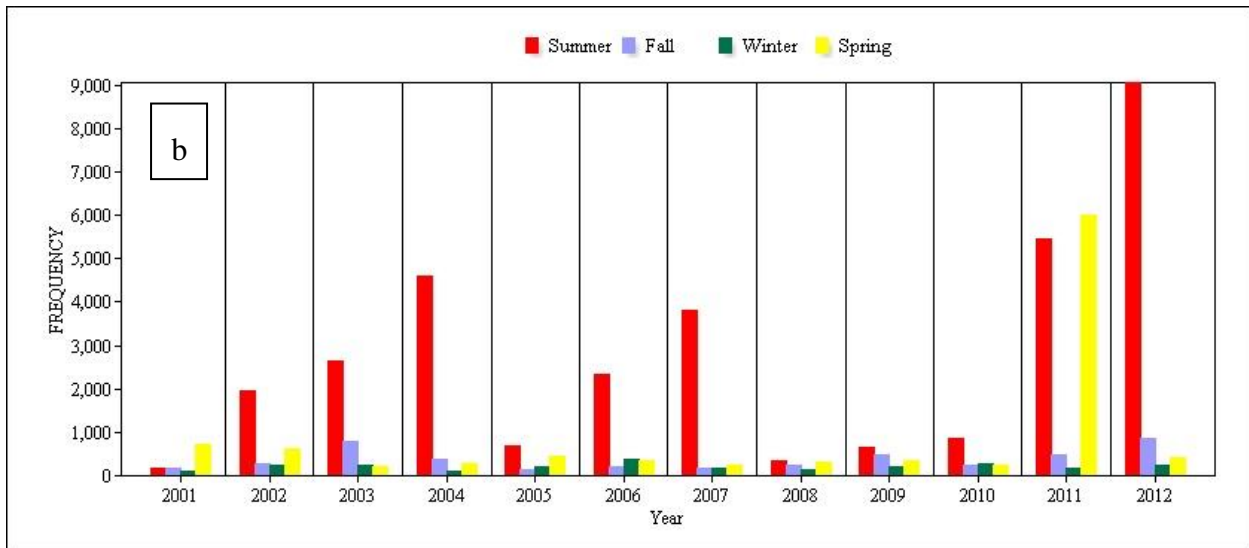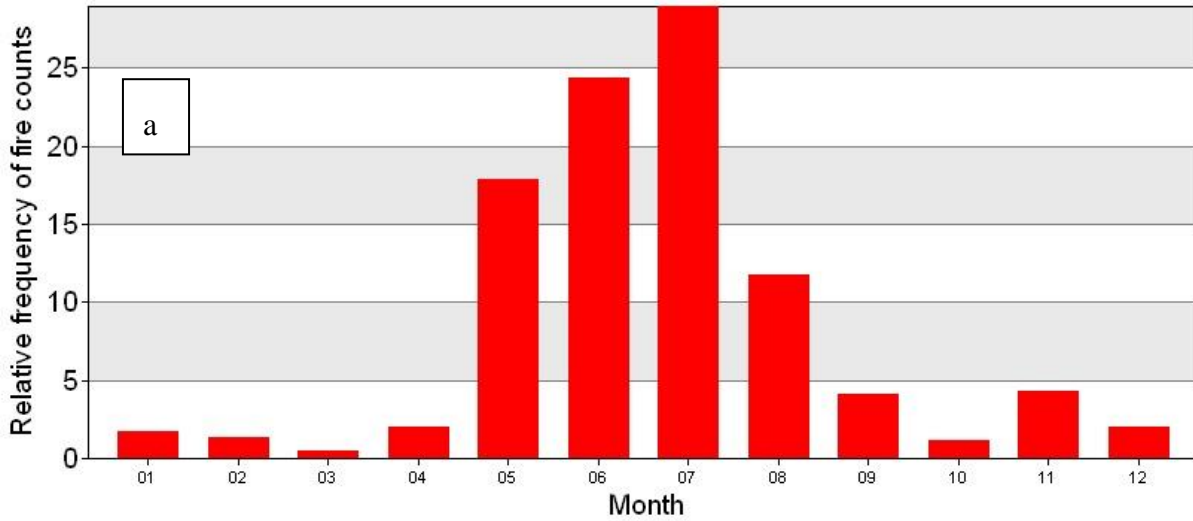
Figure 12. Monthly variations of MODIS fire counts for the study period (2001 to 2012) over Alberta (a) and inter-annual variations of seasonal fire frequency (b).

To analyze in further detail the impact of fire emissions on CO levels and their transport, the variability of fire counts during July 2012 is examined as a case study. The daily time series of fire frequency in summer 2012 (not shown) shows a severe fire period from July 4 to 18 with maximum number on July 10 and 11 when the fire counts exceeded 1,200 and the fire radiative power (FRP[29]) reached 9,510 MW. Figures 13a and b display the MODIS Terra image combined with fire hot spots indicated by red points for July 10 and 11, 2012, respectively. It is.

_____

[29] FRP is the measure of thermal heat emitted from detected fires.
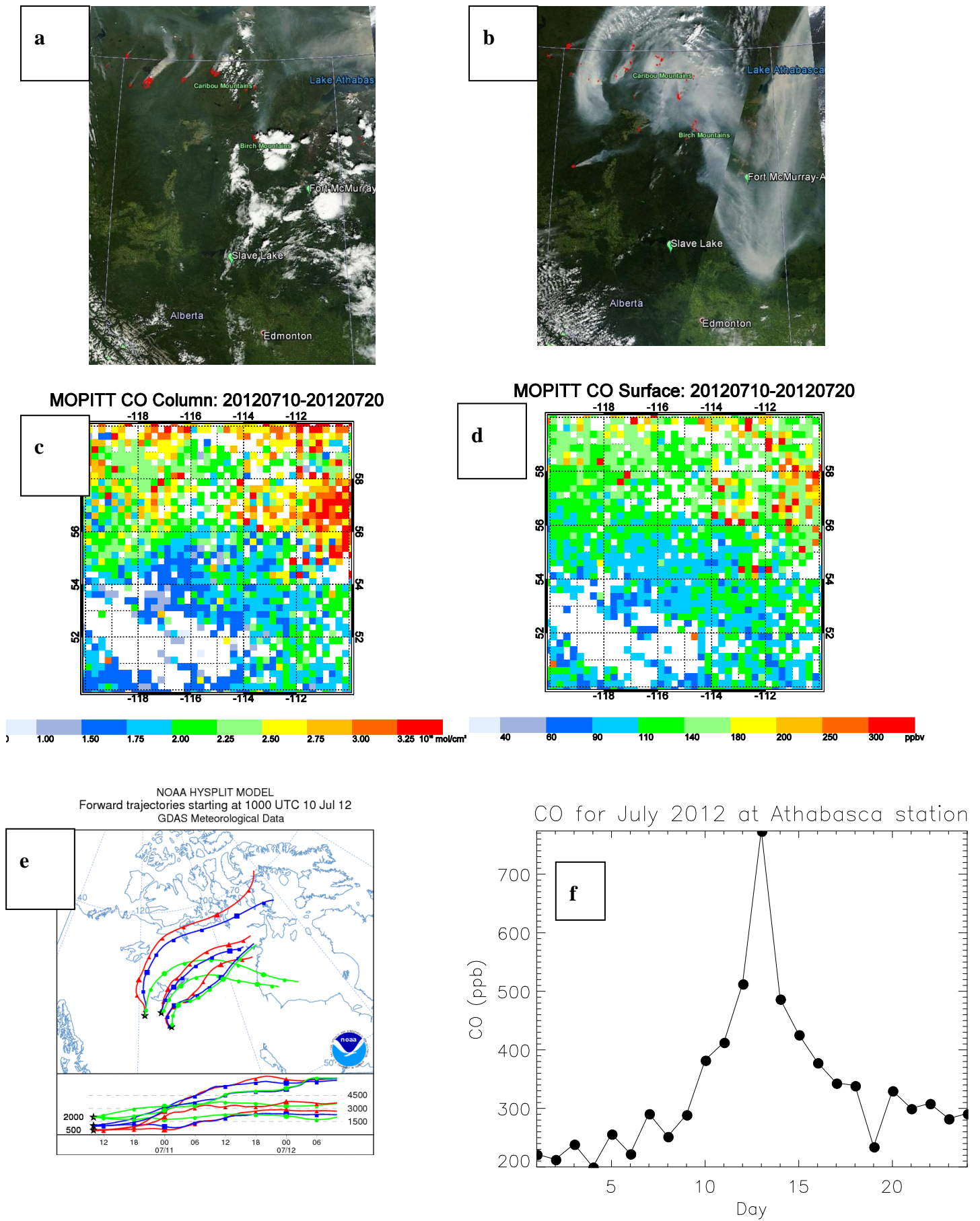
Figure 13. MODIS true image combined with fire points (red) (a) on July 10, 2012 and (b) on July 11, 2012, (c) MOPITT CO total column from July 10 to 20, 2012 over Alberta, (d) MOPITT surface CO from July 10 to 20, 2012 over Alberta, (e) 48 HYSPLIT forward trajectory started on July 10, 2012, and (f) daily CO at Athabasca Valley station for July 2012.

clear that most of the red fire points are included in or headed the smoke plumes, indicating that the plumes originated from those fires.

On July 10, 2012, the air mass was transported across Alberta to the north then on July 11 it went east at which time it split, with part of the air mass being transported south to the Fort McMurray area. To verify the transport pathway of smoke plumes, HYSPLIT forward trajectories analyses were performed for July 10, 2012 for a 48 hour period (Figure 13e). The starting conditions for these analyses included three fire point locations chosen from the MODIS fire data. The blue circles in the trajectories represent time intervals of 6 hours. Analyses were done for 500, 1,000, and 2,000 m heights, and it seems that the plumes stayed in the PBL during the first 12 hours, then all of the plumes moved upward reaching heights up to 3,000 m. Moreover, the trajectories indicate that the air parcels traveled from the northwest toward the northeast which coincides with MODIS smoke plume paths (Figures 13a and 13b). Therefore, the HYSPLIT forward trajectory analysis provides evidence that some cities in Alberta such as Fort McMurray could be affected by fire emissions after a short time (24 to 48 h) depending on the starting plume height.

CO total column and surface composites for July 10 to 20 are displayed in Figure 13c and 13d. The CO plume expanded across northeastern Alberta where the CO total column and surface exceeded $3.25 \cdot 10^{18}$ molecules cm^{-2} and 300 ppb, respectively. Despite the limited vertical resolution of MOPITT measurements, a general enhancement of CO can be clearly seen for surface measurements where the CO mixing ratio close to fires was as high as 300 ppbv, in comparison with a CO mixing ratio of 60 to 90 ppb in the background. However, the spatial pattern of total column and surface CO are not similar where the former is more distinct in the west area of Alberta where fires originated than the latter. This suggests that the enhanced CO was transported vertically as well as horizontally.

Although most of the summer of 2012 fires originated in the northwest area of Alberta, MOPITT images revealed the intense CO plumes in the east which match remarkably well with MODIS and HYSPLIT trajectories. This implies the substantial influence of long range transport on CO levels where its long lifetime allows plumes with elevated CO to travel long distances affecting air quality downstream of the point source emissions. Zhao et al. (2007) indicated that a high CO episode at a remote area can result from long-range transport from active biomass burning and biofuel burning areas rather than local air pollution.

Daily time series of in-situ measurements at the Athabasca Valley station for July 2012 reveals elevated CO concentrations during the intense forest fire period (Figure 13f). Although the total number of hotspots peaked on July 10, the enhancement of CO was found to reach the maximum value later on July 12 where it exceeded 700 ppb. This further confirms the important effect of transport on atmospheric CO values.

Generally, the in-situ measurements are in good agreement with MOPITT data, however the magnitude of in-situ measurements is higher than surface MOPITT data. The reason could be due to the larger spatial resolution of MOPITT data (22 km × 22 km) while in-situ measurements represent point data. In addition, since MOPITT is not very sensitive to the CO in the boundary

layer, it is possible that the sharp surface features are masked and hence the retrieved CO values in the boundary layer are lower than reality during biomass burning emissions.

SUMMARY AND CONCLUSIONS

This study demonstrated the potential use of MOPITT CO measurements to better understand and quantify the CO sources over Alberta. MOPITT-based climatology and inter-annual variations were evaluated for 13 years (2000 to 2012) on spatial and temporal scales. MOPITT V5 multispectral product that uses both near-infrared and the thermal-infrared radiances for CO retrieval were used. Available MOZAIC/IAGOS aircraft CO profiles over Calgary were used to validate MOPITT CO data. Additionally, CO ground measurements were compared to satellite data. The MODIS thermal anomaly product from 2001 to 2012 was employed to investigate the effect of seasonal variations of fires on climatological and inter-annual CO levels. To further recognize the fate and the impact of biomass burning emissions on air quality, forest fires on a severe day have been analyzed as a case study.

Seasonal climatological maps for CO total columns indicated conspicuous spatial variations in all seasons except in winter where the CO spatial variations are less prominent. High CO loadings are observed to extend from the northeast to northwest of Alberta, with highest values (2.5 to 2.75 • 10^{18} molecules cm^{-2}) in spring. The CO mixing ratios at the surface level in winter and spring seasons exhibited dissimilar spatial distribution patterns, where enhancements are detected in central Alberta (east of Edmonton) rather than north, with a mixing ratio range of 250 to 300 ppb. Analyzing spatial distributions of Omega at pressure level 850 mb for four seasons implied that conditions in northeast Alberta are more favorable for uplifting while in the south subsidence of CO emissions is more likely. Thus, meteorological parameters may affect the CO spatial distribution profile where the CO total columns show remarkable enhancements in the north while the surface CO experiences high values in the south area.

Time altitude CO profile climatology, as well as the inter-annual variability, were investigated for Fort McMurray and Edmonton regions to compare impact of various sources on CO loading. Monthly variations over Edmonton region are consistent with the general seasonal cycle of CO in the Northern Hemisphere (Edwards et al. 2004) – significant enhancement in winter and spring, and minimum mixing ratios in summer. The typical seasonal CO variations over Fort McMurray area are less prominent, where there is an obvious rise of CO in summer. The same seasonal patterns are detected at various surface monitoring stations; however the magnitudes of in-situ measurements are higher. Inter-annual variations of satellite data display a slightly decreasing trend for both regions while the decline trend is more evident from ground observations, especially in Edmonton. These discrepancies (between satellite and ground data) may be explained by larger MOPITT spatial resolution and its lower sensitivity to the surface CO.

MOPITT CO profiles are validated by comparing them to the available MOZAIC/IAGOS aircraft profiles after applying averaging kernel (Emmons et al. 2009). Both vertical distributions showed good agreement within the standard deviations at all pressure levels.

Time altitude CO profile measurements over the Edmonton region illustrated relatively elevated CO values in the lower troposphere than the corresponding values (over the same elevations) over Fort McMurray area. However, the total column CO values are similar. This striking feature suggests that Edmonton and Calgary regions may be affected by regional pollution while Fort McMurray area (northern Alberta) may be influenced by CO plumes transported either vertically or horizontally which could be from industry and/or regional biomass burning. Temporal analysis of fire frequency showed that the main biomass burning season is from May to July where the largest fires are clustered spatially in northern and central Alberta. The spatial distributions of fires match remarkably the spatial distributions of MOPITT CO total column in spring and summer. Additionally, there is a consistency between the time evolutions of high CO episodes that are monitored by satellite and ground measurements in the Fort McMurray area and the fire frequency peak time. This finding implies that biomass burning and its transport have interesting consequences for the tropospheric CO distribution in northern Alberta, given the complex meteorology that prevails in this area.

Since 2012 had high fire frequency, July 10, 2012 was selected to analyze the biomass burning smoke plumes. Daily time series of ground measurements in Fort McMurray revealed elevated CO concentrations on July 12 (> 700 ppb) which is two days after peak fire frequency (July 10). Furthermore, the MOPITT composite image for the fire severity period (July10 to 20) displayed a more intense CO plume in the east rather than west area where most of the fires originated. This result reflects the significant influence of long range transport of biomass burning emissions on CO levels which is further confirmed by MODIS smoke plume images and HYSPLIT forward trajectories.

REFERENCES

Alberta Environment, 2008. Alberta Air emissions trends and projections. http://environment.gov.ab.ca/info/library/7964.pdf

Alberta Environment, 2012. Oil sands, the resources. http://www.oilsands.alberta.ca/FactSheets/Resource_FSht_June_2012_Online.pdf

Alberta Environment, 2013. Ambient Air Monitoring Methods. http://environment.alberta.ca/documents/AAMonitMethods.pdf

Amiro, B.D., J.B. Todd, B.M. Wotton, K.A. Logan, M.D. Flannigan, B.J. Stocks, J.A. Mason, D.L. Martell and K.G. Hirsch, 2001. Direct carbon emissions from Canadian forest fires, 1959–1999. Canadian Journal of Forest Research 31: 512-525.

Bytnerowicz A., W. Fraczek, S. Schilling, and D. Alexander, 2010. Spatial and temporal distribution of ambient nitric acid and ammonia in the Athabasca Oil Sands Region, Alberta. Journal of Limnology 69(1): 11-21.

Canadian Association of Petroleum Producers, 2012. Crude oil forecast, marketing and pipelines. http://www.strategywest.com/downloads/CAPP201206.pdf.

Colarco, P.R., M.R. Schoeberl, B.G. Doddridge, L.T. Marufu, O. Torres and E. J. Welton, 2004. Transport of smoke from Canadian forest fires to the surface near Washington, D.C.: Injection height, entrainment and optical properties. Journal of Geophysical Research 109, D06203. doi:10.1029/2003JD004248.

Cullen, R.M. and S.J. Marshall, 2011. Mesoscale temperature patterns in the Rocky Mountains and foothills region of Southern Alberta. Atmosphere-Ocean 49(3): 189-205. doi: 10.1080/07055900.2011.592130.

Daniel, J.S. and S. Solomon, 1998. On the climate forcing of carbon monoxide. Journal of Geophysical Research 103: 13249-13260.

Deeter, M.N., D P. Edwards, J.C. Gille and J.R. Drummond, 2007. Sensitivity of MOPITT observations to carbon monoxide in the lower troposphere. Journal of Geophysical Research 112: D24306. doi:10.1029/2007JD008929.

Deeter, M.N., D.P. Edwards, J.C. Gille, L.K. Emmons, G. Francis, S-P. Ho, D. Mao, D. Masters, H. Worden, J.R. Drummond and P.C. Novelli, 2010. The MOPITT version 4 CO product: Algorithm enhancements, validation, and long-term stability. Journal of Geophysical Research 115: D07306. doi:10.1029/2009JD013005.

Deeter, M.N., L.K. Emmons, G.L. Francis, D.P. Edwards, J.C. Gille, J.X. Warner, B. Khattatov, D. Ziskin, J.F. Lamarque, S.P. Ho, V. Yudin, J.L. Attie, D. Packman, J. Chen, D. Mao and J.R. Drummond, 2003. Operational carbon monoxide retrieval algorithm and selected results for the MOPITT instrument. Journal of Geophysical Research 108: 4399. doi:10.1029/ 2002JD003186.

Deeter, M.N., S. Martínez-Alonso, D.P. Edwards, L.K. Emmons, J.C. Gille, H.M. Worden, J.V. Pittman, B.C. Daube and S.C. Wofsy, 2013. Validation of MOPITT Version 5 thermal-infrared, near-infrared, and multispectral carbon monoxide profile retrievals for 2000-2011. Journal of Geophysical Research 118: 6710-6725. doi:10.1002/jgrd.50272.

Deeter, M.N., H.M. Worden, D.P. Edwards, J.C. Gille and A.E. Andrews, 2012. Evaluation of MOPITT retrievals of lower-tropospheric carbon monoxide over the United States. Journal of Geophysical Research 117: D13306. doi:10.1029/2012JD017553.

Deeter, M.N., H.M. Worden, D.P. Edwards, J.C. Gille, D. Mao, and J.R. Drummond, 2011. MOPITT multispectral CO retrievals: Origins and effects of geophysical radiance errors. Journal of Geophysical Research 116: D15303. doi:10.1029/2011JD015703.

Draxler, R.R. and G.D. Hess, 1998. An overview of the HYSPLIT_4 modelling system for trajectories, dispersion and deposition. Australian Meteorological Magazine 47 (4): 295-308.

Draxler, R.R. and G.D. Rolph, 2013. HYSPLIT (HYbrid Single-Particle Lagrangian Integrated Trajectory) Model access via NOAA ARL READY Website. (http://www.arl.noaa.gov/HYSPLIT.php). NOAA Air Resources Laboratory, College Park, Maryland.

Drummond, J.R., 1992. Measurements of Pollution in the Troposphere (MOPITT). IN: Gille, J.C. and G. Visconti (Eds.). The Use of EOS for Studies of Atmospheric Physics. Elsevier Science Publications, New York. pp. 77-101.

Duncan, B.N., J.A. Logan, I. Bey, I.A. Megretskaia, R.M. Yantosca, P.C. Novelli, N.B. Jones, and C.P. Rinsland, 2007. Global budget of CO, 1988–1997: Source estimates and validation with a global model. Journal of Geophysical Research 112: D22301. doi:10.21029/22007JD008459.

Edwards, D.P., L.K. Emmons, D.A. Hauglustaine, D.A. Chu, J.C. Gille, Y.J. Kaufman, G. Pétron, L.N. Yurganov, L. Giglio, M.N. Deeter, V. Yudin, D.C. Ziskin, J. Warner, J-F. Lamarque, G.L. Francis, S.P. Ho, D. Mao, J. Chen, E.I. Grechko and J.R. Drummond, 2004. Observations of carbon monoxide and aerosols from the Terra satellite: Northern Hemisphere variability. Journal of Geophysical Research 109: D24202. doi:10.1029/2004JD004727.

Emmons, L.K., M.N. Deeter, J.C. Gille, D.P. Edwards, J.-L Attié, J. Warner, D. Ziskin, G. Francis, B. Khattatov, V. Yudin, J.-F Lamarque, S.-P Ho, D. Mao, J.S. Chen, J. Drummond, P. Novelli, G. Sachse, M.T. Coffey, J.W. Hannigan, C. Gerbig, S. Kawakami, Y. Kondo, N. Takegawa, H. Schlager, J. Baehr, H. Zierei, 2004. Validation of Measurements of Pollution in the Troposphere (MOPITT) CO retrievals with aircraft in situ profiles. Journal of Geophysical Research 109: D03309. doi:10.1029/2003JD004101.

Emmons, L.K., D.P. Edwards, M.N. Deeter, J.C. Gille, T. Campos, P. Nédélec, P. Novelli and G. Sachse, 2009. Measurements of Pollution in the Troposphere (MOPITT) validation through 2006. Atmospheric Chemistry and Physics 9: 1795-1803. doi:10.5194/acp-9-1795-2009.

Emmons, L.K., G.G. Pfister, D.P. Edwards, J.C. Gille, G. Sachse, D. Blake, S. Wofsy, C. Gerbig, D. Matross and P. Nédélec, 2007. Measurements of Pollution in the Troposphere (MOPITT) validation exercises during summer 2004 field campaigns over North America. Journal of Geophysical Research 112: D12S02. doi:0.1029/ 2006JD007833.

Environment Canada, 2011. Total air pollutants emissions for Alberta. http://www.ec.gc.ca/inrp-npri/default.asp?lang=en&n=0EC58C98#Emission_Summaries

Flannigan, M.D., K.A. Logan, B.D. Amiro, W.R. Skinner and B.J. Stocks, 2005. Future area burned in Canada. Climate Change 72: 1-16.

Galanter, M., H. Levy II and G.R. Carmichael, 2000. Impacts of biomass burning on tropospheric CO, NO_x, and O_3. Journal of Geophysical Research 105: 6633-6653.

Giglio, L., 2007. MODIS Collection 4 Active Fire Product User's Guide, Version 2.3. SSAI, Lanham, Maryland. http://maps.geog.umd.edu/products/MODIS_Fire_Users_Guide_2.3.pdf

Giglio, L., J. Descloitres C.O. Justice and Y.J. Kaufman, 2003. An enhanced contextual fire detection algorithm for MODIS. Remote Sensing of Environment 87: 273-282.

Gillett, N.P., A.J. Weaver, F.W. Zwiers and M.D. Flannigan, 2004. Detecting the effect of climate change on Canadian forest fires. Geophysical Research Letters 31: L18211. doi:10.1029/2004GL020876.

Girardin, M.P., 2007. Interannual to decadal changes in area burned in Canada from 1781 to 1982 and the relationship to Northern Hemisphere land temperatures. Global Ecology Biogeography 16: 557- 566.

Howell, S.G., A.D. Clarke, S. Freitag, C.S. McNaughton, V. Kapustin, V. Brekovskikh, J-L. Jimenez and M.J. Cubison, 2014. An airborne assessment of atmospheric particulate emissions from the processing of Athabasca oil sands. Atmospheric Chemistry and Physics 14: 5073-5087.

Hyer, E.J., D.J. Allen and E.S. Kasischke, 2007. Examining injection properties of boreal forest fires using surface and satellite measurements of CO transport. Journal of Geophysical Research 112: D18307. doi:10.1029/2006JD008232.

Jacob, D.J., J.H. Crawford, H. Maring, A.D. Clarke, J.E. Dibb, L.K. Emmons, R.A. Ferrare, C.A. Hostetler, P.B. Russell, H.B. Singh, A.M. Thompson, G.E. Shaw, E. McCauley, J.R. Pederson and J.A. Fisher, 2010. The Arctic Research of the Composition of the Troposphere from Aircraft and Satellites (ARCTAS) mission: Design, execution, and first results. Atmospheric Chemistry and Physics 10: 5191-5212. doi:10.5194/acp-10-5191-2010.

Jiang, J.H., N.J. Livesey, H. Su, L. Neary, J.C. McConnell and N.A.D. Richards, 2007. Connecting surface emissions, convective uplifting, and long-range transport of carbon monoxide in the upper troposphere: New observations from the Aura Microwave Limb Sounder. Geophysical Research Letters 34: L18812. doi:10.1029/2007GL030638.

Jiang, Z., D.B.A. Jones, H.M. Worden, M.N. Deeter, D.K. Henze, J. Worden, K.W. Bowman, C.A.M. Brenninkmeijer and T.J. Schuck, 2013. Impact of model errors in convective transport on CO source estimates inferred from MOPITT CO retrievals. Journal of Geophysical Research 118. doi:10.1029/jgrd.50216.

Kalnay, E., M. Kanamitsu, R. Kistler, W. Collins, D. Deaven, L. Gandin, M. Iredell, S. Saha, G. White, J. Woollen, Y. Zhu, A. Leetmaa, R. Reynolds, M. Chelliah, W. Ebisuzaki, W. Higgins, J. Janowiak, K.C. Mo, C. Ropelewski, J. Wang, R. Jenne and D. Joseph, 1996. The NCEP/NCAR 40-Year Reanalysis Project. Bulletin of the American Meteorological Society 77(3): 437-471.

Kaufman, Y.J., D.D. Herring, K.J. Ranson and G.J. Collatz, 1998a. Earth Observing System AM1 mission to Earth. IEEE Transactions on Geoscience and Remote Sensing 36(4): 1045-1055.

Kaufman, Y.J., C. Justice, L. Flynn, J. Kendall, E. Prin, L. Giglio, D.E. Ward, P. Menzel and A. Setzer, 1998b. Potential global fire monitoring from EOS-MODIS. Journal of Geophysical Research 103(D24): 32215-32338. doi:10.1029/98JD01644.

Kean, S., 2009. Eco-alchemy in Alberta. Science 326(5956): 1052-1055.

Liu, J., J.R. Drummond, Q. Li and J.C. Gille, 2005. Satellite mapping of CO emission from forest fires in Northwest America using MOPITT measurements. Remote Sensing of Environment 95(4): 502-516.

Liu, J., J.A. Logan, N.J. Livesey, I. Megretskaia, C. Carouge and P. Nedelec, 2010. Analysis of CO in the tropical troposphere using Aura satellite data and the GEOS-Chem model: Insights into transport characteristics of the GEOS meteorological products. Atmospheric Chemistry and Physics 10: 12207-12232. doi:10.5194/acp- 10-12207-2010.

Livesey, N.J., J.A. Logan, M.L. Santee, J.W. Waters, R.M. Doherty, W.G. Read, L. Froidevaux and J.H. Jiang, 2013. Interrelated variations of O_3, CO and deep convection in the tropical/subtropical upper troposphere observed by the Aura Microwave Limb Sounder (MLS) during 2004-2011. Atmospheric Chemistry and Physics 13: 579-598. doi:10.5194/acp-13-579-2013.

Marenco, A., V. Thouret, P. Ned´ elec, H. Smit, M. Helten, D. Kley, F. Karcher, P. Simon, K. Law, J. Pyle, G. Poschmann, R. Von Wrede, C. Hume and T. Cook, 1998. Measurement of ozone and water vapor by Airbus in-service aircraft: The MOZAIC airborne program, an overview. Journal of Geophysical Research 103: 631-642.

Marlon, J.R., P.J. Bartlein, C. Carcaillet, D.G. Gavin, S.P. Harrison, P.E. Higuera, F. Joos, M.J. Power and I.C. Prentice,2008. Climate and human influences on global biomass burning over the past two millennia. Nature Geoscience 1: 69-702.

Martin, R.V., 2008. Satellite remote sensing of surface air quality. Atmospheric Environment 42: 7823-7843.

Masuoka, E., A. Fleig, R.W. Wolfe and F. Patt, 1998. Key characteristics of the MODIS data products. IEEE Transactions on Geoscience and Remote Sensing 36(4): 1313-1323. doi:10.1109/36.701081.

McLinden, C.A., V. Fioletov, K.F. Boersma, N. Krotkov, C.E. Sioris, J.P. Veefkind and K. Yang, 2012. Air quality over the Canadian oil sands: A first assessment using satellite observations. Geophysical Research Letters 39: L04804. doi:10.1029/2011GL050273.

Morris, G.A., S. Hersey, A.M. Thompson, S. Pawson, J.E. Nielsen, P.R. Colarco, W.W. McMillan, A. Stohl, S. Turquety, J. Warner, B.J. Johnson, T.L. Kucsera, D.E. Larko, S.J. Oltmans and J.C. Witte, 2006. Alaskan and Canadian forest fires exacerbate ozone pollution over Houston, Texas, on 19 and 20 July 2004. Journal of Geophysical Research 111: D24S03. doi:10.1029/2006JD007090.

National Energy Board, 2013. Canada's oil sands: Opportunities and challenges to 2015. http://www.neb.gc.ca/clf-nsi/rnrgynfmtn/nrgyrprt/lsnd/pprtntsndchllngs20152004/qapprtntsndchllngs20152004-eng.html

Nedelec, P., J-P. Cammas, V. Thouret, G. Athier, J-M. Cousin, C. Legrand, C. Abonnel, F. Lecoeur, G. Cayez and C. Marizy, 2003. An improved infrared carbon monoxide analyser for routine measurements aboard commercial Airbus aircraft: technical validation and first scientific results of the MOZAIC III programme. Atmospheric Chemistry and Physics 3: 1551-1564. doi:10.5194/acp-3-1551-2003.

Novelli, P.C., K.A. Masarie and P.M. Lang, 1998. Distributions and recent changes in carbon monoxide in the lower troposphere. Journal of Geophysical Research 103: 19015-19033.

Pétron, G., C. Granier, B. Khattotov, V. Yudin, J-F. Lamarque, L. Emmons, J. Gille and D.P. Edwards, 2004. Monthly CO surface sources inventory based on the 2000–2001 MOPITT satellite data. Geophysical Research Letters 31: L21107. doi: 10.1029/2004GL020560.

Percy, K.E., 2013. Geoscience of climate and energy 11. Ambient air quality and linkage to ecosystems in the Athabasca oil sands, Alberta. Geoscience Canada. http://dx.doi.org/10.12789/geocanj.2013.40.014 .

Preston, C.M. and M.W.I. Schmidt, 2006. Black (pyrogenic) carbon: A synthesis of current knowledge and uncertainties with special consideration to boreal regions. Biogeosciences 3: 397-420. http://www.biogeosciences.net/3/397/2006/

Ridley, B.A., S. Madronich, R.B. Chatfield, J.G. Walega, R.E. Shetter, M.A. Carroll and D.D. Montzka, 1992. Measurements and model simulations of the photostationary state during the Mauna Loa Observatory Photochemistry Experiment: Ozone production and loss rates. Journal of Geophysical Research 97: 10375-10388.

Rolph, G.D., 2013. Real-time Environmental Applications and Display sYstem (READY) Website (http://www.ready.noaa.gov). NOAA Air Resources Laboratory, College Park, Maryland.

Siddique, T., P.M. Fedorak and J.M. Foght, 2006. Biodegradation of short-chain n-alkanes in oil sands tailings under methanogenic conditions. Environmental Science and Technology 40: 5459-5464.

Siddique, T., P.M. Fedorak, M.D. MacKinnon and J.M. Foght, 2007. Metabolism of BTEX and naphtha compounds to methane in oil sands tailings. Environmental Science and Technology 41: 2350-2356.

Simpson, I.J., S.K. Akagi, B. Barletta, N.J. Blake, Y. Choi, G.S. Diskin, A. Fried, H.E. Fuelberg, S. Meinardi, F.S. Rowland, S.A. Vay, A.J. Weinheimer, P.O. Wennberg, P. Wiebring, A.Wisthaler, M. Yang, R.J. Yokelson and D.R. Blake, 2011. Boreal forest fire emissions in fresh Canadian smoke plumes: C1–C10 volatile organic compounds (VOCs), CO_2, CO, NO_2, NO, HCN and CH_3CN. Atmospheric Chemistry and Physics 11: 6445-6463. doi:10.5194/acp-11- 6445-2011.

Simpson, I.J., N.J. Blake, B. Barletta, G.S. Diskin, H.E. Fuelberg, K. Gorham, L.G. Huey, S. Meinardi, F.S. Rowland, S.A. Vay, A.J. Weinheimer, M. Yang and D.R. Blake, 2010. Characterization of trace gases measured over Alberta oil sands mining operations: 76 speciated C2–C10 volatile organic compounds (VOCs), CO2, CH4, CO, NO, NO_2, NOy, O_3 and SO_2. Atmospheric Chemistry and Physics 10: 11931-11954. doi:10.5194/acp-10-11931-2010.

Skinner, W.R., M.D. Flannigan, B.J. Stocks, D.M. Martell, B.M. Wotton, J.B. Todd, J.A. Mason, K.A. Logan and E.M. Bosch, 2002. A 500 mb synoptic wildland fire climatology from large Canadian forest fires, 1959–1996. Theoretical and Applied Climatology 71: 157-169.

Soja, A.J., N.M. Tchebakova, N.H.F. French, M.D. Flannigan, H.H. Shugart, B.J. Stocks, A.I. Sukhinin, E.I. Varfenova, F.S. Chapin and P.W. Stackhouse Jr, 2007. Climate induced boreal forest change: predictions versus current observations. Global Planet Change 56: 274-296.

Stocks, B.J., M.A. Fosberg, T.J. Lynham, L. Mearns, B.M. Wotton, Q. Yang, J.Z. Jin, K. Lawrence, G.R. Hartley, J.A. Mason and D.W. McKenney, 1998. Climate change and forest fire potential in Russian and Canadian boreal forests. Climate Change 38(1): 1–13. doi:10.1023/A:1005306001055.

Strausz, O., K.N. Jha and D.S. Montgomery, 1977. Chemical composition of gases in Athabasca bitumen and in low-temperature thermolysis of oil sand, asphaltene and maltene. Fuel 56: 114-120. doi:10.1016/0016-2361(77)90128-4.

Thompson, A.M., 1992. The oxidizing capacity of the Earth's atmosphere: Probable past and future changes. Science 256: 1157-1165.

Timoney, K. and P. Lee, 2009. Does the Alberta tar sands industry pollute? The scientific evidence. The Open Conservation Biology Journal 3: 65-81.

Wood Buffalo Environmental Association, 2013. http://www.wbea.org/

Worden, H.M., M.N. Deeter, D.P. Edwards, J.C. Gille, J.R. Drummond and P.P. Nedelec, 2010. Observations of near-surface carbon monoxide from space using MOPITT multispectral retrievals. Journal of Geophysical Research 115: D18314. doi: 10.1029/2010JD014242.

Zhao, C., L. Peng, X.X. Tie, Y. Lin, C. Li, X. Zheng and Y. Fang, 2007. A high CO episode of long-range transport detected by MOPITT. Water, Air and Soil Pollution 178: 207-216. doi:10.1007/sl11270-006-9191-1.

LIST OF OSRIN REPORTS

OSRIN reports are available on the University of Alberta's Education & Research Archive at http://hdl.handle.net/10402/era.17209. The Technical Report (TR) series documents results of OSRIN funded projects. The Staff Reports (SR) series represent work done by OSRIN staff.

OSRIN Technical Reports – http://hdl.handle.net/10402/era.17507

BGC Engineering Inc., 2010. Oil Sands Tailings Technology Review. OSRIN Report No. TR-1. 136 pp. http://hdl.handle.net/10402/era.17555

BGC Engineering Inc., 2010. Review of Reclamation Options for Oil Sands Tailings Substrates. OSRIN Report No. TR-2. 59 pp. http://hdl.handle.net/10402/era.17547

Chapman, K.J. and S.B. Das, 2010. Survey of Albertans' Value Drivers Regarding Oil Sands Development and Reclamation. OSRIN Report TR-3. 13 pp. http://hdl.handle.net/10402/era.17584

Jones, R.K. and D. Forrest, 2010. Oil Sands Mining Reclamation Challenge Dialogue – Report and Appendices. OSRIN Report No. TR-4. 258 pp. http://hdl.handle.net/10402/era.19092

Jones, R.K. and D. Forrest, 2010. Oil Sands Mining Reclamation Challenge Dialogue – Report. OSRIN Report No. TR-4A. 18 pp. http://hdl.handle.net/10402/era.19091

James, D.R. and T. Vold, 2010. Establishing a World Class Public Information and Reporting System for Ecosystems in the Oil Sands Region – Report and Appendices. OSRIN Report No. TR-5. 189 pp. http://hdl.handle.net/10402/era.19093

James, D.R. and T. Vold, 2010. Establishing a World Class Public Information and Reporting System for Ecosystems in the Oil Sands Region – Report. OSRIN Report No. TR-5A. 31 pp. http://hdl.handle.net/10402/era.19094

Lott, E.O. and R.K. Jones, 2010. Review of Four Major Environmental Effects Monitoring Programs in the Oil Sands Region. OSRIN Report No. TR-6. 114 pp. http://hdl.handle.net/10402/65.20287

Godwalt, C., P. Kotecha and C. Aumann, 2010. Oil Sands Tailings Management Project. OSRIN Report No. TR-7. 64 pp. http://hdl.handle.net/10402/era.22536

Welham, C., 2010. Oil Sands Terrestrial Habitat and Risk Modeling for Disturbance and Reclamation – Phase I Report. OSRIN Report No. TR-8. 109 pp. http://hdl.handle.net/10402/era.22567

Schneider, T., 2011. Accounting for Environmental Liabilities under International Financial Reporting Standards. OSRIN Report TR-9. 16 pp. http://hdl.handle.net/10402/era.22741

Davies, J. and B. Eaton, 2011. Community Level Physiological Profiling for Monitoring Oil Sands Impacts. OSRIN Report No. TR-10. 44 pp. http://hdl.handle.net/10402/era.22781

Hurndall, B.J., N.R. Morgenstern, A. Kupper and J. Sobkowicz, 2011. Report and Recommendations of the Task Force on Tree and Shrub Planting on Active Oil Sands Tailings Dams. OSRIN Report No. TR-11. 15 pp. http://hdl.handle.net/10402/era.22782

Gibson, J.J., S.J. Birks, M. Moncur, Y. Yi, K. Tattrie, S. Jasechko, K. Richardson, and P. Eby, 2011. Isotopic and Geochemical Tracers for Fingerprinting Process-Affected Waters in the Oil Sands Industry: A Pilot Study. OSRIN Report No. TR-12. 109 pp. http://hdl.handle.net/10402/era.23000

Oil Sands Research and Information Network, 2011. Equivalent Land Capability Workshop Summary Notes. OSRIN Report TR-13. 83 pp. http://hdl.handle.net/10402/era.23385

Kindzierski, W., J. Jin and M. Gamal El-Din, 2011. Plain Language Explanation of Human Health Risk Assessment. OSRIN Report TR-14. 37 pp. http://hdl.handle.net/10402/era.23487

Welham, C. and B. Seely, 2011. Oil Sands Terrestrial Habitat and Risk Modelling for Disturbance and Reclamation – Phase II Report. OSRIN Report No. TR-15. 93 pp. http://hdl.handle.net/10402/era.24547

Morton Sr., M., A. Mullick, J. Nelson and W. Thornton, 2011. Factors to Consider in Estimating Oil Sands Plant Decommissioning Costs. OSRIN Report No. TR-16. 62 pp. http://hdl.handle.net/10402/era.24630

Paskey, J. and G. Steward, 2012. The Alberta Oil Sands, Journalists, and Their Sources. OSRIN Report No. TR-17. 33 pp. http://hdl.handle.net/10402/era.25266

Cruz-Martinez, L. and J.E.G. Smits, 2012. Potential to Use Animals as Monitors of Ecosystem Health in the Oil Sands Region – July 2013 Update. OSRIN Report No. TR-18. 59 pp. http://hdl.handle.net/10402/era.25417

Hashisho, Z., C.C. Small and G. Morshed, 2012. Review of Technologies for the Characterization and Monitoring of VOCs, Reduced Sulphur Compounds and CH_4. OSRIN Report No. TR-19. 93 pp. http://hdl.handle.net/10402/era.25522

Kindzierski, W., J. Jin and M. Gamal El-Din, 2012. Review of Health Effects of Naphthenic Acids: Data Gaps and Implications for Understanding Human Health Risk. OSRIN Report No. TR-20. 43 pp. http://hdl.handle.net/10402/era.26060

Zhao, B., R. Currie and H. Mian, 2012. Catalogue of Analytical Methods for Naphthenic Acids Related to Oil Sands Operations. OSRIN Report No. TR-21. 65 pp. http://hdl.handle.net/10402/era.26792

Oil Sands Research and Information Network and Canadian Environmental Assessment Agency, 2012. Summary of the Oil Sands Groundwater – Surface Water Interactions Workshop. OSRIN Report No. TR-22. 125 pp. http://hdl.handle.net/10402/era.26831

Valera, E. and C.B. Powter, 2012. Implications of Changing Environmental Requirements on Oil Sands Royalties. OSRIN Report No. TR-23. 21 pp. http://hdl.handle.net/10402/era.27344

Dixon, R., M. Maier, A. Sandilya and T. Schneider, 2012. Qualifying Environmental Trusts as Financial Security for Oil Sands Reclamation Liabilities. OSRIN Report No. TR-24. 32 pp. http://hdl.handle.net/10402/era.28305

Creasey, R., 2012. Professional Judgment in Mineable Oil Sands Reclamation Certification: Workshop Summary. OSRIN Report No. TR-25. 52 pp. http://hdl.handle.net/10402/era.28331

Alberta Innovates – Technology Futures, 2012. Investigating a Knowledge Exchange Network for the Reclamation Community. OSRIN Report No. TR-26. 42 pp. http://hdl.handle.net/10402/era.28407

Dixon, R.J., J. Kenney and A.C. Sandilya, 2012. Audit Protocol for the Mine Financial Security Program. OSRIN Report No. TR-27. 27 pp. http://hdl.handle.net/10402/era.28514

Davies, J., B. Eaton and D. Humphries, 2012. Microcosm Evaluation of Community Level Physiological Profiling in Oil Sands Process Affected Water. OSRIN Report No. TR-28. 33 pp. http://hdl.handle.net/10402/era.29322

Thibault, B., 2012. Assessing Corporate Certification as Impetus for Accurate Reporting in Self-Reported Financial Estimates Underlying Alberta's Mine Financial Security Program. OSRIN Report No. TR-29. 37 pp. http://hdl.handle.net/10402/era.29361

Pyper, M.P., C.B. Powter and T. Vinge, 2013. Summary of Resiliency of Reclaimed Boreal Forest Landscapes Seminar. OSRIN Report No. TR-30. 131 pp. http://hdl.handle.net/10402/era.30360

Pyper, M. and T. Vinge, 2013. A Visual Guide to Handling Woody Materials for Forested Land Reclamation. OSRIN Report No. TR-31. 10 pp. http://hdl.handle.net/10402/era.30381

Mian, H., N. Fassina, A. Mukherjee, A. Fair and C.B. Powter, 2013. Summary of 2013 Tailings Technology Development and Commercialization Workshop. OSRIN Report No. TR-32. 69 pp. http://hdl.handle.net/10402/era.31012

Howlett, M. and J. Craft, 2013. Application of Federal Legislation to Alberta's Mineable Oil Sands. OSRIN Report No. TR-33. 94 pp. http://hdl.handle.net/10402/era.31627

Welham, C., 2013. Factors Affecting Ecological Resilience of Reclaimed Oil Sands Uplands. OSRIN Report No. TR-34. 44 pp. http://hdl.handle.net/10402/era.31714

Naeth, M.A., S.R. Wilkinson, D.D. Mackenzie, H.A. Archibald and C.B. Powter, 2013. Potential of LFH Mineral Soil Mixes for Land Reclamation in Alberta. OSRIN Report No. TR-35. 64 pp. http://hdl.handle.net/10402/era.31855

Welham, C. and B. Seely, 2013. Oil Sands Terrestrial Habitat and Risk Modelling for Disturbance and Reclamation: The Impact of Climate Change on Tree Regeneration and Productivity – Phase III Report. OSRIN Report No. TR-36. 65 pp. http://hdl.handle.net/10402/era.31900

Eaton, B., T. Muhly, J. Fisher and S-L. Chai, 2013. Potential Impacts of Beaver on Oil Sands Reclamation Success – an Analysis of Available Literature. OSRIN Report No. TR-37. 65 pp. http://hdl.handle.net/10402/era.32764

Paskey, J., G. Steward and A. Williams, 2013. The Alberta Oil Sands Then and Now: An Investigation of the Economic, Environmental and Social Discourses Across Four Decades. OSRIN Report No. TR-38. 108 pp. http://hdl.handle.net/10402/era.32845

Watson, B.M. and G. Putz, 2013. Preliminary Watershed Hydrology Model for Reclaimed Oil Sands Sites. OSRIN Report No. TR-39. 193 pp. http://hdl.handle.net/10402/era.34250

Birks, S.J., Y. Yi, S. Cho, J.J. Gibson and R. Hazewinkel, 2013. Characterizing the Organic Composition of Snow and Surface Water in the Athabasca Region. OSRIN Report No. TR-40. 62 pp. http://hdl.handle.net/10402/era.36643

De Corby, R.G., 2013. Development of Silicon-Based Optofluidic Sensors for Oil Sands Environmental Monitoring. OSRIN Report No. TR-41. 19 pp. http://hdl.handle.net/10402/era.36936

Iqbal, M., T.K. Purkait, J.G.C. Veinot and G.G. Goss, 2013. Benign-by-Design: Synthesis of Engineered Silicon Nanoparticles and their Application to Oil Sands Water Contaminant Remediation. OSRIN Report No. TR-42. 30 pp. http://hdl.handle.net/10402/era.37308

Oil Sands Research and Information Network, 2013. Future of Shrubs in Oil Sands Reclamation Workshop. OSRIN Report No. TR-43. 71 pp. http://hdl.handle.net/10402/era.37440

Smreciu, A., K. Gould and S. Wood, 2013. Boreal Plant Species for Reclamation of Athabasca Oil Sands Disturbances. OSRIN Report No. TR-44. 23 pp. plus appendices. http://hdl.handle.net/10402/era.37533

Pereira, A.S. and J.W. Martin, 2014. On-Line Solid Phase Extraction – HPLC – Orbitrap Mass Spectrometry for Screening and Quantifying Targeted and Non-Targeted Analytes in Oil Sands Process-Affected Water and Natural Waters in the Athabasca Oil Sands Region. OSRIN Report No. TR-45. 33 pp. http://hdl.handle.net/10402/era.37793

Liang, J., F. Tumpa, L.P. Estrada, M. Gamal El-Din and Y. Liu, 2014. Ozone-Assisted Settling of Diluted Oil Sands Mature Fine Tailings: A Mechanistic Study. OSRIN Report No. TR-46. 43 pp. http://hdl.handle.net/10402/era.38226

Rochdi, N., J. Zhang, K. Staenz, X. Yang, D. Rolfson, J. Banting, C. King and R. Doherty, 2014. Monitoring Procedures for Wellsite, In-Situ Oil Sands and Coal Mine Reclamation in Alberta. OSRIN Report No. TR-47. 156 pp. http://hdl.handle.net/10402/era.38742

Taheriazad, L., C. Portillo-Quintero and G.A. Sanchez-Azofeifa, 2014. Application of Wireless Sensor Networks (WSNs) to Oil Sands Environmental Monitoring. OSRIN Report No. TR-48. 51 pp. http://hdl.handle.net/10402/era.38858

OSRIN Videos – http://hdl.handle.net/10402/era.29304

Rooney Productions, 2012. Assessment Methods for Oil Sands Reclamation Marshes. OSRIN Video No. V-1. 20 minutes. Also available on the University of Alberta You Tube Channel (recommended approach).

Rooney Productions, 2012. Assessment Methods for Oil Sands Reclamation Marshes. OSRIN Video No. V-1. Nine-part mobile device version. Also available on the University of Alberta You Tube Channel (link to Part 1 - recommended approach).

OSRIN Staff Reports – http://hdl.handle.net/10402/era.19095

OSRIN, 2010. Glossary of Terms and Acronyms used in Oil Sands Mining, Processing and Environmental Management – December 2013 Update. OSRIN Report No. SR-1. 123 pp. http://hdl.handle.net/10402/era.17544

OSRIN, 2010. OSRIN Writer's Style Guide – November 2013 Update. OSRIN Report No. SR-2. 29 pp. http://hdl.handle.net/10402/era.17545

OSRIN, 2010. OSRIN Annual Report: 2009/2010. OSRIN Report No. SR-3. 27 pp. http://hdl.handle.net/10402/era.17546

OSRIN, 2010. Guide to OSRIN Research Grants and Services Agreements - June 2011 Update. OSRIN Report No. SR-4. 21 pp. http://hdl.handle.net/10402/era.17558

OSRIN, 2011. Summary of OSRIN Projects – March 2014 Update. OSRIN Report No. SR-5. 108 pp. http://hdl.handle.net/10402/era.20529

OSRIN, 2011. OSRIN Annual Report: 2010/11. OSRIN Report No. SR-6. 34 pp. http://hdl.handle.net/10402/era.23032

OSRIN, 2011. OSRIN's Design and Implementation Strategy. OSRIN Report No. SR-7. 10 pp. http://hdl.handle.net/10402/era.23574

OSRIN, 2012. OSRIN Annual Report: 2011/12. OSRIN Report No. SR-8. 25 pp. http://hdl.handle.net/10402/era.26715

OSRIN, 2013. OSRIN Annual Report: 2012/13. OSRIN Report No. SR-9. 56 pp. http://hdl.handle.net/10402/era.31211

OSRIN, 2014. OSRIN Annual Report: 2013/14. OSRIN Report No. SR-10. 66 pp. http://hdl.handle.net/10402/era.38508